An Evaluation of Trend and Anomalies of Arctic Sea Ice Concentration, 1979–2006

by

Peiyao Daniel Xia

A thesis
presented to the University of Waterloo
in fulfilment of the
thesis requirement for the degree of
Master of Environmental Studies
in
Geography

Waterloo, Ontario, Canada, 2013

AUTHOR'S DECLARATION

I hereby declare that I am the sole author of this thesis. This is a true copy of the thesis, including any required final revisions, as accepted by my examiners.

I understand that my thesis may be made electronically available to the public.

ABSTRACT

As a part of the Cyrosphere ecosystem, Arctic sea ice is one of the focal points when studying Arctic climate change. Arctic sea ice image has been documented by remotely sensed data since the 1970s. By examining these data, some climate patterns can be revealed. In this research, Arctic region is divided into 9 sections to analyze the regional differences of the ice coverage and variability. Data used are bootstrapped 1979 to 2006 SSM/I and SMMR images from NSIDC to perform a time series analysis to examine the sea ice trends and spatial/temporal anomalies detection by conducting a descending sort of sea ice coverage by years in the sub-regional scale. Then, the temporal mixture analysis developed by Piwowar & LeDrew is applied to the data to reveal the variability within each subregion. Fractional images produced by TMA highlight the temporal signature concentration in the entire Arctic region. And the color-mix image derived from TMA highlights and overlaps temporal signatures that have over 80% concentrations from highest to lowest. The color mix image can reveal the spatial distribution of similar temporal characteristics and the evolution of time series in the same area during the 30-year period. Through this analysis, the spatial and temporal variability of Arctic sea ice can be perceived that in the subpolar regions, Arctic sea ice has a higher seasonal pattern which varies a lot each other. The Arctic sea ice extent endures an overall decline trend, which the decline speed increases every ten years. But this trend is not statistically significant in every subregion. The spatial/temporal anomaly analysis reveals several patterns of Arctic sea ice variability. The seasonal variability of Arctic sea ice in the eastern and western side of the Arctic Basin resemble each other in

the long term, which may coincide with the North Atlantic Oscillation. In addition, within a subregion, different areas may have significantly different temporal characteristics, such as the Greenland Sea and Seas of Okhotsk. Moreover, the temporal characteristics some areas in the Arctic region have changed through time significantly regarding early melt or late freeze. Hopefully this analysis will provide undiscovered temporal evolution through time and some new insights on the dynamics of the Arctic sea ice cover.

ACKNOWLEDGEMENTS

First of all, I need to give my full gratitude to Dr. Ellsworth LeDrew for his guidance, patience, and wisdom to help me finish this thesis. He leads me through all obstacles and makes things happen. Secondly, I'd like to thank Dr. Richard Kelly for his useful comments and guidance through the progress of this thesis.

TABLE OF CONTENTS

LIST OF FIGURES

CHAPTER ONE

INTRODUCTION

The Arctic region is surrounded by Eurasia and North America continents, and largely covered by the Arctic Ocean and a number of smaller seas, such as, Laptev Sea, Greenland Sea, and Baffin Bay. In climatology, the climate in the Arctic region plays an important role in global climate change. Since the Arctic Ocean is covered mostly by ice most of time, the variability of the ice reflects local climate change. Recently, due to global warming, the polar cap ice began to melt at an accelerating rate. As the ice melts, there is reflective surface to reflect the solar radiation and results more absorbing of the sun heat. This creates a positive feedback cycle that leads to more melting of the ice cap.

From previous research of sea ice variability, a decadal oscillation pattern for Arctic sea ice was in the eastern and western side of the Arctic Ocean due to North Atlantic Oscillation (Wang and Ikeda, 2000).

In this research, the question to be examined is how does the sea ice extent vary in time and in space in the Arctic region, where and when these changes happened, and are there regional differences. In order to answer these questions, a general analysis of sea ice extent variability is performed, followed by a small-scale regional ice extent ranking, then the temporal mixture analysis.

The following gives an introduction of Arctic sea ice and its role in the global ecosystem. Next, a brief summary of the recent development of remote sensing and its significance in monitoring sea ice is provided. Last, the North Atlantic Oscillation is introduced and its significance when applied with Arctic sea ice.

1.1 Introduction of Arctic Sea Ice and its Importance to Ecosystem

According to the National Snow and Ice Data Centre (NSIDC, 2006), sea ice is defined as sea water that freezes and becomes ice that floats on the ocean surface. Arctic sea ice is a major form of surface water in the Arctic Ocean. Sea ice covers the Arctic Ocean and its adjacent areas with a thin, uneven sheet of sea ice formed by frozen ocean surface water, all year round or seasonally.

Sea ice is a major component of the polar environment on the planet. In the northern hemisphere, sea ice covers approximately 15.9 million km^2 of the north polar and sub-polar oceans in midwinter and typically 6 million km^2 at its summer minimum (NSIDC, 2006). Sea ice limits energy exchange between the ocean and the atmosphere, reflecting a high percentage of the solar radiation. Furthermore, as sea ice forms and ages, salt is rejected to the deeper ocean, so that sea ice tends to have lower salinity than sea water. Consequently, as the ice forms and melts, the salinity content of the underlying ocean increases and decreases, impacting overturning and ocean circulation (Parkinson and Cavalieri, 2008). When the ice moves, it transports cold, low-salinity mass, affecting surface temperature and salt gradients (Aagaard and Carmack, 1989; Barry et al., 1993; Parkinson, 1996). Changes in the sea ice volume hence have potential broad-range climate consequences. For instance, a numerical model demonstrates that 37% of the global warming simulated for a doubled CO_2 scenario was attributable explicitly to a changing sea ice volume (Rind et al., 1995).

Sea ice in the Arctic region undergoes a seasonal variability. Based on past research, the maximum extent of sea ice is expected on March, while the minimum is

expected in September (Carsey, 1992). The seasonal melting and freezing period is different in various regions. In terms of annual variability, the melting period may be delayed by two or three months in the summer. In most cases, there is a layer of snow on top of sea ice covering ice from wind and direct solar insulation (Parkinson, 1996), which causes the freezing and melting delay. In addition, the latent heat in the ocean is also a factor. Ocean storages heat applies buffer effect on the sea ice freezing and melting when the season changes by releasing or absorbing large amount of energy. Figure 1.1 gives a brief illustration of the air-sea-ice interaction and microwave emissions and scattering from various surfaces.

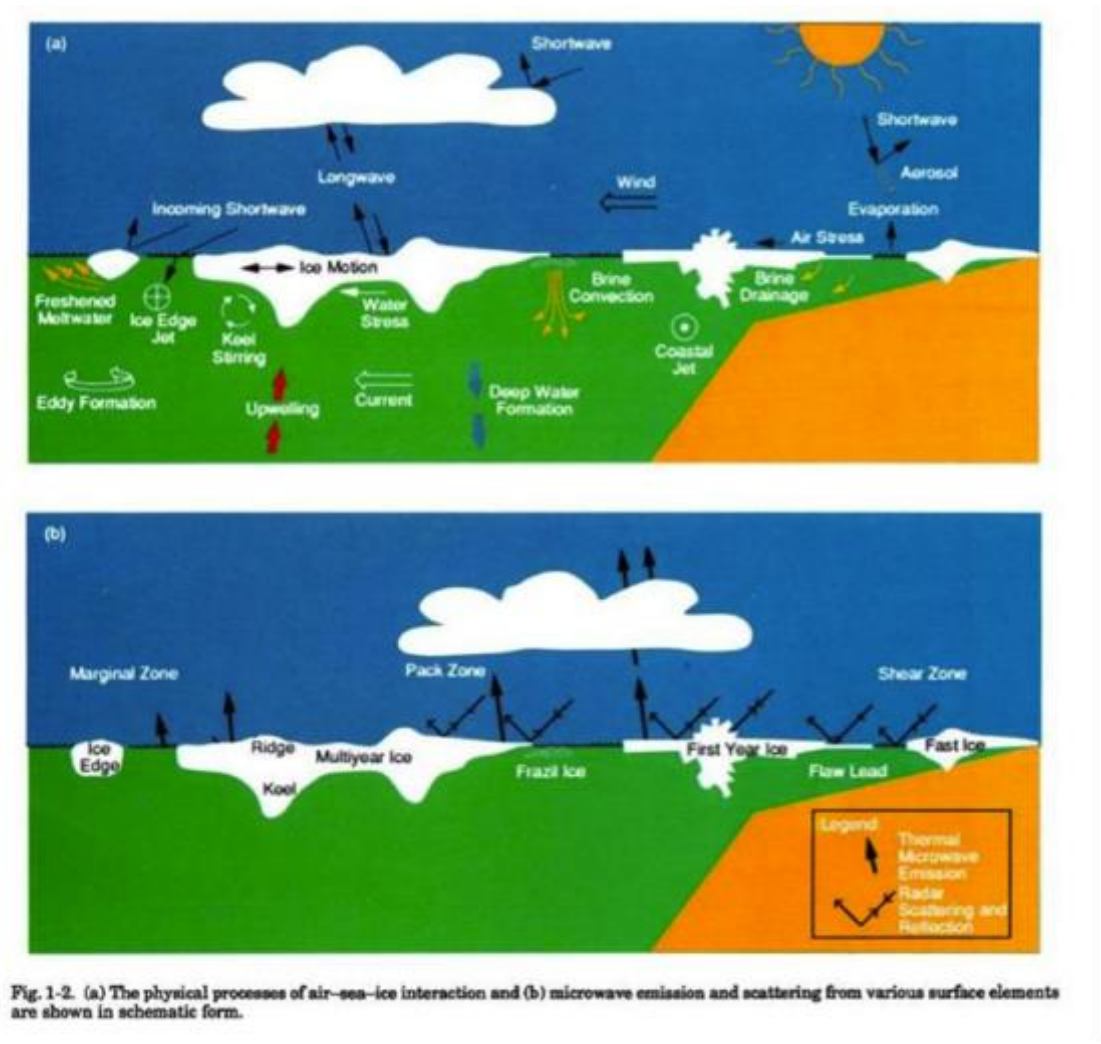

Fig. 1-2. (a) The physical processes of air–sea–ice interaction and (b) microwave emission and scattering from various surface elements are shown in schematic form.

Figure 1.1 Physical process of air sea ice interaction (Carsey, 1992)

Sea ice buffers the interaction between ocean and atmosphere constantly (see Figure 1.1). The incoming solar insolation will be partly absorbed by sea ice/water and becomes heat which changes the sea temperature, sea ice freeze/melt time, and sea ice extent. Because both sea ice extent and thickness is very sensitive to the temperature of the ocean surface, solar insolation can greatly influence sea ice variability. Beneath the ocean surface, the melt ice rises to the sea surface can increase the melt of small floes. While under a large floating multiyear sea ice, water stirring, upwelling warm sea water,

and water stress can greatly influence the sea ice melt process. If these phenomena happened in the center of a large floe, these might be a significant chance to form polynyas and leads.

In Arctic regions, sea ice endures seasonal freeze and melt cycle, which is influenced by a combination of factors, including age of ice, air temperature, and solar insolation. The freshly formed sea ice is called the first-year ice (FYI), while sea ice that survived at least one melt season is called the multi-year ice (MYI) (Parkinson, 1996). The multi-year ice is usually thicker than first year ice.

A few Arctic sea ice characteristics have been summarized: sea ice extent, concentration, type, thickness, and seasonality (Piwowar & LeDrew, 1995). Generally, sea ice is considered to play an important role in the Arctic biosphere from the following perspective which is solar radiation reflection, thermal connection with the ocean and atmosphere, brine capacitance, and the physical conditions, thickness and concentration. Any analysis of climate change and variability using sea ice as a proxy indicator must ultimately reference one or more of these physical properties (Piwowar & LeDrew, 1995).

Sea ice concentration indicates the relative amount of sea space covered by ice. Usually sea ice concentration is compared to some reference area. While sea ice extent is defined as the cumulative areas of all grid cells having at least 15% sea ice concentration, and sea ice area is the sum of the pixel areas times the ice concentration for all pixels with ice concentration of at least 15%. Therefore, sea ice extent is often larger than sea ice area.

Research regarding the sea ice extent from satellite images has accelerated since

the 1970s. Numerous studies have investigated the changes of Arctic sea ice extent, area, and concentration. In general, the regression analysis of average mean Arctic sea ice extent in September for the past 30 years showed an undoubted downward tendency. From 1979 to 2006, the three minimum summer Arctic sea ice extents are within 2001 to 2006. A later start of freeze-up and an earlier start to the melt season leading to longer melt period contributes to the severe sea ice loss (Serreze et al. 2007). Western arctic, including the Beaufort Sea, Chukchi Sea, East Siberian Sea, Laptev Sea and Kara Sea, has the most significant summer sea ice loss in 2007 when compared to the averaged summer sea ice extent for 1979-2000 (Comiso et al., 2008).

Sea ice thickness is a very important feature for the estimation of sea ice volume. Unlike sea ice extent which is easily retrieved from remote sensing technology, sea ice thickness is much harder to attain. Sea ice thickness determines a number of important fluxes such as heat flux between the air and ocean surface as well as salt and fresh water fluxes. Any decline in sea ice extent might indicate loss of sea ice and serves as signal for warm or cold year, sea ice thickness is also very critical in this issue. According to NASA, (2008), the Arctic sea ice thickness has dramatically declined which leads a wide concern about global warming and sea level rising.

Table 2: Sea Ice as a Climatic Indicator

Sea Ice Parameter	Observations	Potential* Indicators	Ideal[1] Spatial Requirements	Ideal[1] Temporal Requirements
extent	• has been shown to influence weather and to be influenced by weather • extreme variability; oscillations on a 10-12 year period noted; no consistent trends found	+ Baffin Bay[2,3] + Labrador Sea[2,4] + Greenland Sea[5,6] – Hudson Bay[6] – Bering Sea[6,7,8] – Sea of Okhotsk[6,7,9] – Kara Sea[3,6]	>1 km	3 days
type	• composition of multiyear ice pack is a potential repository for accumulated climatic changes • it has not been studied for trends or variability		> 1 km	3 days
concentration	• areas of low concentration are significant areas for atmosphere-ocean interaction • high variability in the marginal ice zone; no trends found	+ Baffin Bay[6] + Bering Sea[6] + Labrador Sea[6] + Sea of Okhotsk[6] + Kara Sea[6,10]	> 1 km	3 days
thickness	• relative thickness of sea ice reflects average winter and early spring temperatures as well as the magnitude of mid-summer solar radiation	– shorefast ice[11]	10 km	3 days
dynamics	• motion changes can lead to changes in ice concentration; long-term motion is a potential repository for accumulated climatic changes • high variability; sometimes reverses; no trends found		10 km	1 day
sesonality: melt onset	• closely related to winter and spring air temperatures; long-term variation is a potential indicator of climatic changes • high variability; no long term trend studies made	+ Chukchi Sea[12] + Kara Sea[12,13] + Barents Sea[12,13] – Labrador Sea[6,12]	10 km	3 days

*potential regions for which consistent deviation from an established norm for that ice parameter might indicate a change of climate; '+': likely candidate; '-': region to avoid

[1]Barber *et al.*, 1992b
[2]Chapman and Walsh, 1992
[3]Barry, 1993
[4]Ikeda, 1990a,b
[5]Kelly *et al.*, 1987
[6]Parkinson, 1991
[7]Cavalieri and Parkinson, 1987
[8]Niebauer, 1983
[9]Parkinson, 1989
[10]Crane and Anderson, 1989
[11]Brown and Cote, 1992
[12]Anderson, 1987

Figure 1.2 Sea ice physical features and relationship with ocean, atmosphere, and solar radiation (Piwowar & LeDrew, 1995)

1.2 Sea Ice Observation and Monitoring using Remote Sensing

Routine observations of the Polar Regions are necessary to examine changes of sea ice. Thanks to the incredible technological advancements that have undergone in the last thirty years, the development of satellite observation and imagery contributes significantly in understanding the polar geophysical processes. Remote sensing provides a relatively easy-to-obtain source of data with which we can view the entire planet and monitor changes in the nature of the surface of large areas through time, in a consistent, integrated, and numerical manner (Davis, et al., 1991). Since the electrically scanning microwave radiometer (ESMR) in 1972, a multichannel satellite passive microwave data record that began with the deployment of the Scanning Multichannel Microwave Radiometer (SMMR) following the launch on NASA's Nimbus 7 satellite in October 1978 makes scientists capable to examine the Arctic sea ice coverage on a large scale. In 1987, the Defense Meteorological Satellite Program (DMSP) Special Sensor Microwave Imagers (SSM/I) was launched and continued to operate since then. A few of those Arctic researches are based solely on the SMMR data, while the most are based also on data from SSM/I. (Johannessen et al., 1995; Maslanik et al., 1996; Bjørgo et al., 1997; Cavalieri et al., 1997; Parkinson et al., 1999; Stroeve et al., 2005; Comiso, 2006; Meier et al., 2007)

Apart from measurement of Arctic sea ice coverage, the remote sensing technology nowadays can measure the thickness and volume of Arctic sea ice. Laxon *et al*., (2013) stated in paper "*CryoSat-2 estimates of Arctic sea ice thickness and volume*" that results from the Pan-Arctic Ice-Ocean Modeling and Assimilation system (PIOMAS)

suggest the decline in sea ice extent has been accompanied by a decline in volume. Using data from the European Space Agency CryoSat-2 (CS-2) mission, validated with in situ data, sea ice volume for winters of 2010/11 and 2011/12 can be estimated. In addition, Kwok, (2011) described a method of estimating sea ice thickness by using altimeter-derived free-board together with the assumption of hydrostatic equilibrium in paper "*Satellite remote sensing of sea-ice thickness and kinematics: a review*". The basic idea of measuring sea ice thickness is to measure the surface elevation of the ocean and the surface elevation of ice first. And then, given the volume of sea ice above the ocean surface, the whole volume of sea ice can be extrapolated. To convert freeboard to thickness, sophisticated approaches are employed by modifying the snow loading from Warren et al (1999) and ice density (Kwok, 2011).

1.3 North Atlantic Oscillation

Climate change and global warming have caused much discussion recently. From previous research, the North Atlantic Oscillation (NAO) is the most prominent and recurrent pattern of atmospheric variability in high latitudes.

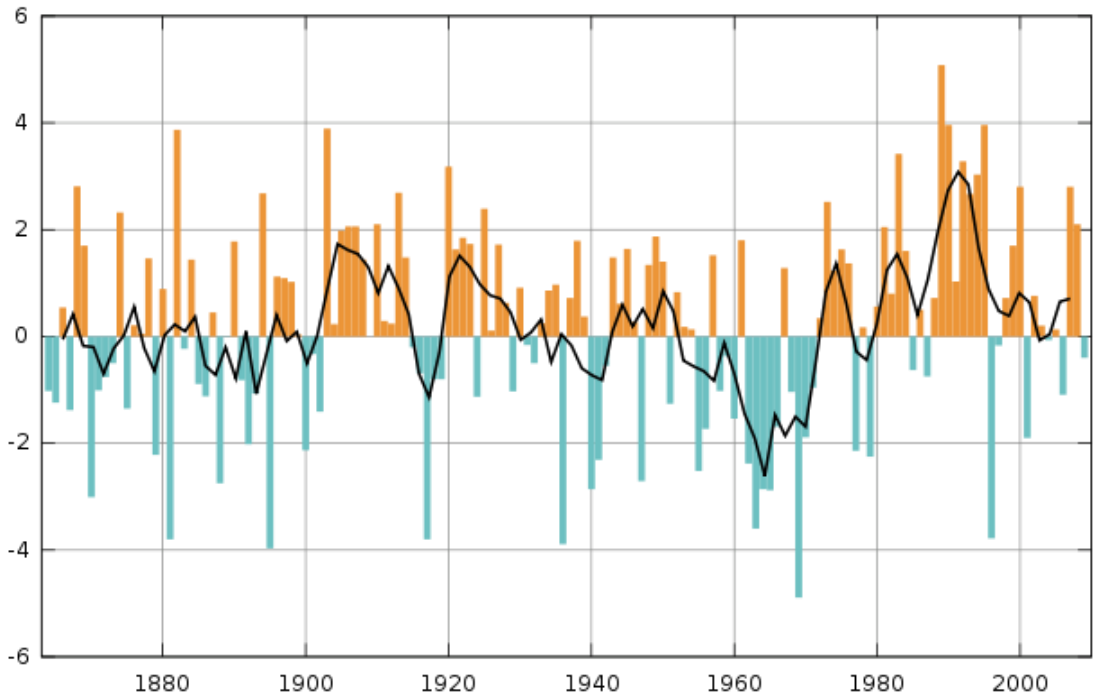

Figure 1.3 North Atlantic Oscillation Index (Marsupilami, 2010)

The North Atlantic Oscillation refers to the swings in the atmospheric sea level pressure difference between the Arctic and the subtropical Atlantic that are most noticeable during the boreal cold season (November - April). The oscillations are associated with changes in seasonal heat and moisture transport between the Atlantic and the neighboring continents, as well as the intensity and paths of storms (Hurrell, Kushnir, Ottersen, & Visbeck, 2003). Similar changes can also be induced by NAO(Hurrell, Kushnir, Ottersen, & Visbeck, 2003).

From the background research, North Atlantic Oscillation, the atmosphere, and sea ice are widely considered to be highly correlated with each other. These climatic fluctuations affect agricultural harvests, water management, energy supply and demand, and fisheries yields (Hurrell, Kushnir, Ottersen, & Visbeck, 2003). According to recent observations, sea ice coverage and thickness in the north Arctic have dramatically decreased (NSIDC, 2007) , which makes finding the interaction mechanism between these climate factors necessary. Any climate mitigation and adaptation measurements must be based on the full and thorough understanding of the natural environment and its relevant climate factors.

North Atlantic Ocean and the Arctic Ocean are also under the influence of North Atlantic Oscillation. The responses of the marine ecosystems, terrestrial ecosystems, and the freshwater ecosystems to the climate variability are highly correlated with the North Atlantic Oscillation. Speaking of the ocean's response to the NAO alone, which is highly interested in this research, can be divided into the following subtopics: the sea surface temperature response pattern; the air sea flux interaction pattern including momentum flux, heat flux, water flux, and the buoyancy flux; the response of the ocean circulation, including the wind driven ocean circulation, buoyancy driven ocean circulation, poleward heat transport affect to circulation changes, and the ocean circulation response in dynamical ocean models; and changes in water masses, including observed NAO induced changes in the subtropical mode water, Labrador sea water, and in the Nordic Seas (Visbeck et al., 2003).

Since NAO has a profound influence on the polar atmosphere and ocean

ecosystems and the polar ice consequently. There are a number of key processes that influences the sea ice more than others, such as the changes in the air ice flux momentum and the heat and the changes in the divergence of the oceanic heat transport (Visbeck et al., 2003). Variations in cloud interact with the heat flux in changing the Arctic radiation budget, which are the main factors contributing to the ice change. As for sea ice motion, enhanced wind stress associated with a positive NAO index generally forces the sea ice edge southward in the Labrador Sea and further to the northeast in the Barents Seas (Deser et al., 2000). During a positive NAO index phase, strong winds bring warm air masses towards the Nordic Seas and Arctic Ocean thus reducing the winter sea ice production (Dickson et al., 2000).

From the sea ice extent variability research by Parkinson and Cavalieri, (2008), Arctic sea ice coverage has a decrease rate of approximately 3% per decade. The NAO impacts might also be involved in this downward trend. Modeling studies of Zhang et al. (2008) suggest that the NAO impacts the winter time sea ice thickness in the Arctic, which may precondition the summer ice concentrations even in the absence of additional anomalous atmospheric forcing during summer. Coincidentally, the long term decline of the summer sea ice cover shares the same period of increasing NAO index since the mid-1960s. Through this coincidence cannot be used to for any conclusion, it provides a hint for future research. However, reliable long term Arctic sea ice data are mostly restricted to the position of the sea ice edge during the pre-satellite era and sea ice concentration thereafter. Only a few decades of satellite recorded sea ice motion, and only the Fram Strait has a continuous record of sea ice thickness for several years (Vinje et al., 1997).

1.4 LITERATURE REVIEW

1.4.1 Synthesis of Arctic sea ice variability and trend during the recent 30 years

In the paper "Arctic sea ice variability and trends, 1979-2006 by Claire L. Parkinson and Donald J. Cavalieri", the analysis of arctic sea ice extents is performed, derived from satellite passive microwave data for the 28 years 1979-2006. The analysis yields an overall negative trend of -45,100 ± 4,600 km2/a (-3.7 ± 0.4%/decade) in the yearly averages, with negative ice extent trends also occurring for each of the four seasons and each of the 12 months. And separate analyses have also been done within different Arctic sections, such as the Kara and Barents Seas, Arctic Ocean, Baffin Bay/Labrador Sea, the Greenland Sea, Hudson Bay, Seas of Okhotsk and Japan, the Bering Sea, Canadian Archipelago, and Gulf of St. Lawrence.

Monthly sea ice extents in this article are retrieved by calculating sea ice extents on a daily basis (or every other day in the case of SSMR data) and then combined to monthly, seasonal, and yearly averages. The monthly sea ice extents are displayed temporally to present the overall long term variation and seasonal changes inside each individual year. Monthly deviations were extracted by taking the individual monthly averages and subtracting the 28 year average of a particular month. A line of linear least squares fit is used to determine the monthly deviations from the long term averages. In addition, seasonal averages are calculated (Spring, Summer, Fall, and Winter) to show the seasonal variation of each year. Seasonal variations can be used to identify whether sea ice in this region is dominated by non-seasonal or seasonal characteristics. Yearly and seasonally averaged sea ice extents for the years 1979–2006 divides the winter (W),

spring (Sp), summer (Su), and autumn (A) values cover the periods January–March, April–June, July–September, and October–December, respectively (Parkinson and Cavalieri, 2008).

All these regions showed a negative trend of sea ice extent but with different confidence level. The 28 year trends in ice areas for the Northern Hemisphere total are also statistically significant and negative in each season, each month, and for the yearly averages.

In this article, a perspective is provided for analyzing the long term Arctic sea ice time series by displaying the monthly data in their temporal order as well as their averaged seasonal variations. However, this Arctic seasonal sea ice extent view does not give a straightforward method in analyzing the long-term sea ice variability trend. Therefore, average monthly sea ice data of each month is compared with average sea ice extent data of each month with individual monthly data. The difference in this comparison formed a line that greatly helped in analyzing the long-term sea ice variability trend. In addition, the author utilized a linear regression analysis to test whether sea ice extent has decreased. The linear least squares fit analysis was chosen to create a line with its slope and estimated standard deviation. These methods provide a way in analyzing the general variability and trend of Arctic sea ice extent for this research. However, because of limited sample size of the remote sensing sea ice extent data, it is difficult to determine the parametric or nonparametric nature of these data. In addition, the seasonal effects and the both spatial and temporal autocorrelation have not been taken into consideration. Therefore, in this research, these problems will be avoided.

Arctic Sea Ice Extent and Anomalies, 1953-1984. Lawrence A. Mysak and Davinder K. Manak, 1989. Atmosphere-Ocean, 27:2, 376-405

In this article, s 32-year period of seasonal and interannual variability of sea ice extent in the Arctic region from 1953 to 1984 is investigated. The major findings of this article can be summarized in the following 4 sections.

The first section is the climatological ice edge positions in the various sub-regions of the Arctic are closely related to the surface ocean circulation patterns at high latitudes.

The second section is the time scale of the areal sea ice anomaly fluctuations varies across the Arctic region exhibited an approximate 4-6 year cycle, and according to the author, this cycle is most likely due to the interannual variability of the sea level pressure in the North Pacific and the Beaufort Sea region. Also, a strong decadal cycle in the smoothed anomalies for the Kara and Barents Seas is found. Though the data are highly correlated, they do not imply a causal relationship between the decadal pattern and the North Atlantic Oscillation/Arctic Oscillation. The time scale of these cycle fluctuation appears to vary from interannual to decadal.

The third section is the anomalies found in the Beaufort and Chukchi sea region. There are plausible atmospheric pressure anomalies associated with the see-saw in winter air temperature between northern Europe and western Greenland. The air temperature and pressure see-saw pattern is also very similar with the NAO/AO patterns in the Arctic region, but no interaction is found between sea ice variability and atmospheric pressure and temperature anomalies.

The fourth section is to propose a plausible explanation for the sea ice anomalies, especially the maximum sea ice extent observations. The plausible explanation could be the presence of a large negative salinity anomaly that moved cyclonically around the subarctic region. Apart from interactions with salinity, other environmental factors such as wind, sea surface temperatures can also be related to sea ice extent anomalies.

Overall, this article studies the Arctic sea ice extent and anomalies in the 1989 in different Arctic sub-regions. Also, other climatological data such as sea ice motion, salinity, air pressure/temperature, are used to find variability patterns. Apart from the anomalies, the seasonal cycles of sea ice are also found in some sub-regions.

In another paper "*Sea ice conditions and melt season duration variability within the Canadian Arctic Archipelago (CAA): 1979-2008"* by Howell *et al.* (2009), the sea ice conditions and melt season duration within the Canadian Arctic Archipelago are investigated with a conclusion of sea ice extent within the Canadian Arctic Archipelago decreases in average September sea ice area at -8.7% per decade and the melt season duration increased by 7 days per decade. Unlike the Parkinson paper, this paper focuses more on the variability of first year ice and multiyear ice. Also, the Canadian Ice Service Digital Ice Chart Archive (CISDA) data is used to explore the links between sea ice conditions and melt season duration as well as the SMMR and SSM/I data.

The September and October sea ice extent in CAA is analyzed in this paper to show the spatial distribution of average September multiyear ice concentration. And the linear least squares fit average method is used to create the long-term trend of average September total ice and multiyear ice. In addition, the melt duration analysis concludes

that the 7 days per decade increase contains a 3.1-days per decade earlier melt and a 3.9-days per decade later freeze.

In this paper, the author noted that the majority of CAA's multiyear ice is generated within or imported into the Queen Elizabeth Islands region from the Arctic Ocean and multiyear ice flow into the Northwest Passage. In addition, the input source of CAA multiyear ice changes through time with multiyear sea ice flow into the Northwest Passage and a anomaly year that in 2007, multiyear ice within the Northwest Passage was removed. Some physical dynamics examined the sea ice variability through ice import from the Arctic Ocean and the sea level pressure, and concluded the future conditions of the current variability trend that the supply of multiyear ice from the Arctic Ocean to CAA could reduce but unlike to stop (Howell, 2008). The physical process of Arctic sea ice variability helped analyze the sea ice motion between CAA and the Arctic Ocean, understanding the dynamics of sea ice.

The change of speed of Arctic sea ice decline is not fully analyzed in the Howell (2008) study. In the paper "Accelerated decline in the Arctic sea ice cover" by Comiso *et al.* (2008) examined the evolution of speed of Arctic sea ice extent decline. First of all, sea ice extent in summer 2007 was observed as the minimum. Furthermore, it is 24% lower than the previous record minimum observed in 2005. The acceleration in the decline is evident and area trends of the entire ice cover have shifted from -3% per decade in 1979-1996 to -10.7% per decade from 1997 to 2007 (Comiso *et al.*, 2008).

Overall, Arctic sea ice extent in the summer of 2007 shows a very large low anomaly of 37% less than the climatological averages. And the surface temperature data

indicated that the growth of sea ice was likely hindered and the retreat likely enhanced by the anomalously high temperatures in previous months (Comiso *et al*., 2008). This phenomenon is probably due to the result of pre-conditioning of Arctic Ocean through abnormally low perennial ice coverage in recents (Serreze *et al*., 2007). According to this paper, the rate of Arctic sea ice decline dramatically increased in the last decade compared to the 1979 to 1997 average, especially in the summer period. And this provides a view to analyze the decline trend and rate in this thesis that in the 30 year time series how Arctic sea ice extent decline by decade.

There is another paper "*Arctic sea ice decline: Faster than forecast*" by Juliene Stroeve *et al*., (2007) which found the decline rate is faster than anticipated. In this paper, late September Arctic sea ice extents are analyzed from 1953 to 2006, and compare actual sea ice extent observations with several forecasting models in the Intergovernmental Panel on Climate Change Fourth Assessment Report (IPCC AR4). All participating models show that sea ice cover declines over the 50 year period. The atmospheric greenhouse gas (GHG) loading response to the variability of Arctic sea ice extent is also examined.

In particular, Stroeve *et al*., (2012) wrote another paper "*Trend in Arctic sea ice extent from CMIP5, CMIP3 and observations*" that specific described two climate model comparisons, the World Climate Research Program Coupled Model Intercomparison Project Phase 3, and updated that to CMIP5. Similar conclusions are made that trends from most ensemble members and models nevertheless remain smaller than the observed value, pointing to strong impacts of internal climate variability (Stroeve *et al*., 2012).

The Hadley Center sea ice and sea surface temperature data set are the primary data source. And estimates of sea ice concentration before 1979 are based on early satellite observations, aircraft and ship reports. Through a number of IPCC AR4 simulations, it concludes that observations indicating a downward trend in September Arctic sea ice extent from 1953 to 2006 are larger than any of the model estimates. In addition, the current summer minimum extent is approximately 30 years ahead of the ensemble mean model forecast (Stroeve *et al*., 2007). Also, the impact of GHG loading on the Arctic sea ice extent in September is strong and growing, and may also impact the March sea ice extent.

The seasonal variability of the Arctic sea ice extent involves an important part of the melt onset dates. Anderson *et al*., (2010) studied the calculation of melt onset dates of the Arctic sea ice in paper "*A comparison between SSM/I passive microwave melt onset dates and satellite-derived albedo melt onset dates in the Arctic*". In this paper, the rapid decline of Arctic sea ice extent in the past few years is also noted. Many factors contribute to the melting of sea ice, among which the ice albedo feedback plays an important role in energy absorbing and melt intensification. In order to study the albedo conditions during the melt season, the start of melt could help to determine when albedos change due to melting. As it is difficult to obtain albedo data directly from satellite remote sensing due to cloud cover, especially in the polar regions, passive microwave remote sensing data have a large chance to see through clouds and determine snow characteristics such as melting on the sea ice surface (Anderson *et al*., 2010). Satellite derived passive microwave brightness temperature data has been used to determine the

onset of sea ice melt in the Arctic region since 1997 (Anderson *et al*., 2010). The change in the passive microwave emissivity from crystallization changes in the snow ice continuum can be used to determine the onset dates of sea ice melt. Hence, passive microwave data during melt onset could be used as a proxy for the changing albedo conditions during melt (Anderson *et al*., 2010).

1.4.2 Synthesis of climatology dynamics of Arctic sea ice variability

After the 2007 record minimum Arctic sea ice cover was observed, the following deformation of the Arctic sea ice cover was examined by Kwok and Cunningham (2012) in "*Deformation of the Arctic Ocean ice cover after the 2007 record minimum in summer ice extent*".

The behavior of sea ice cover after significant thinning at the end of summer is of great interest in studying the response of the ice cover to external forcing of the environment (Kwok and Cunningham, 2012). If the significant deformation at the beginning of the growth season were unaccounted for in the mass and area balance of ice cover, any deformation-induced decrease in ice coverage could be incorrectly attributed to ice export with a concurrent decrease in Arctic sea ice volume when in fact the ice volume is conserved but compensated by redistributions in thickness (Kwok and Cunningham, 2012). This paper quantifies the deformation of ice cover after the summer of 2007 using RADARSAT-1 imagery and ice drift sampling from the radar imagery.

Generally speaking, the high resolution ice drift data from sequence of radar imagery provides a view of how sea ice cover behaves after the significant thinning at the end of this record -setting summer. The net divergence and vorticity are ~3% and -0.43 respectively. The ice cover is divergent with a rotation in the same sense as that of circulation pattern imparted by the persistent high sea level pressure pattern centered in the southern Beaufort Sea (Kwok and Cunningham, 2012). In addition, two distinct regimes of ice motion and deformation with differing characteristics that contributed to the observed mean: one poleward of 80°N and the other to the south. Poleward of 80°N,

we find a net convergence of more than 14% over the period that is a result of the strain rates associated with the response to on-shore wind and motion (Kwok and Cunningham, 2012). The divergence and drift of sea ice cover after an anomalously low extent can help explain the similarities of Arctic sea ice seasonal characteristics. The decreased stability by the water column and thus promoting overturning with warmer and deeper waters can affect the brine rejection interference with the ice cover. McPhee *et al*. (2005) suggest that confined zones of upwelling of the pycnocline associated with significant shear motion of sea ice may greatly enhance local ocean-to-ice heat transfer and thinning of the winter ice cover. Therefore, the relationship between sea ice extent variability with other environmental factors can be explored. In addition, in the anomaly analysis of this thesis, the deformation process plays an important role in influencing the sea ice cover in the following years. Also, in analyzing similar seasonal characteristics across the Arctic region, the sea ice cover divergence would help in explaining these phenomena.

The causes of Arctic sea ice coverage decline have gain much research since the last decade. In paper "*Recent changes of Arctic multiyear sea ice coverage and the likely causes*" by Polyakov *et al.* (2012), the multiyear Arctic sea ice variability is studies and the causes of the variability are explored. Over the period 1979 to 2010, Arctic sea ice extent for September declined by 11% per decade and steeper for the last decade. Winter ice extents also declined but in a slower speed. The reason of the variability of Arctic multiyear sea ice is that a large fraction of MYI area loss is due to wind-driven export of sea ice through the straits connecting the Arctic Ocean with the subpolar basins (Polyakov *et al.*, 2012), among which the Fram Strait in the Greenland Sea contributed

the majority of Arctic sea ice export. The atmospheric thermodynamics and melt also contributed to the Arctic MYI variability. Warming in the Arctic since 1987 is evident in the time series of sea air temperature anomalies from three coastal stations. Strong warming in the central Arctic is also evident in fields from the ERA-Interim reanalysis. In addition to atmospheric thermodynamics, Arctic sea ice cover is affected by the thermal state of the Arctic Ocean. Observational and modeling results suggest that gradual warming of intermediate waters of Atlantic origin, the so-called Atlantic Water (AW) of the Arctic Ocean helped precondition the polar ice cover for the extreme ice loss observed in recent years (Polyakov *et al.*, 2012). In this paper, the possible causes of Arctic MYI variability are explored. Three environmental factors: wind-driven sea ice export, atmospheric thermodynamics, and the ocean heat contributed to the MYI decline during last 30 years. And it provides further research opportunities of quantifying the relationship between other environmental factors with sea ice variability.

In the paper "Wind-driven trends in Antarctic sea ice drift" by Holland and Kwok, (2012) through data of satellite tracked sea ice motion from 1992 to 2010, it reveals large and statistically significant trend in Antarctic sea ice drift can be linked to local winds in most sectors. The dynamic and thermodynamic processes in the internal ice pack are quantified and wind driven changes in ice advection are the dominant driver of ice concentration trend around much of West Antarctica. The strong correlation between observed ice motion and reanalysis winds in most of the sea ice zone implies that ice motion trends are largely caused by wind trends (Holland and Kwok, 2012). In conclusion, the fundamental importance of this paper is to rectify the failure of current

climate models to hindcast the recent increase of Antarctic sea ice. The large scale climate variability of the southern hemisphere is the substantial cause of the wind and ice changes in the Antarctic areas.

Stroeve *et al*. (2012) summarized the processes influencing the sea ice cover in 2011 in "*The Arctic's rapidly shrinking sea ice cover: a research synthesis*". In this study, the phenomenon that accelerated sea ice decline over the past decade was also noted. And from the paper "*Arctic sea ice decline: Faster than forecast"* by Stroeve *et al.* (2007) noted that September Arctic sea ice extent decline becomes steeper with time lower than any of the IPCC AR4 simulation. Stroeve *et al.* (2012) stated that although the statistical evidence for accelerating ice loss is only beginning to emerge, a couple of physical evidences of growing non-linear response to external climate forcing has already showed up. The linked processes through analysis of satellite derived sea ice extent, ice concentration, ice age, and atmospheric data are synthesized to provide evidence. Apart from several environmental factors raised by Polyakov *et al.* (2012), the summer ice albedo feedback and ice cover thickness are taken into consideration.

As the synthesis points out, Arctic air temperatures are rising in all seasons which leads to more open water in September and thinner ice cover in the coming spring. The summer ice albedo would also promote more open water in September. Warm atmosphere in autumn enhances the sea ice melting. And atmospheric patterns that favor ice retention are becoming less effective than they used to be (Stroeve *et al*., 2012). As Arctic continues to be warm in the most recent years, the probability of a sequence of unusually cold years in the Arctic that could bring recovery declines (Stroeve *et al*.,

2012).

Ocean forcing is another potential major player in affecting the sea ice retreat, which hasn't been fully understood. There are evidences showing warm Atlantic waters enter the Arctic Ocean through eastern Fram Strait and the Barents Sea and form an intermediate layer as they subduct below colder and less dense Arctic surface waters (Stroeve *et al*., 2012). However, it is still not clear to know how much heat it will bring to the surface to influence the ice cover. As with the Pacific water inflow, Shimada *et al*. (2006) noted a concurrence between increases in Pacific Surface Water temperature in the Arctic Ocean beginning in the late 1990s and the onset of sharp summer sea ice reductions in the Chukchi and Beaufort seas (Stroeve *et al*., 2012). An imbalance between winter ice growth and summer melt results acceleration of sea ice reduction in a large area. Jackson *et al*., (2010) focus on changes in the near surface temperature maximum in the Canada Basin. And a near surface halocline forms below the mixed layer which stores heat gained in summer. Compared with data in the early 1990s, the near surface temperature maximum warmed and expanded northward in shallower depth that increases ice melt for longer periods of time (Jackson *et al*., 2010).

In conclusion, after the 2007 record September sea ice minimum, it is widely speculated that Arctic Ocean is rapidly changing to seasonally ice free conditions. And the above-summarized processes worked together to support further ice loss, anomalous atmospheric forcing, and dramatic summer ice loss. However, because of the short time series of Arctic sea ice, the current apparent steepening downward trend may not be sustained (Stroeve *et al*., 2012). Also, because of the natural variability in the ice-ocean-

atmosphere system, sea ice recovery happened in 2007 and 2009 should come in the future.

1.4.3 Spatial-Temporal Variability of Northern Hemisphere Sea Ice Concentrations and Concurrent Atmospheric Teleconnections. M. Piwowar and C.P. Derksen, 2008

In this research, the authors explored the spatial and temporal variability of Arctic sea ice and its relationship with concurrent atmospheric teleconnections. The paper explores the relationship between global warming and polar ice cap variations.

- Introduction

Since the Earth's climate is always changing, the analysis of temperature records shows that the Earth has warmed an average of 0.6 degree Celsius over the past century (NRC, 2000). From 1980s and 1990s, there was an overall decrease in the Arctic sea ice extent of approximately 5% (Parkinson et al., 1999). The variability of sea ice can greatly impact the radiation reflection and absorption conditions. When the sea ice cover retreats, therefore, lower albedo ocean is exposed to the radiation, absorbing more energy. The ocean layers are thus heated, setting up a positive feedback loop further enhancing the warming of the polar regions (Piwowar, 08).

The primary research objective in this research is to find a better way of exploring the Arctic sea ice cap by comparing its spatial and temporal characteristics with the atmospheric circulation patterns. Also, the sea ice atmospheric teleconnections can be used to validate observed climate changes in the future.

The remote sensing sea ice concentration data was obtained from the National Ice and Snow Data Center (NSIDC), which were calculated from microwave brightness temperatures using the Bootstrap algorithm (Comiso et al., 1997). The passive microwave brightness temperatures were collected from SMMR and SSM/I sensors, which were on

the Nimbus-7 and DMSP series satellites (Piwowar, 2008). The atmospheric data were from the National Center for Environmental Prediction gridded data product from the National Center for Atmospheric Research) (Jenne, 1970). Additional Pacific Decadal Oscillation, and the Arctic Oscillation data were acquired from University of Washington.

- Methodology

The Principal Components Analysis is used to analyze the remote sensing and atmospheric data. The main objective of a PCA analysis is to enhance the separability, hence discriminability, of elemental features in the original data (Piwowar, 2008). The PCA analysis can help remove the inter-variable correlation, and create new channels which have no correlation between them.

In this research, the first five components will be analyzed to create a component image and corresponding loadings plot. The component image shows the spatial associations by each component. The component loadings are derived from the eigenvectors calculated during the PCA procedure, which can reveal the similarity between the PCA component and the original data ranging from -1 to +1. The larger the loadings are, the more similar the PCA component and its original data will be. The component image will be utilized to interpret where the component is correlated with the original data and when the spatial pattern of that component was strongest.

The processing procedure was conducted by analyzing the positive and negative mode of each PCA component by identifying their strongest positive ice anomalies. These anomalies can be found on the component image and compare with the original data image in both positive and negative model. Also, the atmospheric 500Z Composite

image went through a rotated PCA to assess the within group variability, which means the greater the similarity among the pentads, the greater the variance that will be explained by the leading atmospheric component and the greater the predictive potential of this analysis (Piwowar, 2008). From the 500Z Composite image, the sea ice extent anomalies can be implied. Also, by comparing the observed anomaly patterns with the AO indexes, the relationship between sea ice extent variability and the atmospheric teleconnections can be examined by providing the observational evidence for the linkages between the ice and the global atmospheric system.

From results of this research, the author captured the five largest temporally repeating ice concentration anomaly patterns in the Northern Hemisphere and identified their contemporary 500Z pressure patterns using the Principal Component Analysis. The strongest spatial-temporal ice concentration anomaly pattern over the 1980 to 1999 was the phase-shifted anomalies between the Greenland and Barents Seas and the Labrador Sea and in Davis Strait (Piwowar, 2008). Each PCA component has revealed a relationship with certain climatic phenomenon in the Arctic region, such as anomalies, oscillations, El Nino series, etc. However, only did a study of finding the linkages between the ice and the global atmospheric system, and did not perform a follow-up study to identify the cause and affect relationships. Therefore, all these results and conclusions were based on observations and any relationship between ice and atmospheric system were from sheer data coincidence, which statistically might be the ecological fallacy. However, this research does provided a benchmark of sea ice-atmospheric teleconnections for the two decades from 1980 to 1999, which gives the

follow-up researches to validate the actual ice and atmospheric conditions with the observations in this paper.

1.4.4 Sea ice response to an extreme negative phase of the Arctic Oscillation during winter 2009/2010. Julienne C. Stroeve, James Maslanik, Mark C. Serreze, Ignatius Rigor, Walter Meier, and Charles Fowler, 2010

Based on previous studies, there exists a relationship between Arctic Oscillation and the Arctic sea ice extent variability. The Arctic sea ice extent is very sensitive to changes in the atmospheric circulation, where in the Arctic region, the Arctic Oscillation is generally considered as an important component of this atmospheric variability.

In this research, the authors examined an extreme negative phase of Arctic Oscillation during winter 2009/2010, and analyzed the sea ice response. According to the research, the Arctic sea ice extent in September 2010 was the third lowest in the satellite record. This phenomenon reflects the differences in atmospheric circulation during the winter 2009/2010 compared to the mean anomaly pattern based on past negative AO winters, low ice volume at the start of the melt season, and summer melt of much of the multiyear ice that had been transported into the warm southerly reaches of the Beaufort and Chukchi seas (Stroeve, et al., 2011).

Temporal behavior of the AO has been implicated in the downward trend in summer sea ice extent evident in the passive microwave satellite record, 1979 to present [e.g., Rigor et al., 2002; Rigor and Wallace, 2004]. Also, traditionally defined as the leading stationary mode of northern hemisphere sea level pressure (SLP) variability based on Empirical Orthogonal Function (EOF) analysis, the AO can be interpreted as an exchange of atmospheric mass between the Arctic and the mid‐latitudes [Thompson and Wallace, 1998].

The author indicates that Arctic sea ice was motivated by an anticyclone centered over the northern Beaufort Sea, known as the Beaufort Sea High (BSH), and a trough of low pressure from the Icelandic Low northeastward into the Kara Sea. These surface winds drive the sea ice motion, and the Transpolar Drift Stream, indicating sea ice motion from the Siberian across the Arctic and into the North Atlantic through the Fram Strait. Otherwise when the winter AO is in its positive mode, the cyclone is counter clockwise and drives sea ice motion because of the weak BSH, which can be represented as decreased ice transport from the Beaufort Sea to the Chukchi Sea, and increased ice transport out of the Arctic Ocean through the Fram Strait (Rigor et al., 2002). In winter 2009/2010, the AO was strongly negative. According to established relationships, this phenomenon should favor the survival of ice through the 2010 melt season. However, the sea ice extent in summer 2010 ended up third lowest in the satellite record.

The author used monthly sea ice concentration from 1979 to 2010 obtained from the National Snow and Ice Data Center. Also, the sea ice motion data at 250km spatial resolution was utilized in this research. Fields of SLP and air temperature at T925 were obtained from the National Centers for Environmental Prediction/National Center for Atmospheric Research (NCEP/NCAR) reanalysis data (Kalnay et al., 1996). The author focuses on winter months (December through February), and derive anomalies of SIC, SLP and T925 relative to baseline means for 1979–2009. Changes in ice age and ice transport between October and March are also evaluated. Net transports were calculated through several gates: Western Beaufort, Eastern Beaufort, and western portion of the ocean area adjacent to the Canadian Archipelago, Transpolar Drift Stream and Fram

Strait (Stroeve et al., 2010). The weekly ice motions were used to calculate the velocity component. These were totaled across the gate and by time to get net areal transports by month.

Typically, the negative phase of the winter AO is associated with a strong Beaufort Gyre that sequesters sea ice in the Canada Basin where it can thicken and survive summer melt (e.g., Proshutinsky and Johnson, 1997). The winter of 2009/2010 had the most extreme negative phase of AO since 1951; however the September of 2010 sea ice extent ended up third lowest. The explanation of this phenomenon lies in the differences of atmospheric circulation compared to other normal negative AO events. The wind field may drive the older sea ice directly across the Beaufort into Chukchi Sea as opposed to curving northward in the western Beaufort. While lending credence to arguments that the character of the AO may be changing (e.g., Wang et al., 2009; Overland and Wang, 2010), one must also recognize that the AO only explains roughly 50% of the SLP variability (Rigor et al., 2002). Furthermore, ice conditions can be sensitive to slight shifts in the position of high and low pressure centers (e.g., Maslanik et al., 2007a) that are not captured by EOF loading patterns. In the 80s, wind associated with the strong Beaufort Gyre during negative AO winters would carry the older and thicker sea ice from the Canadian Arctic towards the Eurasian Arctic, and older and thicker ice in the Eurasian Arctic towards the Canadian and central Arctic (Stroeve et al., 2010).

1.4.5 Synthesis of Temporal Mixture Analysis

- *Temporal Mixture Analysis of Arctic Sea Ice Imagery: A New Approach for Monitoring Environmental Change. Joseph M. Piwowar, Derek R. Peddle, and Ellsworth F. LeDrew, 1998*

Temporal mixture analysis is a new change detection approach for spectral mixture analysis. Spectral mixture analysis utilizes the isolation of the main spectral contributions in each pixel to estimate the components in mixed pixels. Summing the fractional components of a set of spectral end members drives spectral mixture analysis (Piwowar, Peddle, & LeDrew, 1998). End members represent the most extreme or "pure" spectra for a certain land cover feature in the image. Images are assumed to contain a number of spectrally mixed data and then unmixed to find the fractional contribution of each of its end members.

In temporal mixture analysis, it is expected that an overview of the temporal characteristics of Arctic sea ice processes could be derived and subsequently used as a proxy of the long term normal (Piwowar, Peddle, & LeDrew, 1998).

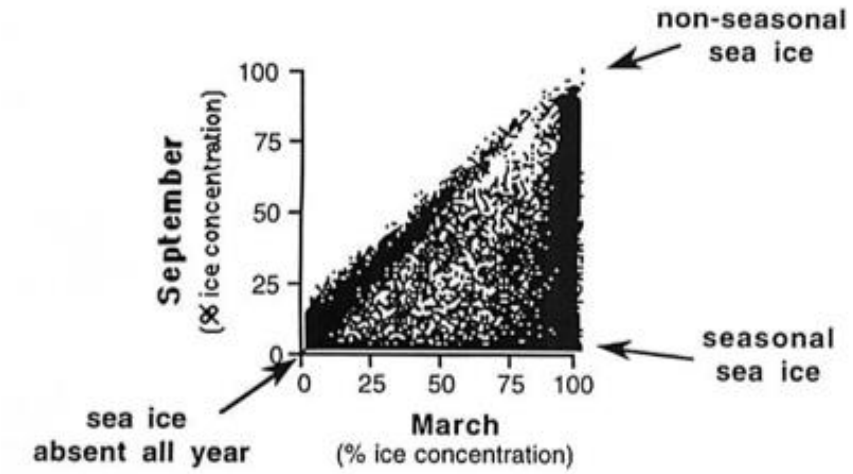

Figure 1.4 Endmember selection using scatterplot in TMA (Piwowar, Peddle, & LeDrew, 1998)

Three end members will be selected which are the non-seasonal sea ice, and open water. End members should be the "purest" spectra in the image. In spectral mixture analysis, this indicates pixels that represent a certain land cover component best or "purest". Whereas in the temporal mixture analysis, end members can be selected in a purification formula developed by Piwowar to derive pure end member spectra from a sampled set of image spectra.

$$EM_i = \begin{cases} \text{MAX}_i \text{ if } \text{MEAN}_i > \text{MEDIAN}_I \\ \text{MIN}_i \text{ if } \text{MEAN}_i < \text{MEDIAN}_I \end{cases} \quad (2)$$

where:

EM_i is the endmember spectral value for the ith spectral interval (where i is represented by *month* in the present context)

MAX_i is the maximum of all sampled spectral values at the ith spectral interval

MIN_i is the minimum of all sampled spectral values at the ith spectral interval

MEAN_i is the mean of all sampled spectral values at the ith spectral interval

MEDIAN_I is the median of all sampled spectral values at all spectral intervals

Figure 1.5 Endmember selection in each spectral (Piwowar, Peddle, & LeDrew, 1998)

Once the end members are selected, temporal mixture analysis can be conducted in a similar way with spectral mixture analysis. In temporal mixture analysis, pixel unmixing will be applied to pixels belong to different time while they share the same geographical location.

THE TWO-ENDMEMBER MODELING

The two end members: nonseasonal ice and seasonal sea ice were used to extract

their relative fractions from the SMMR data. Hudson and Baffin Bays and the Barents, Kara, and Chukchi Seas have very high ice concentrations in March and become ice free in September. In the RMS error image, lighter tones show areas where the model has a good fit with the data.

THE FOUR-ENDMEMBER MODELING

The RMS error image from the two-endmember model highlighted areas that were not well described by that model, suggesting the need for additional end members. New seasonal ice end members were added to the model by using an empirical approach. The spectrum for each end member was defined from a purified selection of temporal spectra extracted at locations with high RMS errors. Two end members were added to the original spectra.

The RMS error image generally reveals a well-fitting model with low errors, particularly in the non-seasonal sea ice zone, with some slightly higher errors observable in the areas covered by the seasonal end members. Thus, we can conclude that there are four basic temporal models that can be used to describe the annual cycle of the sea ice concentration for any point in the arctic.

TMA AS A TOOL FOR CHANGE ANALYSIS

If they were applied to annual subsets of the SMMR data, it was expected that the fractional images could serve as a historical record or summary describing the spatial distribution of ice for each year. Further, they could form the basis for inter-annual comparison by relating the spatial distributions of each end member.

This method is primarily used in this research to analyze the spatial distribution of different temporal signatures selected from different Arctic sub-regions. However, at that time, the author performed the two-endmember analysis and the four end-member analysis was based on the error image created in the two end-member analysis. However, if the endmembers could be selected from Arctic regions with different temporal signatures, the accuracy and representativeness of these endmembers can be greatly improved. Also, in the original paper, even in the second analysis, only four endmembers are selected to unmix the entire Arctic region, which are not enough to describe the various temporal characteristics across the Polar region. After the analysis is done, the error image is the sole source for error analysis, without comparing the fractional images with the actual temporal characteristics in different Arctic regions.

- *The derivation of an Arctic sea ice normal through temporal mixture analysis of satellite imagery, Joseph M. Piwowar, 2008, International Journal of Applied Earth Observation*

Later in 2008, Piwowar further improves the Temporal Mixture Analysis in the endmember selection and unmixing process to create a long-term baseline for the Arctic sea ice data.

Unlike the first paper of TMA, the improved TMA utilizes the minimum noise fraction (MNF) transform to determine the inherent dimensionality of the data, pixel purity index (PPI) to find the most temporally “pure” pixel, and similar unmix processes (Piwowar, 2008). The MNF function can greatly help to remove the redundant and correlation to ensure the effectiveness of TMA procedures. The principal component analysis is well acknowledged transformation to minimize inter-band correlation and

concentrate the information from the original data (Jensen, 2005). And MNF also embodied this concept. After that, the pixel purity index function is applied to find the most extreme representations of different temporal characteristics in the data. Endmembers will then be specified. There're a total of nine endmembers selected across the Arctic from the MNF and PPI functions.

The linear temporal unmixing process was similar with the 1997 TMA paper with endmember description and error analysis. But the temporal mixture images provide a different view with the endmember fraction images. It presents similar endmembers in one image with color compositions assigned to each endmember. These images provide a view of how the endmembers are distributed across the arctic region with their concentrations. In addition, in areas with compositions of different endmembers, the fraction of endmembers is displayed to give a numerical perspective of concentrations of different endmembers in a regional scale.

In the improved TMA process, the endmembers were statistically selected compared to manually select from various Arctic sub-regions for better accuracy and RMS error minimization. And it provides a better view in analyzing the compositions of endmembers in some regional areas. However, the larger scale endmember composition image is also of great interest to researchers and a comprehensive endmember distribution and composition image of the entire Arctic region would greatly help to find similar seasonal variability in different Arctic areas as well as find the evolution of seasonal variability through the 30-year time series.

1.5 Research Rationale of Arctic Sea Ice Variability and Anomalies

Numerous studies have been reported on the study of the sea ice extent variability and anomalies during the past 50 years. From these studies, the anomalies of the Arctic sea ice's spatial and temporal structures provide great value in understanding the processes and mechanisms of sea ice variability and insights in estimating sea ice future trend. As the climate or the regional ecosystem changes, the Arctic sea ice is most likely to change accordingly. In the first literature review, Parkinson and Cavalieri did a research of the Arctic sea ice extent variability and trend over the past few decades, and concluded that sea ice extent is declining at 3.7% per decade in the Arctic region scale. While in different sub-regions, the decline rate varies from 1.5% to 9.5% per decade.

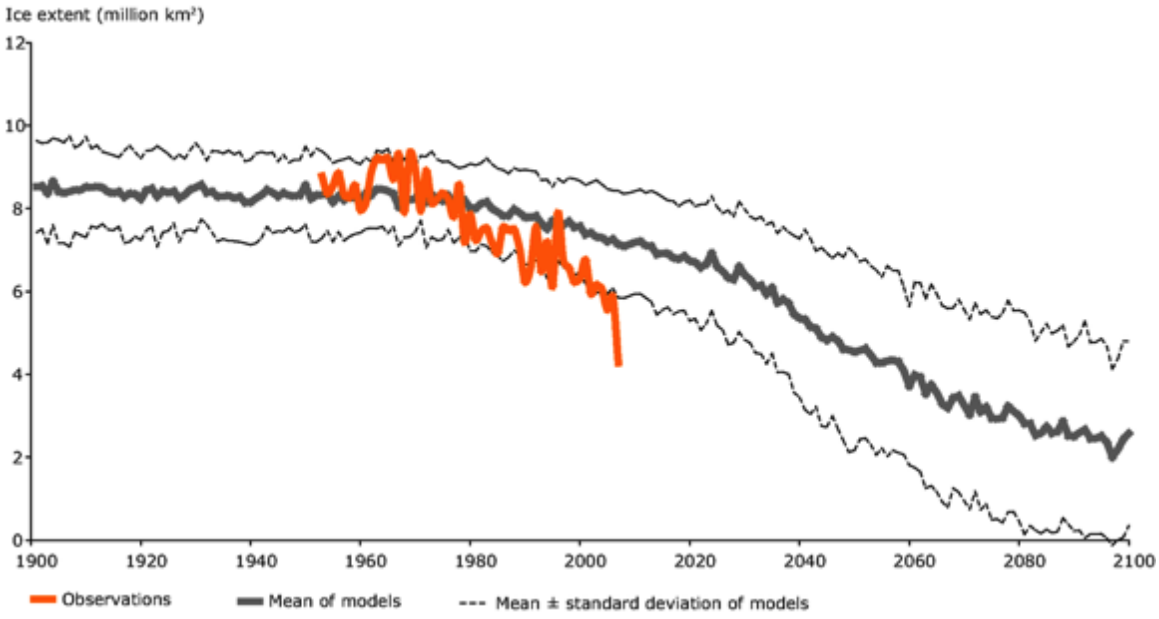

Figure 1.6 Observed and IPCC Model projected Arctic sea ice from 1900 to 2100 (European Environment Agency, 2011)

However, based on previous long-term time series analysis of Arctic sea ice extent variability and its comparison with previously generated forecast models, the

Arctic sea ice extent is decreasing faster than estimated (Figure 1.6) (Stroeve et al., 2012; Holland and Kwok (2012); Comiso et al., 2008). Therefore, the emerging changes would show up as anomalies. And through a period of time, these anomalies would probably be the beginning of a new phase of sea ice decline. Thus the study of Arctic sea ice anomalies can provide useful clue in estimating future trend in the development of the cyrosphere ecosystem. Moreover, by relating these anomalies with a number of Arctic climate phenomena can help explain the air/sea and air/ice/sea interaction processes and mechanisms.

Generally speaking, the anomaly analysis of Arctic sea ice extent focuses on the spatial structures and scales of anomalies in previous researches. For instance, in the second literature review, Mysak and Manak studied the Arctic sea ice variability and anomalies in seven different sub-regions in the Arctic region. At first, the seasonal cycles of sea ice extent variability were found. And the seasonal variation can be used to analyze the freeze and melt time of the year. In addition, the speed of sea ice freeze and melt also provides useful data in interpreting the climate condition of that particular year. Within different sub-regions, the seasonal variation pattern varies accordingly. But the sea ice extent variability or trend in the long term needs more discussion. Also, too few sub-regions were classified and analyzed. The sea ice extent anomalies were studied through various time series analysis focusing on the fluctuations of areal sea ice extent. The deviations from the usual seasonal cycle would represent the structure of high-latitude climatic fluctuations on time-scales of years to decades. But the anomalies were diagnosed by comparing the individual monthly sea ice data with the short or long term

average. From the deviation chart between monthly sea ice data and average, the overall fluctuation and approximate decadal cycle of sea ice variability can be perceived. From the anomaly distribution, the amplitude and scale of anomaly in different sub-regions can be classified. Moreover, the multiyear variation trend of Arctic sea ice extent happened to coincide with other environmental data, such as the atmosphere air temperature, sea surface temperature, and sea level pressure. In other researches, for example, Torrence and Compo, 1998, the wavelet analysis was utilized to model the long term sea ice extent variation compared to the windowed Fourier transform, and deal with edge effects due to finite length time series. The wavelet analysis provides much more detailed insight information for analyzing time series with different time scales and changes in variance. In addition, anomalies classified from the wavelet models are more accurate than the deviation-from-mean method.

The limitation of the previous anomaly researches is obvious that anomalies must be inspected in a pre-designated spatial scale, and this scale is usually too large for a single temporal signature to describe. Hence, no applicable method to combine the spatial and temporal anomaly analysis was introduced in previous sea ice extent anomaly researches. Fortunately, in the fifth literature review, Piwowar and LeDrew developed the temporal mixture analysis, which can separate the temporal features of the remote sensing sea ice image by selected temporal signatures. Although, the original TMA paper only introduced the two-endmember and four-endmember unmix analysis, its concept of unmixing the spatial distribution of different temporal signatures can be implemented by introducing more and carefully selected endmembers. With the improved TMA, the

spatial and temporal characteristics of sea ice extent anomalies can be found, which none of the previous sea ice anomaly researches achieved.

Apart from the variability of Arctic sea ice extent, its relationship with other environmental elements is also a big research interest. The interaction between Arctic sea ice and atmosphere has gained attention decades ago, and the third and fourth literature review indicated severe atmospheric impact to Arctic sea ice variability. These articles provide a useful insight in explaining the anomalies. The variability of Arctic sea ice reflects the overall ecosystem in the Arctic region, and can be used as an index for explaining other environmental phenomena. Moreover, the mechanisms between different cyrosphere environmental elements, such as sea ice, atmosphere, ocean, solar radiation, haven't been thoroughly understood. Hence future research could continue on this topic, especially in the global scale. In addition, the purpose of studying the past Arctic sea ice extent variability history is to construct a better model for forecasting its trend and variability in the future.

1.6 RESEARCH OBJECTIVE

a. What are the long-term sea ice extent variability pattern and trend in entire Arctic region, as well as different subregion? What is the sea ice extent in recent years compared to the 1980s?
b. What are the significant spatial/temporal Arctic sea ice anomalies in the Arctic region from 1979 to 2006?

CHAPTER TWO

METHODOLOGY

In this chapter, the research methodology is introduced to analyze the general variability and trend of Arctic sea ice extent during the past decades. In addition, based on studying its variability, the spatial and temporal anomalies of Arctic sea ice extent in the time series will be detected and analyzed. The structure of this chapter is as follows. First, the data used in this research is introduced as well as the environment situations of the study area. Second, the general sea ice variability and trend analysis utilizing the Sen's Slope. Third, the sea ice extent ranking charts are created to reveal years with unusual sea ice extent and their potential inner relationships. Last, the Temporal Mixture Analysis is applied to further subdivide each subregion to pixels and find sea ice extent anomalies within each subregion.

2.1 DATA DESCRIPTION

The data set is from the National Snow and Ice Data Center (NSIDC) using measurements from the Scanning Multichannel Microwave Radiometer (SMMR) on the Nimbus-7 satellite and from three Special Sensor Microwave/Imager (SSM/I) sensors (Comiso, J. 1999). The most recent version of sea ice concentration data, version 2, is used released in September 2007. The second version of sea ice concentration data has tie-points adjusted to be consistent with the AMSR-E Bootstrap algorithm (Comiso, J. 1999). The time series generated using the AMSR-E Bootstrap algorithm consists of SMMR data from November 1978 to August 1987, and SSM/I data from July 1987 to 2006 (Comiso, J. 1999).

The data set coverage includes the northern and southern Polar Regions. In this research, only the northern Polar Regions are included. Through SSM/I instrument coverage is global, the circular sectors centered over the north pole, 311 km in radius, located poleward of 87.2°, are never measured due to orbit inclination. The 50° scan pattern provided a swath width of 780 km at the Earth's surface. The spatial resolutions at the various frequencies ranged from approximately 27 km at 37 GHz to 148 km at 6.6 GHz. Same situation with the SMMR instrument which has 611 km in radius located poleward of 84.5°.

The bootstrap sea ice concentration data are provided at a resolution of 25km with a temporal coverage from October 26 1978 to December 31 2006 at the time when this research starts in 2010. SMMR data were collected every other day. Monthly means are generated by averaging all available files for each individual month, excluding pixels of missing data (Comiso, J. 1999). Ice concentrations are provided for each day and as monthly means. Monthly mean files are generated by averaging all available daily files for each individual month, excluding pixels of missing data (Comiso, J. 1999).

The bootstrap algorithm used in creating the sea ice concentration data uses basic radiative transfer equations and takes advantage of unique multichannel distributions of sea ice emissivity (Cosmiso and Sullivan, 1986). In order to derive sea ice concentration, the bootstrap algorithm only utilizes two microwave channels, but other additional channels may be required to mask the open ocean (Comiso, 1992). The bootstrap algorithm has several advantages in creating sea ice concentration data, for example, it provides the best resolution from the set of channels, provide better accuracies suitable

for the Arctic region where the percentage of open water is usually less than 5% in winter, it considered the surface temperature variations, the slope of line used to find the tie point for consolidated ice is consistently close 1.0 in every winter data set from either SMMR or SSM/I (Comiso, 1992).

However, the uncertainties of the bootstrap algorithm are mainly from the changing emissive surfaces. For example, errors are higher in seasonal ice region than in the central Arctic because of higher standard deviations of consolidated ice. In addition, when the leads open up in winter, the open water exposed to the cold atmosphere will quickly freeze to grease ice then metamorphoses to nilas, young ice, and then first year ice with snow cover (Comiso, 1992), causing emissivity of the surface change considerably (Grenfell and Comiso, 1986). These situations have not been accounted for in the sea ice concentration algorithm. Also, in spring and summer when the surface of multiyear ice starts to melt, the emissivity of thick ice changes accordingly. Despite all adjustments, the error remains substantial and can be larger than 20% due to spatial variations in melt and effects of meltponding (Comiso, 1992). Apart from the uncertainties in sea ice concentration measurement, validation of satellite ice concentration data is difficult because of the limited coverage of field data compared with large area captured by satellite sensors. Data files are stored in the original Goddard Space Flight Center flat binary two-byte integer format, and are scaled by a factor of 10 in a 304*448 dimension (Comiso, J. 1999). A mask image is provided to retrieve geographical information for these gridded images. By referring the location in the data matrix to the mask image, the coordinates of each pixel can be retrieved.

2.2 Study Area Description

The Arctic Ocean is located on the north end of the earth, surrounded by the Europe, Asia, and North America continent (Michael Pidwirny 2006). The Arctic Ocean covers area of approximately 15 million km^2. The Arctic Ocean is partly covered by sea ice throughout the year. In winter, the Arctic Ocean is almost completely covered by sea ice.

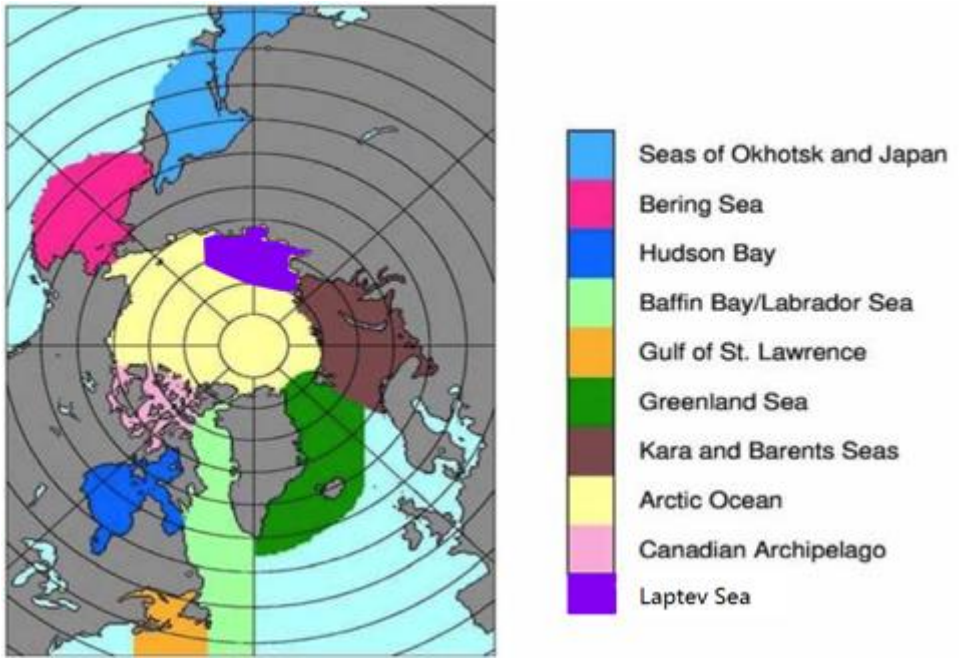

Figure 2.1 Sea Ice sub-regions (Parkinson and Cavalieri, 2008)

For scale studies, the Arctic region is usually divided into nine sections, which is introduced by Parkinson and Cavalieri (2008): the seas of Okhotsk and Japan, the Bering Sea, Hudson Bay, Baffin Bay/Labrador Sea, the Gulf of St. Lawrence, the Greenland Sea, the Kara and Barents seas, the Arctic Ocean, and the Canadian Archipelago. The classification scheme of the subregion was firstly introduced by Parkinson, (1999), which is based on previous empirical data of sea ice variability and dynamics research. These

sub-regions are considered to have their own and unique temporal variability based on previous observations. Also, these sub-regions contain the majority of the sea ice coverage in the northern hemisphere and the sea ice-ocean-atmosphere dynamics are more similar within a sub-region than other areas based on previous researches. Sea ice extents for each year can be examined within each Arctic section. Besides, sea ice extents are measured for both winter and summer time for both maximum and minimum sea ice extent analysis to find the anomalies, freeze, and melt patterns.

2.3 DATA PROCESSING

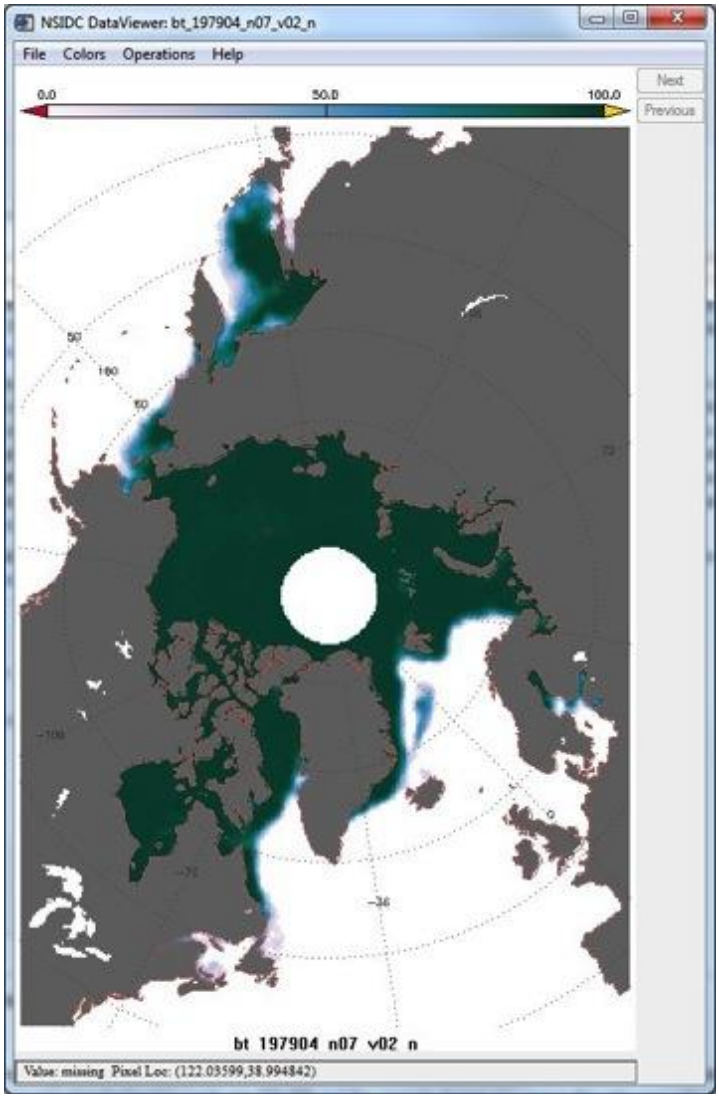

Figure 2.2 Sea ice concentration image

The remote sensing image raw data downloaded from NSIDC is in a flat binary data in a matrix with a 304*448 dimension (Figure 2.2). However these raw data have no geographical information, each number in this matrix represents the sea ice concentration of a 25*25 km^2 area, which is a pixel in the remote sensing image. Fortunately, the pixel coordinates can be retrieved from the mask image. Hence the nine sub-regions in Arctic

can be identified by strict edge segmenting the columns and rows in the matrix.

837 887 924 971 971 992 980 975 974 964 980 965 936 972 968 986

982 987 978 984 988 965 980 972 981 985 992 988 989 983 993 986

985 984 982 983 982 981 974 990 982 983 978 977 983 987 981 992

985 979 978 982 981 969 966 972 977 984 973 976 980 970 972 977

980 984 980 982 977 973 973 969 968 972 980 951 887 877 928 936

1200 1200 1200 969 1200 951 956 980 980 980 975 982 982 961 937 863

791 710 706 706 678 . . . . .

Figure 2.3 Sea ice concentration data matrix

The segmenting process will firstly retrieve the corner coordinates of each subregion. After then, these coordinates will be projected to the mask image. From the mask image, the row and column number of a certain coordinate or the digital number (DN) can be determined. As there is not fuzzy edge process introduced in this research, any edge pixels will be divided evenly to its adjacent sub-regions.

After the monthly sea ice extent data of the entire Arctic Region is divided into 9 sub-regions, sea ice extents in these sub-regions may be extracted individually on a monthly basis. Therefore, monthly sea ice extent data are available for the whole Arctic region and these sub-regions as well. Later, the variability of monthly sea ice extents from 1979 to 2006 can be displayed chronologically for each subregion and the entire Arctic Region.

2.4 TREND ESTIMATION USING SEN'S SLOPE

In order to reveal the long-term sea ice variation trend, Sen's Slope Estimator is introduced for the trend estimation analysis of the residuals between individual monthly sea ice extent and 28-year average of the particular month. However, the long term of sea ice extent variability pattern has large amounts of uncertainties in determining the most suitable statistical model to describe the sea ice variability trend mathematically. The 1979-2006 period of sea ice variability, which is of interest in this research, is only part of the long-term time series. As the Arctic sea ice is always changing in either increase or decrease phase, remote sensing captured sea ice concentration data since 1978 could possibly be one of the increase or decrease phase, even both.

From Figure 1.6, the Arctic sea ice extent trend forms a nonlinear decline which shows that sea ice extents before year 2000 are still within the model estimated range, but after 2000, sea ice extents start to fell below the minimum confidence level threshold. Therefore, theoretically one slope estimation that describes the long-term sea ice variability trend is not the most precise and ideal given the small period of satellite remotely sensed data. A more suitable method is to divide the sea ice variability into two periods, one is the "normal" sea ice trend that coincides with the model estimates, and the other one is the intensified melting period. A big problem from doing so is the difficulty in defining the breakpoint that separates the two periods. In addition, many related articles in Arctic sea ice extent trend analysis computed slopes to give an overall impression of the sea ice extent variability in the recent decades. In this research, given the small sample size and the research methods from other journal articles, the Sen's

Slope is used to find the slope of the sea ice extent variability.

Test Procedure	Applicability	Notes	Reference(s)
Graphical Methods	Visual estimate of trend presence/absence	No quantifiable results	
Linear Regression	Provides an estimate of slope, confidence interval, and quantifies goodness of fit	Allows quantified estimate of influence of multiple independent variables Does not handle missing data Does not handle BD measurements May be greatly affected by outliers and cyclic data	
Box-Jenkins Model	Test for trends in long term, regularly spaced data	Requires large data set Requires constant temporal spacing of data sets	Box and Jenkins (1976)
Mann-Kendall	Yes/No test for existence slope	Non-parametric test Allows missing data Allows reporting of levels BD Not affected by gross data errors and outliers	Mann (1945) Kendall (1980)
Sen's Method	Estimates value and confidence interval for slope	Allows missing data Makes no assumptions on distribution of data Not affected by gross data errors and outliers	Sen (1968) Thiel (1950)

Figure 2.4 Comparisons of Methods for Estimating Trends (Brauner, 1997)

Apart from Sen's Slope Estimator, there are a number of other methods to estimate and/or quantify the trends of a dataset, their applicability and performances vary when applied on different datasets. In Figure 2.4, five trend estimation procedures are listed, namely, the graphical methods using visual estimate of trend, linear regression, Box-Jenkins Model, Man-Kendall Model, and Sen's Slope Method. The visual estimate method apparently does not meet the requirements in this research because of its non-quantifiable results. The linear regression method does provide an estimate of slope, however, its incapability in handling missing data and may be greatly influenced by outliers and cyclic data makes it unsuitable for analyzing the Arctic sea ice extent time series data which has considerable amount of outliers and seasonal/oscillation cyclic pattern. The Box-Jenkins Model is most suited for analyzing long-term and regularly spaced data, which is suitable for estimating the long-term monthly sea ice data. However,

because of the small dataset in this research, it is unsuitable to utilize the Box-Jenkins Model because it requires large data set (Box and Jenkins, 1976). The Mann-Kendall method is not an estimate of a slope, instead it evaluate an existing slope by providing a yes/no test (Kendall, 1980). Since in this research, it is essential to provide trend estimation and after that a slope estimation validation can be performed. The last one is Sen's Slope method which is most suitable for this research with its virtues in allowing missing, making no assumptions on data distribution, and not affected by outliers (Sen, 1968). The introduction of the Sen's Slope Estimator is as follows.

The Sen's Slope Estimator is a robust linear regression analysis which chooses the median slope among all lines through pairs of two-dimensional sample points (Wilcox, Rand R. 2001). In this research, the entire dataset will be used as the test sample with 95% confidence level. Its efficiency in computing and insensitivity to outliers make it more accurate than simple linear regression analysis, which makes it very suitable for this research. Also, the Sen's Slope is widely used in environmental science researches because of its nonparametric technique, which is suitable for time series analysis compared with parametric techniques. Sen's Slope is defined by Theil, (1950), which takes a set of two dimensional points, measures the median of the slopes determined by all pairs of sampled points. Once the slope is determined, a line is drawn through the sample points by setting the intercept to be the median (Rousseeuw, Peter J.; Leroy, Annick M. 2003). The confidence interval of Sen's Slope can be determined as the interval of the 95% of the slopes of lines determined by pairs of points.

In non-parametric statistics, any model or interpretation does not depend on the

parameters or rely on data, which is generally regarded as a robust analysis. Non-parametric statistics, unlike parametric statistics, does not rely on any assumptions that the sample data are drawn from certain probability distribution, indicating less assumptions and parameters compared to parametric statistics (Corder, G.W. & Foreman, D.I. 2009). In this research, since the size of the data is small with 28*12 monthly deviations, there is no need for a test sample data collection and analysis.

The Sen's Slope can be applied in Matlab based on the code developed by Cathy Akritas, 2004, with 95% confidence interval to each subregion and the north hemisphere. The computation algorithm follows the same concept from Sen and Theil that compute slopes for every pair of points and find the medium slope with 95% confidence level.

2.5 SEA ICE EXTENT RANKING

In previous sea ice extent variability and anomalies analysis, sea ice extents are usually displayed according to their temporal order and try to find and analyze anomalies from the wave crests or troughs. A number of journal articles focused on identifying anomalies statistically. In paper "*Arctic Sea Ice Extent and Anomalies, 1953-1984*" by Mysak, sea ice extent data in different sub-regions are compared with each other yearly and seasonally. In addition, the sea ice extent anomalies are statistically detected by comparing individual monthly/yearly data with long-term averages. But this method lacks rigid statistical validation of anomalies. However, in some other journal articles which anomalies are detected in a more sophisticated method, the long term declining nature of Arctic sea ice is not considered. In this research, sea ice extents are ranked according to their actual extents from largest to smallest regardless of their temporal

order. Sea ice extents of close by years are also more likely to be close to each other in the sea ice extent ranking. Therefore, any different year that happened to be among the cluster of other continuous years can be identified as anomalies.

Compared with other types of time series analysis, the sea ice extent ranking analysis provides a different view of the sea ice extent variability and anomalies as well as observing the sea ice extent change with the North Atlantic Oscillation. By performing this ranking analysis, it breaks the temporal autocorrelation pattern in other conventional time series and makes anomaly detection easier and more effective, which no longer requires complicated statistical validation of anomalies and the ranking analysis won't be affected by the sea ice's declining nature because anomalies are detected by colors regardless of the long-term trend. In addition, the long-term trend of sea ice variability would also be easily identified which would otherwise be considered as normal fluctuations in conventional time series analysis.

The data of the Arctic region are ranked using monthly sea ice extent data from January 1979 to December 2006. In this sea ice extent ranking, the yearly sea ice extent (Jan to Dec) is ranked from largest to smallest according to years. And the colors of the bars are used to differentiate the decades to help identify different periods.

This color differentiation of years uses a transitional color scale to present the clustering years. The color transition is from blue to red, and through each year, its color slightly changes. Any sea ice extent anomalies can be identified in the case of a different color among cluster bars of similar colors. Apart from anomalies detection, the clustering of years in the ranking chart can also provide a view of the cold/warm conditions in the

multiyear scale. And through these climate conditions in different sub-regions, the relationship between sea ice extent variation and North Atlantic Oscillation can be explored. In addition, the sea ice extent ranking in different sub-regions provides an insight view of the similarities and differences of climate in adjacent areas.

2.6 Application of Temporal Mixture Analysis for Anomaly Analysis

Temporal Mixture Analysis, developed by Piwowar and LeDrew, (1998) is utilized to create the fractional images, and it's the only technique available nowadays to reveal the spatial distribution of temporal features across the different sub-. The TMA can unmix each pixel into a composition of several endmembers as the temporal characteristics of a particular subregion. Usually, an endmember is considered to have a large number of high concentration pixels in the subregion that it's been selected from. However, as TMA strictly performs the unmixing process based on endmembers, which can reveal pixels that have a high fraction of temporal characteristics of endmembers selected in other areas instead of its own subregion, therefore, TMA can help to analyze the temporal variation of sea ice extent within a subregion, which is very useful in some large sub-regions such as the Greenland Sea and Baffin Bay. Moreover, the clustering of endmembers can be not only found in its selection subregion, it can also be found in other sub-regions. This phenomenon is greatly useful in identifying the North Atlantic Oscillation and climate similarities among different Arctic regions. After the unmixing process, an error image is created to help identify the temporal anomalies within sub-regions, which might not be found in the sea ice extent ranking analysis. The scales of the sea ice extent variability and ranking analysis are the sub-regions while the TMA narrows

the scale of analysis to each pixel, which can reveal the temporal variability and anomalies within each subregion.

The temporal mixture analysis (TMA) is derived from the Spectral Mixture Analysis (SMA). Spectral mixture analysis is a procedure that attempts to extract the fractional radiance components from the pixels in an image. Spectral mixture analysis has been used extensively for the analysis of hyperspectral data from imaging spectrometers where conventional image analysis techniques have been shown to be inadequate (Boardman, 1989; Adams et al., 1993; Harsanyi et al., 1994).

The dataset preparation for TMA is different than SMA. In SMA, a remote sensing image with multiple bands would facilitate the endmember unmixing process, while in TMA, the monthly sea ice extent data from 1979-2006 will be averaged by month to create a 12-month summary of mean sea ice concentrations.

Similar to spectral mixture analysis, TMA also has endmembers, which can be used to identify the fractional contributions of each pixel. In TMA, endmembers are used to represent the time series or seasonal variability of sea ice concentration.

Endmembers, as is the case with spectral mixture analysis, represent the most extreme examples. In time series analysis, the "purest" spectra can be thought of having one of the three fundamental temporal characteristics: ice absent all year long; sea ice varies through the season; perennially present sea ice. The pure non-seasonal sea ice is defined as 100% sea ice concentration all year round. Pure absent sea ice is defined as 0% ice concentration all year. Pure seasonal ice is ideally defined as 100% ice concentration in winter and 0% ice concentration in summer.

In this research, endmembers will be selected within each Arctic subregion through the scatterplot between March and September sea ice concentrations. In Figure 2.4(a), if sea ice concentration in both March and September are 0%, it means open water. However, if in both March and September are 100%, it means non-seasonal sea ice. An endmember will be selected in this scatterplot in the lower right corner, which has 0% sea ice concentration in March, but has 100% in September.

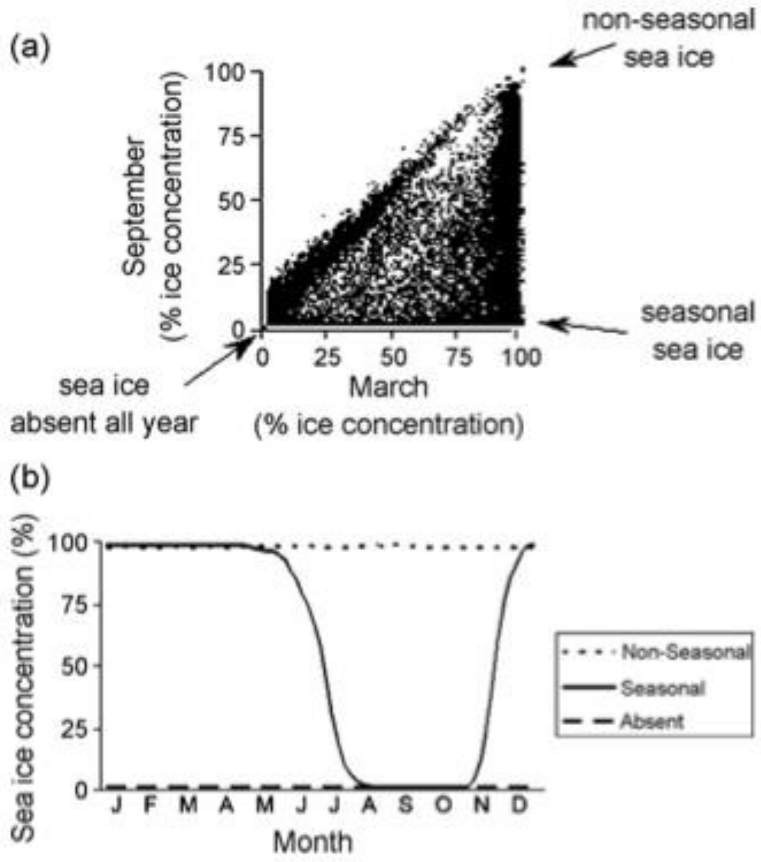

Figure 2.5 (a) TMA endmember selection using scatterplot of sea ice concentration in September vs. March. (b) the temporal characteristics of a endmember presents (Piwowar, 1997)

In each subregion, according to the sea ice concentration scatter plot, a seasonal sea ice endmember will be selected for the unmixing process. And the sea ice absent and

non-seasonal endmembers will not be selected from each subregion, but manually set to default that 0% sea ice concentration as absent sea ice endmembers, and 100% sea ice concentration as non-seasonal sea ice endmembers.

The unmixing model that will be used to determine the temporal feature fractions follows the same algorithm with spectral mixture analysis. For each pixel in the image a linear mixing model is defined as (after Adams et al., 1993):

$$DN = (EM1 * F1) + (EM2 * F2) + ... +(EMn * Fn) + e$$

Where the DN is the pixel number, EM*i* is the spectrum of the *i*th endmember of a total of n endmembers, Fi is the fractional contribution of the *i*th endmember in this particular pixel and e is the residuals. Given the pixel number and endmembers, the fractional contribution of each endmember can be calculated by reverting this equation.

Therefore, the fractional contribution of a certain endmember can be represented as a fraction image. In temporal mixture analysis, it assumes that each pixel is a mixture of several time series; hence each pixel can be represented by several endmembers. For example in spectral mixture analysis, a pixel in the Arctic Ocean can be spatially unmixed as 20% of sea ice endmember selected in the Baffin Bay and 80% of sea ice endmember selected in the Greenland Sea. While in temporal mixture analysis, this pixel can be unmixed as 20% of seasonal sea ice and 80% of non-seasonal sea ice. By revealing the temporal component fraction of each pixel, the sea ice variability attribute of each pixel can be examined. For example, a pixel in the Canadian Archipelago can be unmixed in temporal mixture analysis to be 70% seasonal sea ice and 30% and non-seasonal ice.

In addition, the temporal mixture analysis not only can reveal the seasonal versus non-seasonal sea ice, but it also can reveal the seasonal pattern in different sub-regions. According to the North Atlantic Oscillation, sea ice extent growth generally behaves in a shifting pattern between the eastern and western hemisphere. Hence, the sea ice variability can be quite different between these two regions. In other words, each subregion may have its own temporal variability pattern. For example, the sea ice in the Bering Sea usually has a complete melt in summer and will freeze again in winter; while the sea ice in the Hudson Bay does not complete melt in summer, but has approximately 100000 km2 ice left. Temporal mixture analysis can be utilized to unmix a pixel to show the temporal variability pattern for a number of different sub-regions, which is of great value to reveal the sea ice interactions among these sub-regions.

CHAPTER THREE

RESULTS

The results of this research will be presented in the following sections: sea ice extent variability charts, sea ice extent ranking, and the temporal mixture analysis.

3.1 GENERAL ARCTIC AND REGIONAL SEA ICE VARIABILITY

In the general arctic and regional sea ice variability analysis, the sea ice extent variability from 1978 to 2006 will be presented in the graphs below generated from the monthly sea ice concentration data retrieved from NSIDC. In these graphs, for example, monthly average chart in Figure 3.1, the seasonal variation of sea ice extent can be identified clearly, but the long-term sea ice extent variability trend wasn't identical. In addition, the averages of each individual month are calculated and created a general seasonal sea ice variation chart. Therefore, the seasonal sea ice variation chart will provide an overview of the sea ice freeze and melt pattern of the particular region.

Moreover, a Sen's Slope Estimator will be applied to the monthly deviation data. The Sen's Slope Estimator is used to analyze the subtraction between individual monthly sea ice data and the average of this particular month from 1979 to 2006. From the monthly deviation data and the trend estimation, the long-term sea ice extent variation trend can be identified. Besides, sea ice anomalies can also be seen from the regression line.

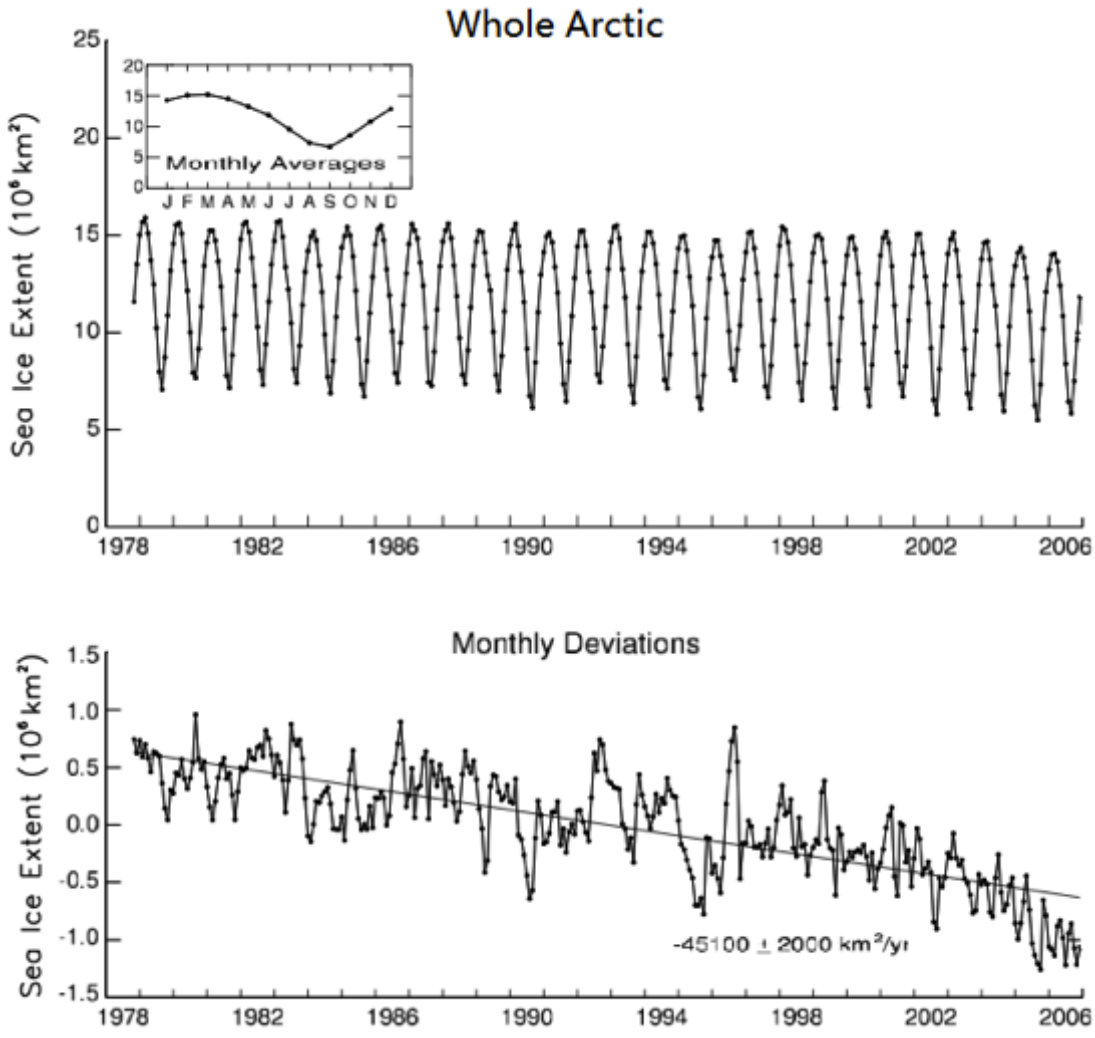

Figure 3.1 Monthly Sea Ice Extent Graph of the Whole Arctic, and Monthly Deviation Trend Estimation

From 1979 to 2006, the Arctic sea ice extent has exhibited seasonal changes (Figure 3.1). Traditional seasonal sea ice usually has maximum coverage in March and melts up to its minimum in September. In the monthly average sea ice extent figure (the upper graph of Figure 3.1) of the whole Arctic from 1979 to 2006, it does not show a clear sign of sea ice extent trend. The entire Arctic sea ice extent usually has a maximum of 15 million km2 while in summer; the entire Arctic sea ice extent decreases to 6 million

km squared. But in the sea in the monthly deviations chart, the 30-year monthly sea ice extent average is calculated and compared with each monthly data. In this chart, linear trend estimation indicates a trend of sea ice extent decrease despite of several anomalies. From 1979 to 1995, the sea ice extent monthly deviations are above the 30-year average. Especially after 2000, the majority of monthly deviations are below the 30-year average. The monthly deviation decline rate is -45000±2000 km^2 per year. But in the long-term trend analysis, this decline rate is not clear enough to conclude that sea ice extent decreased from 1979 to 2006.

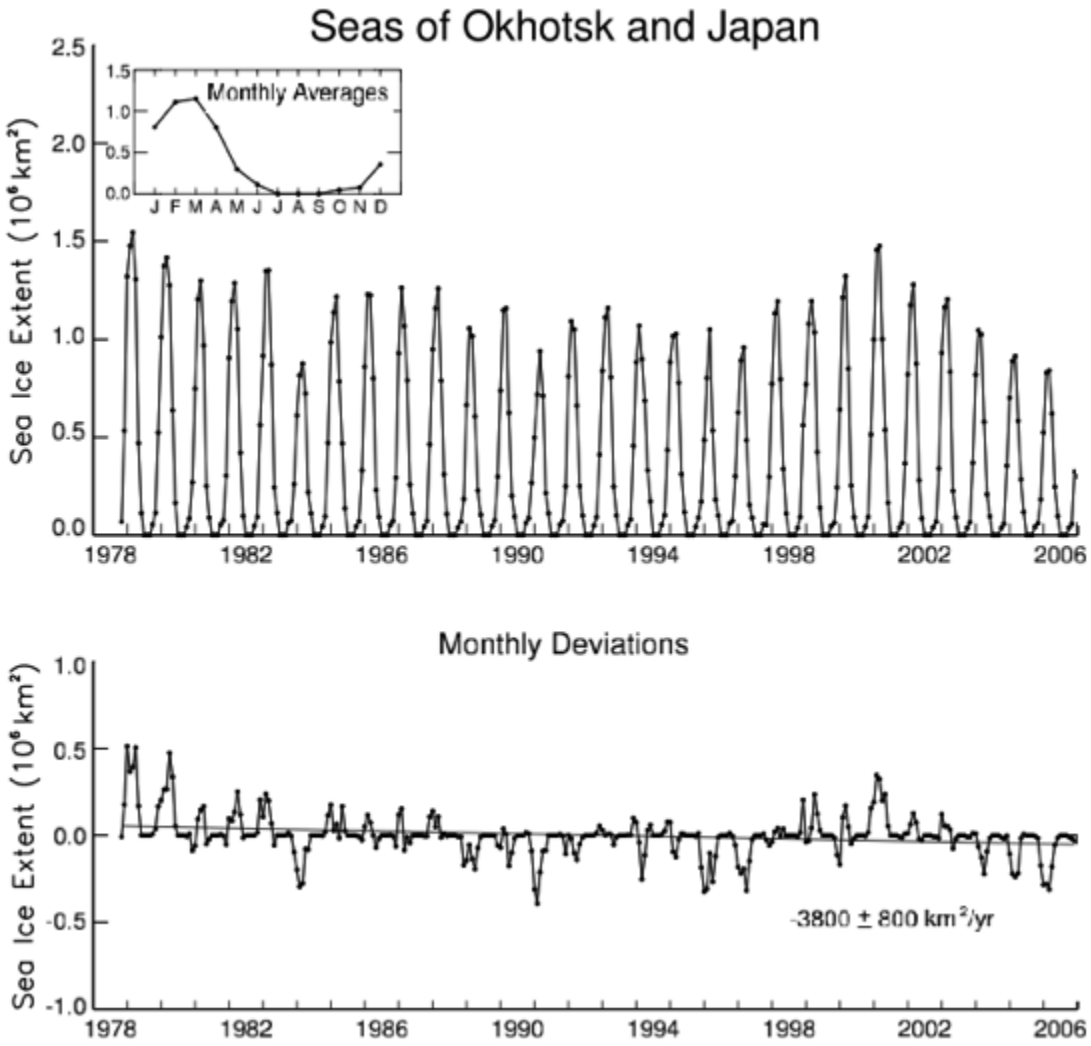

Figure 3.2 Monthly Sea Ice Extent Graph of the Seas of Okhotsk and Japan, and Monthly Deviation Trend Estimation

Sea ice extent variability in the Seas of Okhotsk and Japan (Figure 3.2) freezes up to 1.6 million km2 in winter and usually completely melts in summer with a minimum of 0 sea ice coverage. And the monthly deviation shows a decline trend of -3800 ± 800 km2 per year. The slope of this subregion is very close to zero, but in the 95% confidence level, it still indicates a positive decline trend.

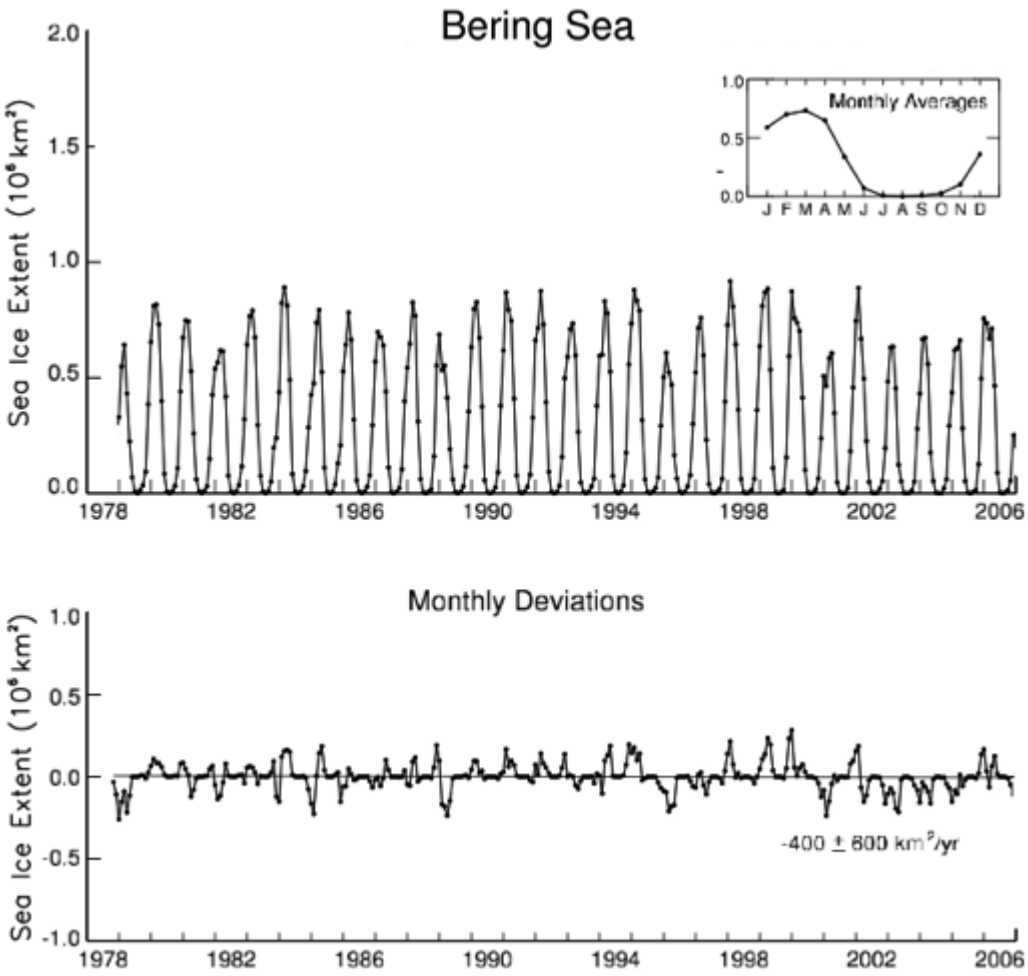

Figure 3.3 Monthly Sea Ice Extent Graph of the Bering Sea, and Monthly Deviation Trend Estimation

Sea ice in the Bering Sea (Figure 3.3) is very similar to that in the Seas of Okhotsk and Japan, which has a maximum of 0.9 million km2 in winter and completely melts in summer. And the majority of monthly deviations are very close to the 30-year average. Both sub-regions are typical seasonal sea ice region. However, in the Sen's Estimator, it is not clear that sea ice extent in this subregion either decreased or increased in the study period. The slope indicates a -400 ± 600 km^2 trend that the upper boundary of the 95% confidence level implies an increase trend. Therefore, the general trend of sea

ice extent variability in this subregion remains uncertain.

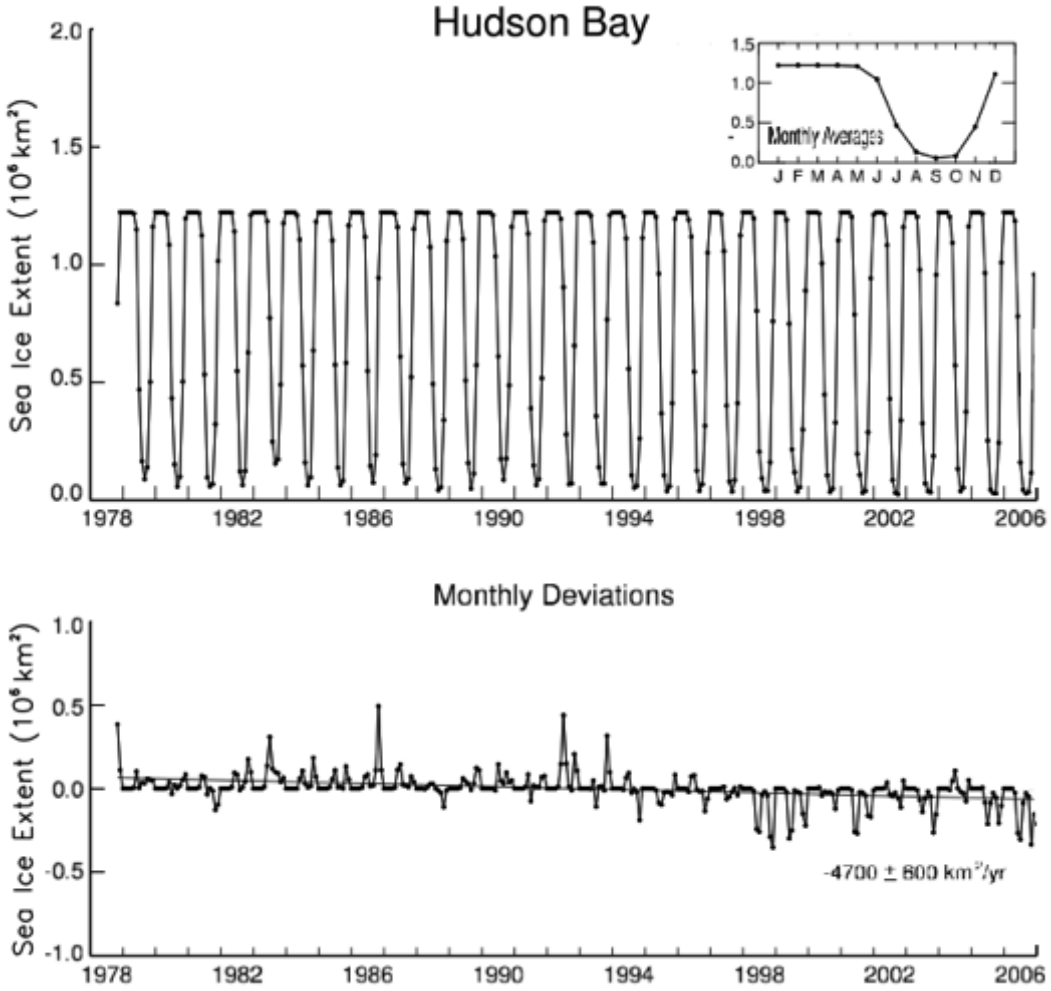

Figure 3.4 Monthly Sea Ice Extent Graph of the Hudson Bay, and Monthly Deviation Trend Estimation

Sea ice in the Hudson Bay (Figure 3.4) is very different from the above two sub-regions, which has a very steady winter freeze ice extent of approximately 1.23 million km2 from January to early May, and in summer, sea ice melt to approximately 0.1 million km2. It can be concluded that the entire region freezes up in winter and only part melt in summer. The monthly deviations have most of above average deviation values

before 1995, and after 1998, sea ice extent deviations are more likely to be below the 28 year average.

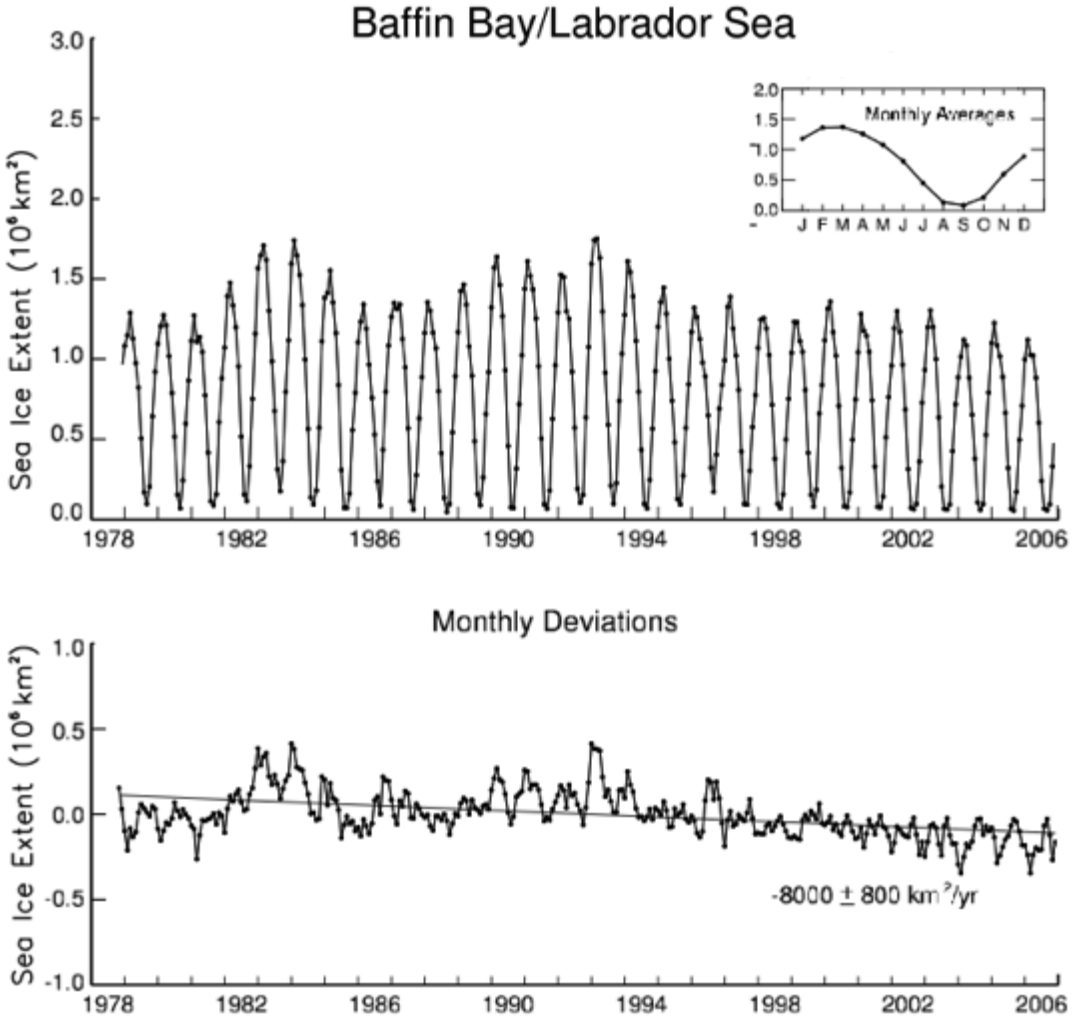

Figure 3.5 Monthly Sea Ice Extent Graph of the Baffin Bay/Labrador Sea, and Monthly Deviation Trend Estimation

Sea ice in the Baffin Bay and Labrador Sea (Figure 3.5) shows a seasonal pattern which freezes up to 1.5 million km2 in winter and melt to 0.1 million km2 in summer. Two top winter sea ice extents happened in 1983 and 1993 and summer sea ice extent is very close. Monthly deviation shows a clear decline trend of -8000±800 km2 per year.

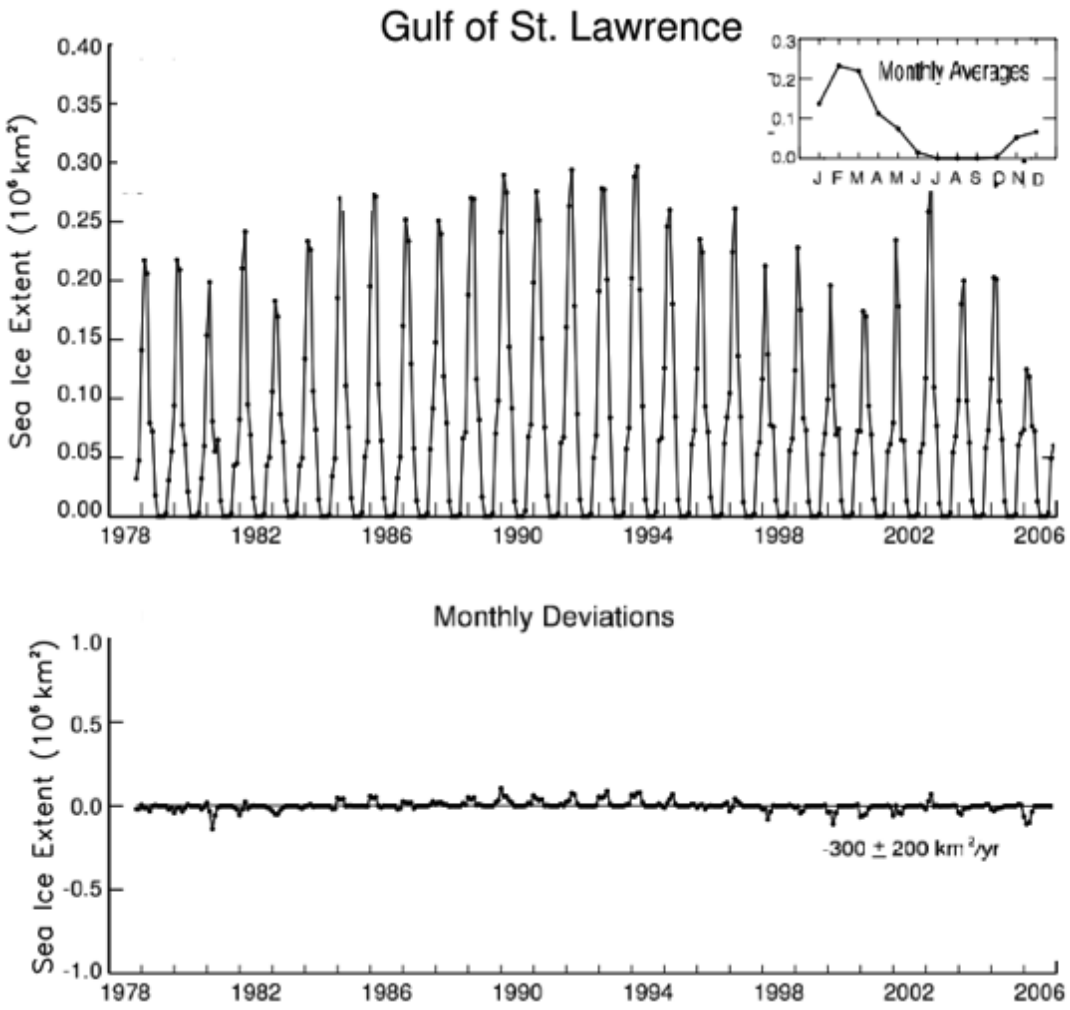

Figure 3.6 Monthly Sea Ice Extent Graph of the Gulf of St. Lawrence, and Monthly Deviation Trend Estimation

Sea ice in the Gulf of St. Lawrence (Figure 3.6) usually completely melts in late June, July, August, September, and early October, while winter freeze up extent varies a lot from 0.2 to 0.3 million km2 compared to summer extent variation. The monthly deviations are very close to 30 year average.

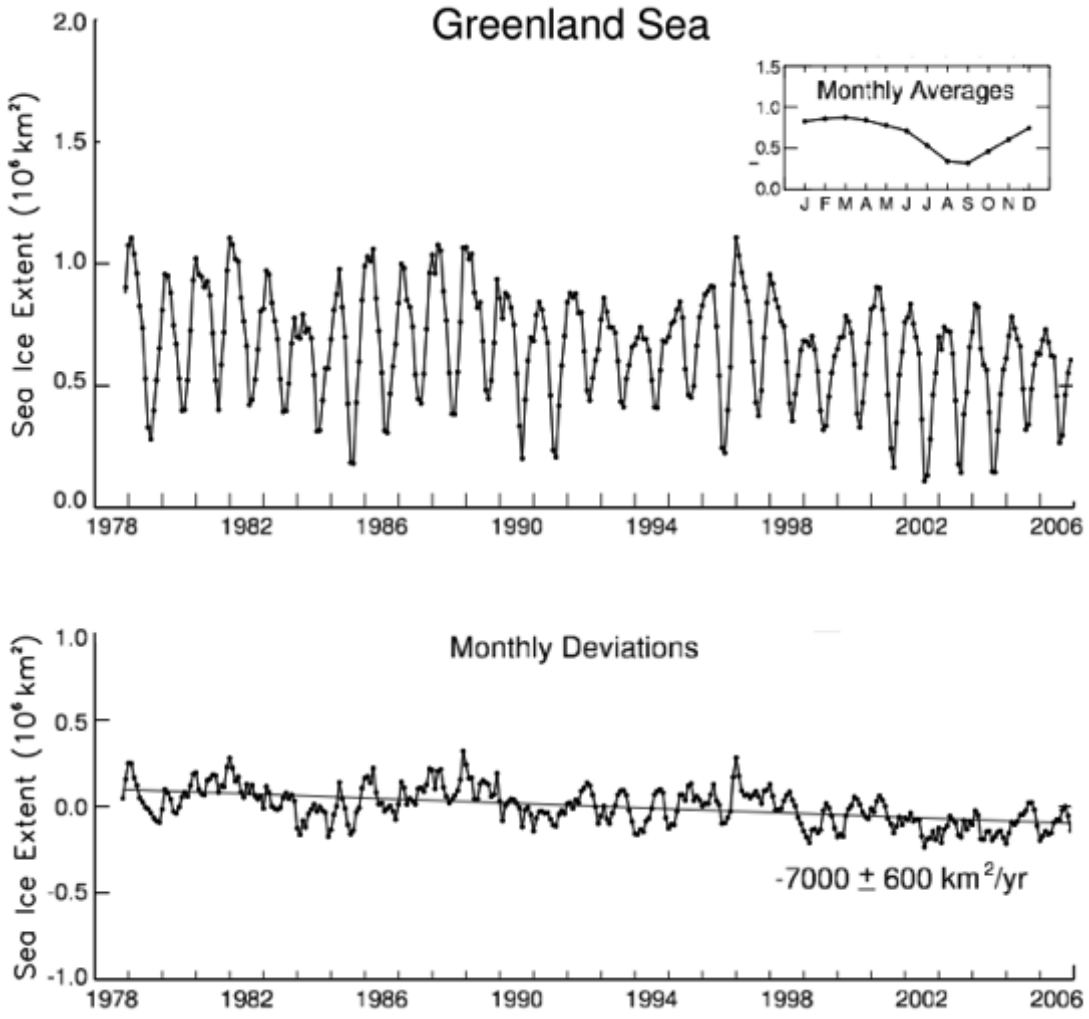

Figure 3.7 Monthly Sea Ice Extent Graph of the Greenland Sea, and Monthly Deviation Trend Estimation

The Greenland Sea ice (Figure 3.7) also shows a strong seasonal pattern, but unlike the other regions whose summer and winter sea ice extents are more likely to be close with its adjacent years, while sea ice extent in Greenland Sea varies a lot each year. The monthly deviation trend is -7000 ±600 km2 per year, and deviations that are above the 30 year average are clustered before 1995; after 2000, deviations are below average.

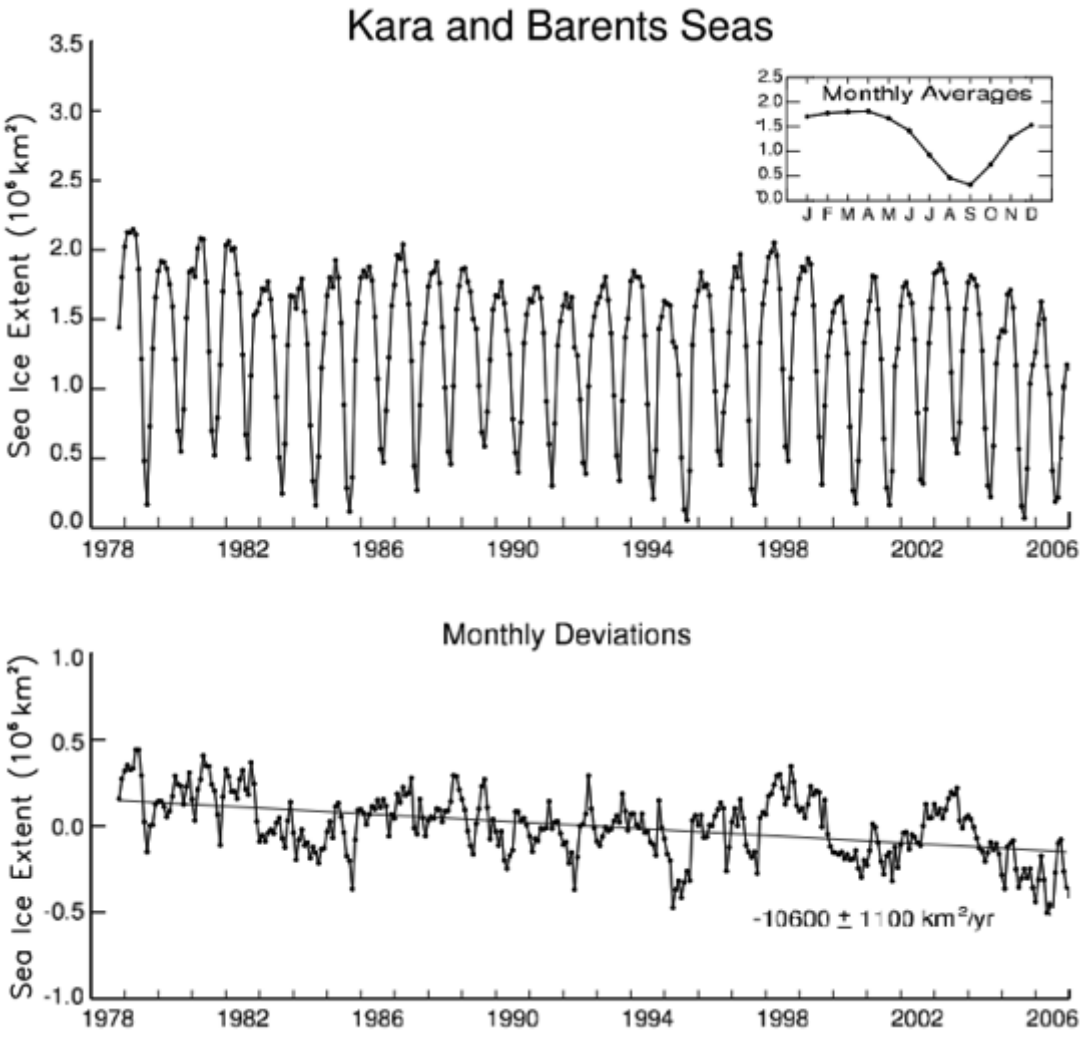

Figure 3.8 Monthly Sea Ice Extent Graph of the Kara and Barents Seas, and Monthly Deviation Trend Estimation

The sea ice in the Kara and Barents Seas (Figure 3.8) is similar to that in the Greenland Sea with an approximately 1.8 million km2 in winter and 0.5 million km2 in summer. In winter, the sea ice extent gradually increases from November to April and reaches the top in April. The monthly deviation trend is -10600±1100 km2 per year.

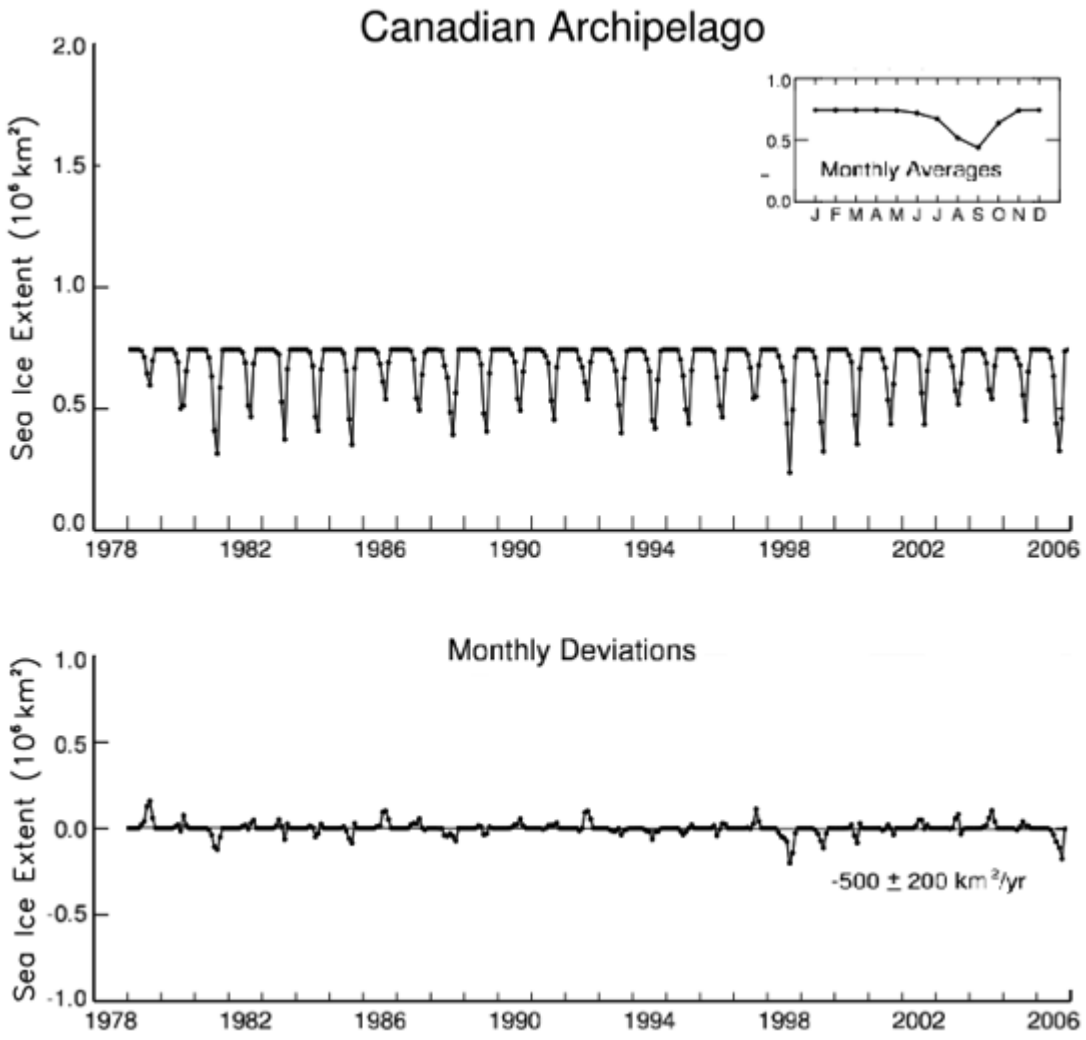

Figure 3.9 Monthly Sea Ice Extent Graph of the Canadian Archipelago, and Monthly Deviation Trend Estimation

Sea ice variability in the Canadian Archipelago (Figure 3.9) is similar to that in the Arctic Ocean which melts from late May to October. In winter, the entire region completely freezes up. And the least summer sea ice extent happened in 1998. And the monthly deviation trend is steady of -500±1100 km2 per year.

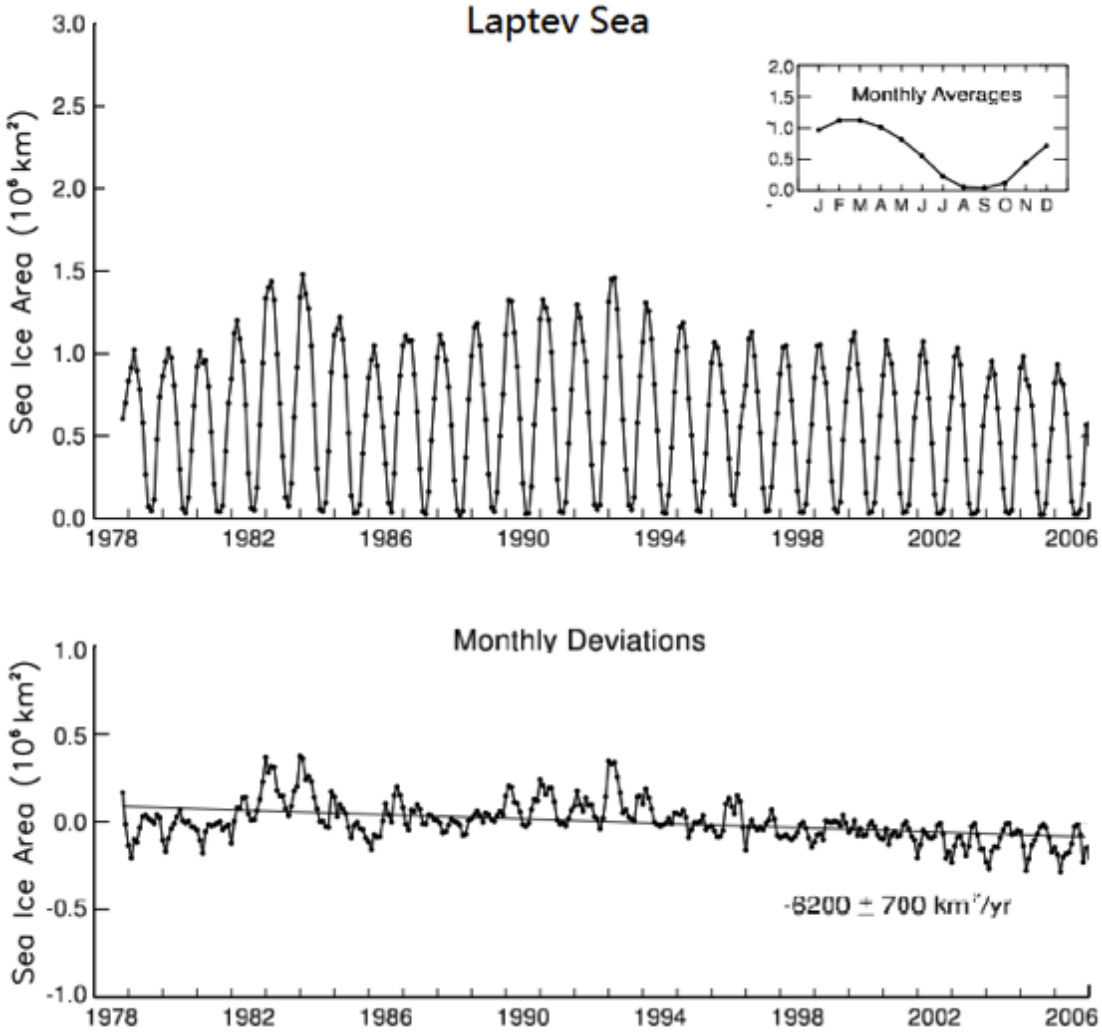

Figure 3.10 Monthly Sea Ice Extent Graph of the Laptev Sea, and Monthly Deviation Trend Estimation

Sea ice in the Laptev Sea (Figure 3.10) shows a string seasonal pattern, which is very similar with sea ice in the Baffin Bay. Sea ice in the Laptev Sea freezes up to 1.5 million km2 in winter and melt to 0.1 million km2 in summer. Two top winter sea ice extents happened in 1983 and 1992 and summer sea ice extent is very close. The monthly deviation shows a clear decline trend of -8200±700 km2 per year. The decline rate is also very similar to that of Baffin Bay.

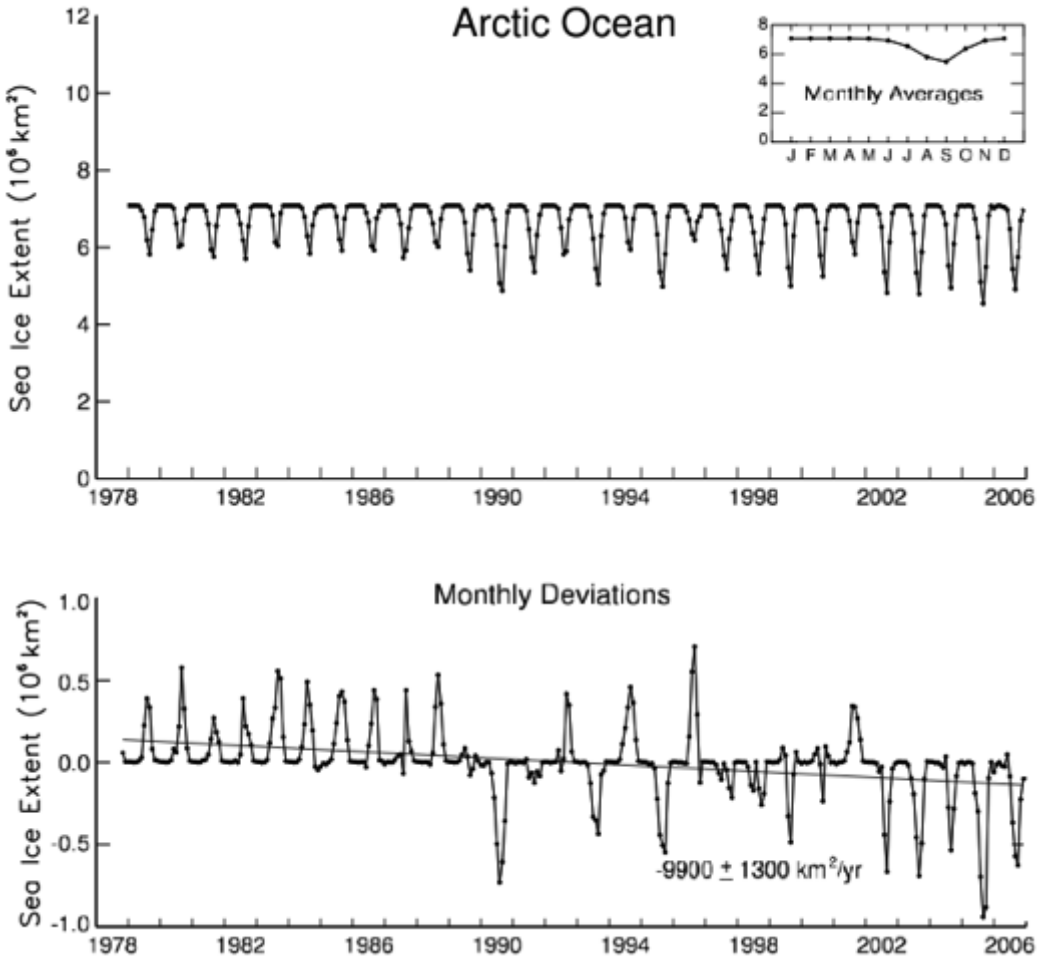

Figure 3.11 Monthly Sea Ice Extent Graph of the Arctic Ocean, and Monthly Deviation Trend Estimation

The Arctic Ocean contains majority of non-seasonal sea ice (Figure 3.11). From December to June, sea ice complete freezes and starts to melt in July and freezes again in late November. The monthly deviation shows a clear decline trend of -9900±1300 km2 per year. The least sea ice extent happened in 1998 and 2005. In addition, in the recent 5 years, the Arctic sea ice extents are far below the average implying global warming resulting Arctic sea ice decrease. Although non-seasonal sea ice is found in the central

Arctic Basin, it is not always identifiable in passive microwave imagery because summer melt water flooding the surface of the ice pack is frequently mistaken as ice with reduced concentration (Kwok, 2000; Meier, 2005).

	Jan	Feb	Mar	Apr	May	Jun	Jul	Aug	Sept	Oct	Nov	Dec
1979	1554	1631	1645	1546	1406	1259	1047	815	720	939	1116	1354
1980	1496	1598	1613	1549	1404	1231	1039	804	785	946	1169	1372
1981	1503	1565	1561	1512	1390	1257	1062	786	725	919	1117	1374
1982	1526	1606	1615	1557	1417	1269	1075	826	745	998	1191	1383
1983	1510	1602	1610	1530	1354	1235	1091	836	752	964	1164	1344
1984	1461	1532	1562	1515	1368	1220	1015	787	717	884	1129	1318
1985	1486	1567	1606	1534	1423	1240	1009	746	693	888	1139	1319
1986	1502	1589	1608	1515	1352	1210	1047	801	754	989	1178	1340
1987	1520	1611	1595	1533	1381	1257	998	769	748	929	1152	1355
1988	1515	1561	1613	1521	1369	1202	1004	790	749	947	1169	1378
1989	1512	1556	1552	1444	1298	1231	1038	792	704	952	1150	1347
1990	1495	1556	1588	1468	1330	1168	962	682	624	935	1131	1327
1991	1446	1526	1550	1493	1351	1223	968	740	655	916	1112	1317
1992	1472	1550	1547	1470	1325	1213	1061	786	755	960	1187	1346
1993	1508	1573	1588	1518	1354	1199	966	729	650	918	1173	1352
1994	1482	1561	1558	1495	1373	1210	1022	761	718	948	1130	1353
1995	1462	1524	1532	1459	1304	1155	915	668	613	894	1097	1298
1996	1421	1517	1513	1422	1306	1210	1036	817	788	939	1056	1314
1997	1447	1552	1558	1459	1332	1191	959	730	674	876	1091	1329
1998	1481	1577	1566	1489	1380	1185	962	749	656	885	1075	1326
1999	1447	1537	1540	1513	1386	1210	959	738	624	910	1099	1288
2000	1441	1518	1527	1463	1318	1171	975	721	632	892	1054	1281
2001	1431	1527	1561	1486	1372	1169	922	747	675	859	1092	1284
2002	1445	1536	1544	1437	1312	1169	949	653	596	881	1078	1282
2003	1446	1525	1549	1457	1300	1177	946	685	615	865	1029	1282
2004	1403	1493	1505	1411	1258	1151	960	683	605	848	1065	1272
2005	1366	1436	1474	1407	1299	1129	893	630	557	845	1047	1247
2006	1360	1442	1443	1397	1262	1106	867	652	592	833	984	1227

Figure 3.12 A chart of monthly sea ice extent in the Arctic region from 1979 to 2006, in 10000 km^2

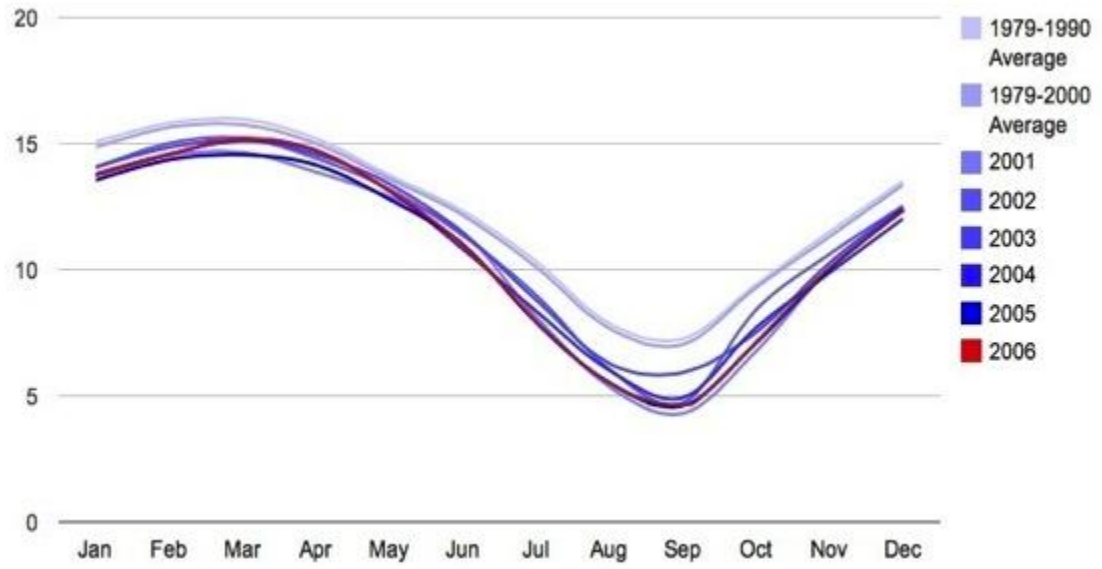

Figure 3.13 Seasonal Sea Ice Extent Average Line (in 10^6 km^2)

From the seasonal sea ice extent averaged line graph (Figure 3.13), it can be seen that sea ice extent seasonal average lines for years after 2000 are significantly below the lines of 1979-1990 average and 1979-2000 average all year round. The 1979-1990 sea ice extent average line gives an overall idea of the seasonal sea ice extent variability in a period which is widely considered with no intensified sea ice extent decline. The 1979-2000 average line gives an idea of the remotely sensed seasonal sea ice extent variability in the last century.

By visual inspection, the sea ice extent difference for years after 2000 and 1979-1990&1979-2000 was minimal in late April and May, which the melting process begins. And in September, the difference reaches maximum throughout the year, which implies intensified melting process in summer. In winter time, the difference decreases gradually and reaches minimum in May. However, the 1979-1990 average line is not far away from the 1979-2000 average line with a slightly visible difference. From the 1979-1990

average line and the 1979-2000 average line, it can be concluded that because the sea ice extent average from 1990-2000 is smaller than the 1979-1990 sea ice extent average, therefore the 1979-2000 average line is lower than the 1979-1990 average line.

From the Arctic sea ice extent variability graph and the trend estimation of the whole Arctic region and its sub-regions, it can be concluded that although there're variations through interannual, regional, and seasonal reasons, the 1979-2006 Arctic sea ice record is overall in a downward trend. According to the trend estimation, the Arctic sea ice shows a downward trend in all the sub-regions. Except the Canadian Archipelago, Bering Sea, and the Gulf of St. Lawrence, the downward trend is very small in the trend estimation, which is not very significant; the downward trend was significant in all other sub-regions. In particular, the trend estimation of the whole Arctic region indicates a strong sea ice extent decrease of 45100±2000 km^2 per year. Also, from the Arctic average lines chart, it can be concluded that Arctic sea ice extent average was highest in year 1979-1990, and become less in year 1990-2000, and even lesser after year 2000.

The reasons for the Arctic sea ice decrease has been studied for decades, and according to Serreze et al. (2000), this decrease has been caused in part by and has impacted the widespread Arctic warming. As warmer temperature increases melt and reduce freezing, less ice cover allows more solar radiation absorbed in the Arctic climate system (Johannessen et al., 2004). The reduced sea ice coverage would increase more open water which reflects less radiation and allows more radiation to be absorbed into the ocean which in turn increases the temperature and accelerates the sea ice melting process.

Numerous studies have focused on the interactions between the Arctic sea ice extent variability and the large scale ice/ocean/atmosphere system (Visbeck, et al., 2003). It is almost certain that the Arctic sea ice cover is impacted by various oscillation patterns in the North Hemisphere, for example, the North Atlantic Oscillation (NAO), the Arctic Oscillation (AO), and the El Nino/Southern Oscillation (ENSO) (Visbeck, et al., 2003). But the actual mechanism of how these oscillation patterns affect the Arctic sea ice extent remains under research. By understanding the real mechanism of the interaction between Arctic sea ice and oscillation patterns, it would provide researchers with opportunities for analyzing various arctic phenomena in the large scale. In addition, researches of the long term climate trend in not only the northern hemisphere, but also the entire earth would benefit a lot from the discovery of interaction mechanism.

3.2 Sea Ice Extent Ranking Analysis

The Arctic sea ice extent will be ranked from the largest to the smallest yearly sea ice extent in the whole Arctic region and the nine sub-regions as well to find the years with sea ice extent anomalies and the long term variability trend.

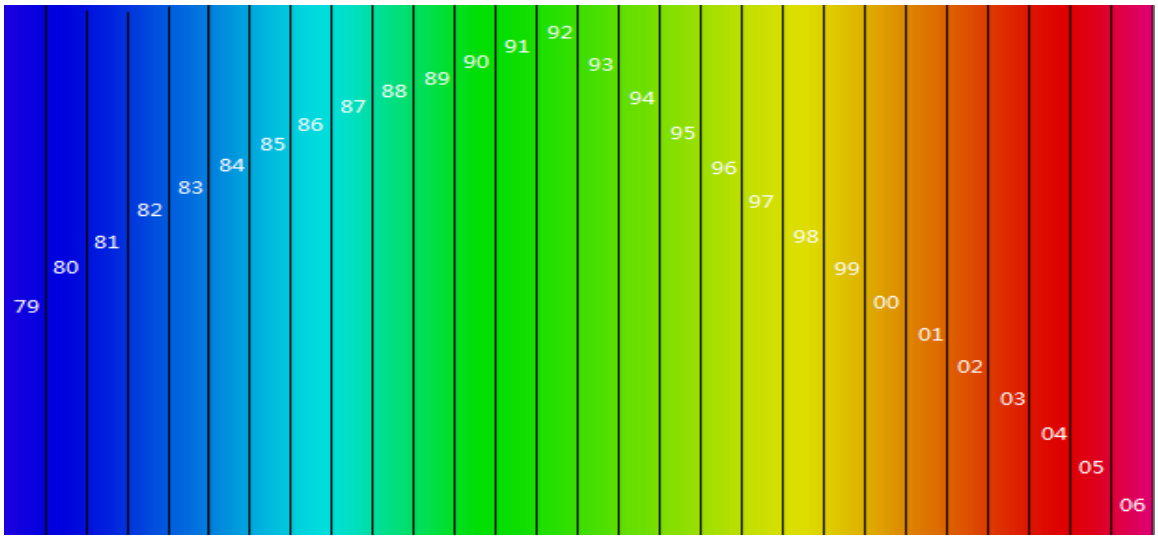

Figure 3.14 Color differentiation chart of the sea ice extent ranking

This chart (Figure 3.14) shows how the color varies by sequential year. This color scale gradually changes from visually cold color (1979 to 1983) to visually warm color (2001 to 2006). In the sea ice extent ranking chart, the color clustering can be used to visually highlight the clustering of adjacent years in sea ice extent ranking. This technique has been used for similar illustrations of temperature by WMO (World Meteorological Organization, 2011).

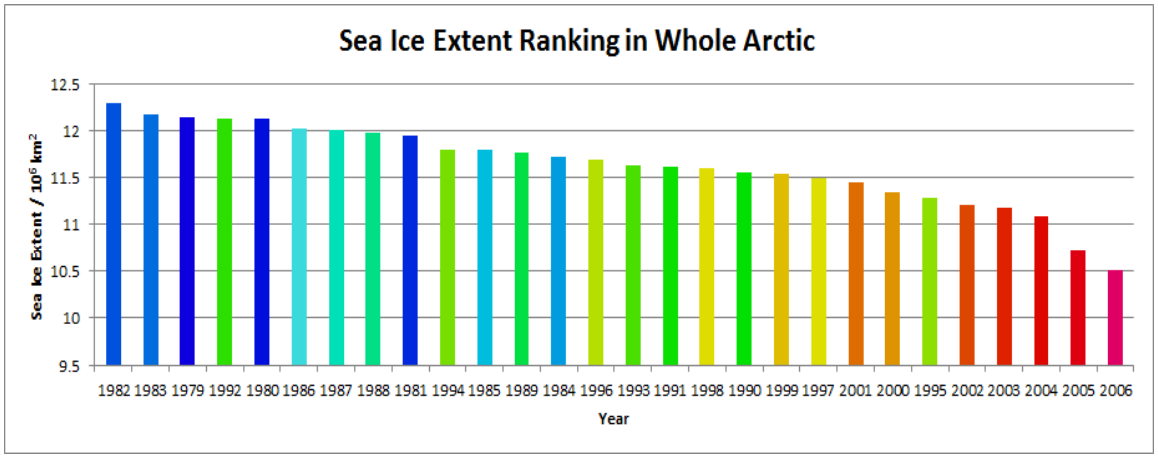

Figure 3.15 Sea Ice Extent Ranking Chart of whole Arctic region

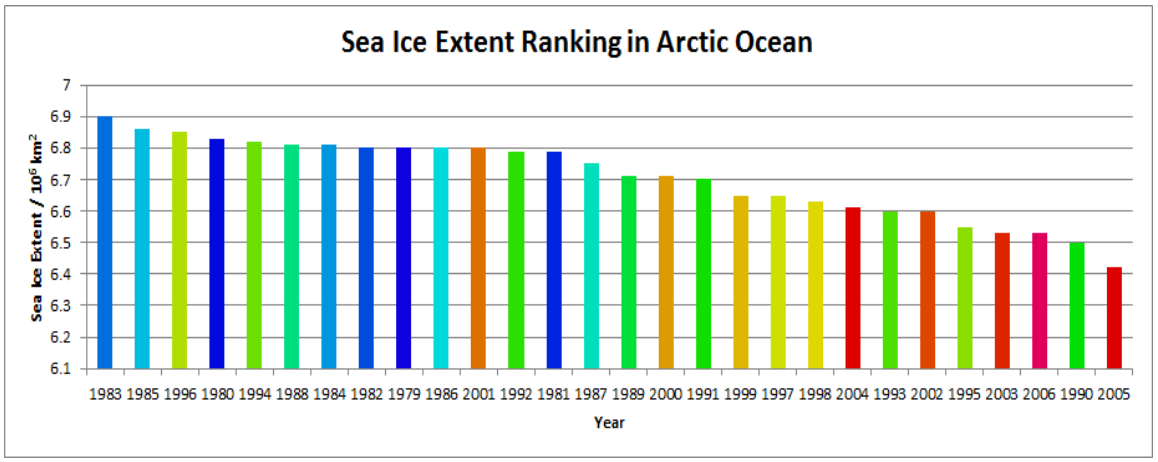

Figure 3.16 Sea Ice Extent Ranking Chart of the Arctic Ocean

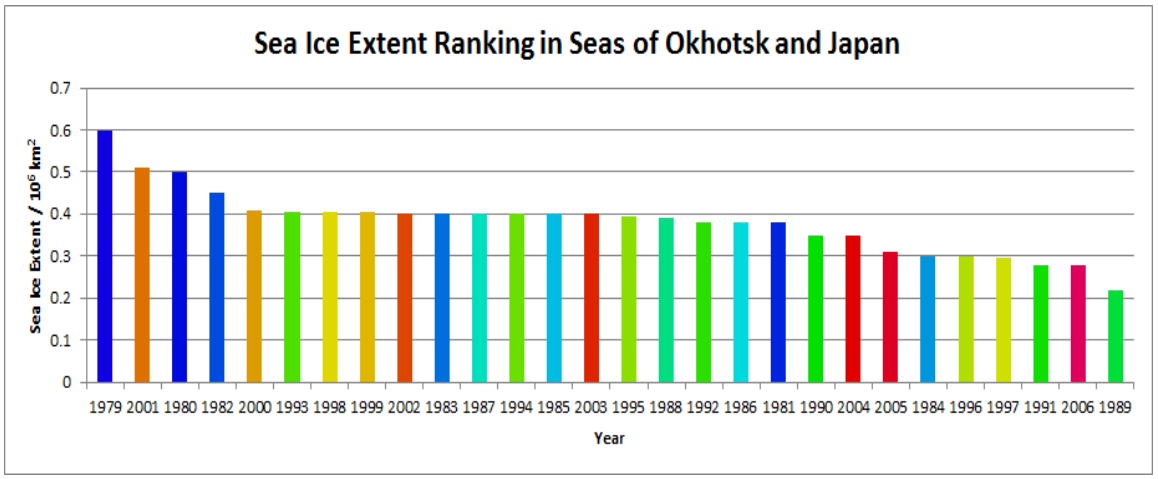

Figure 3.17 Sea Ice Extent Ranking Chart of the Seas of Okhotsk and Japan

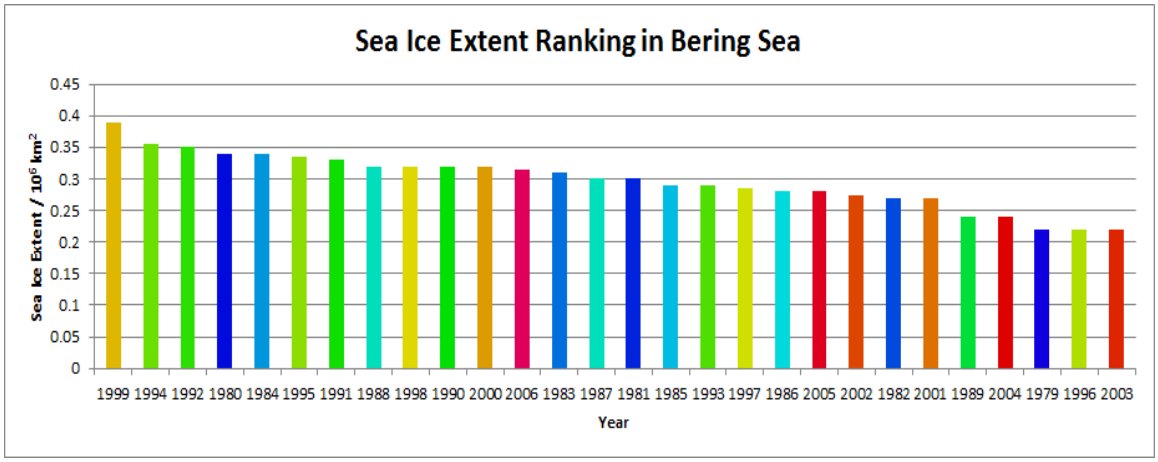

Figure 3.18 Sea Ice Extent Ranking Chart of the Bering Sea

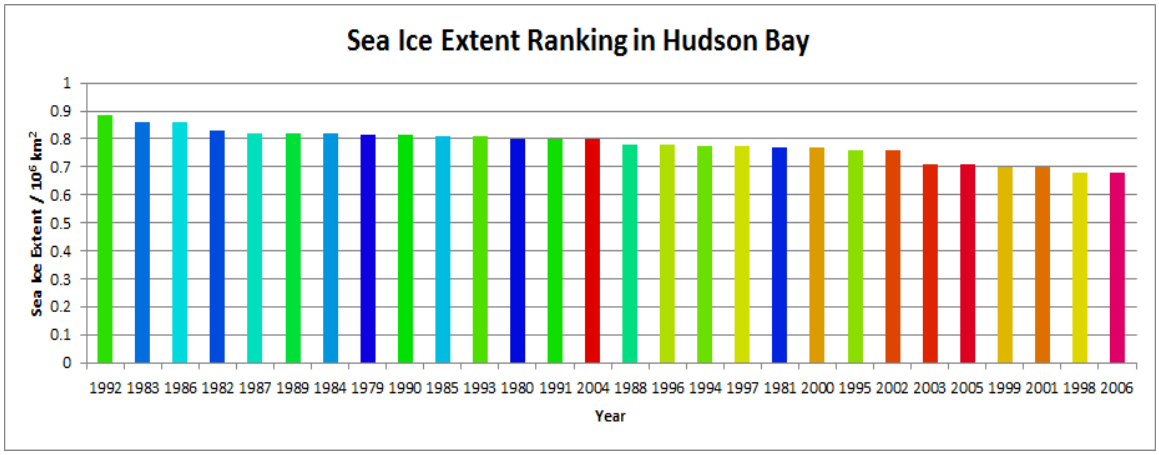

Figure 3.19 Sea Ice Extent Ranking Chart of the Hudson Bay

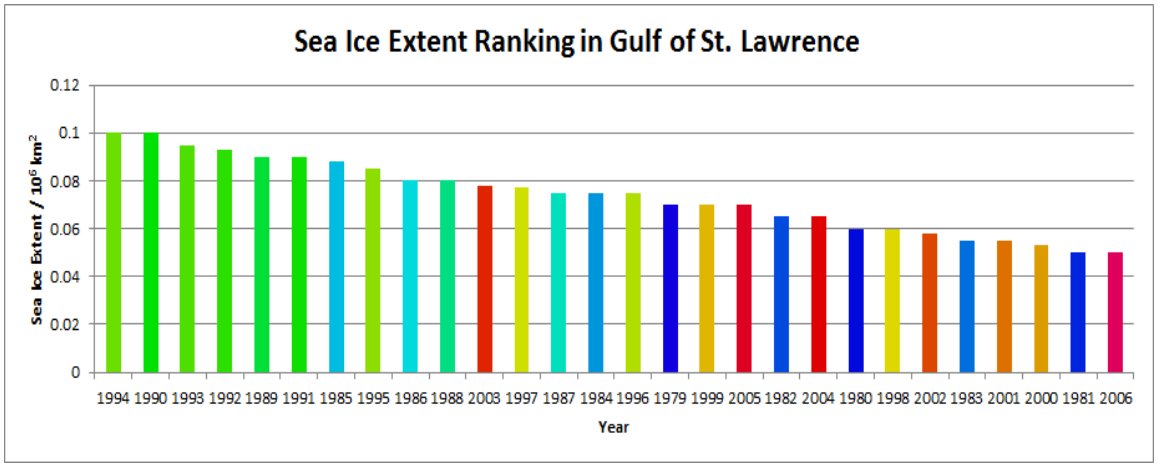

Figure 3.20 Sea Ice Extent Ranking Chart of the Gulf of St. Lawrence

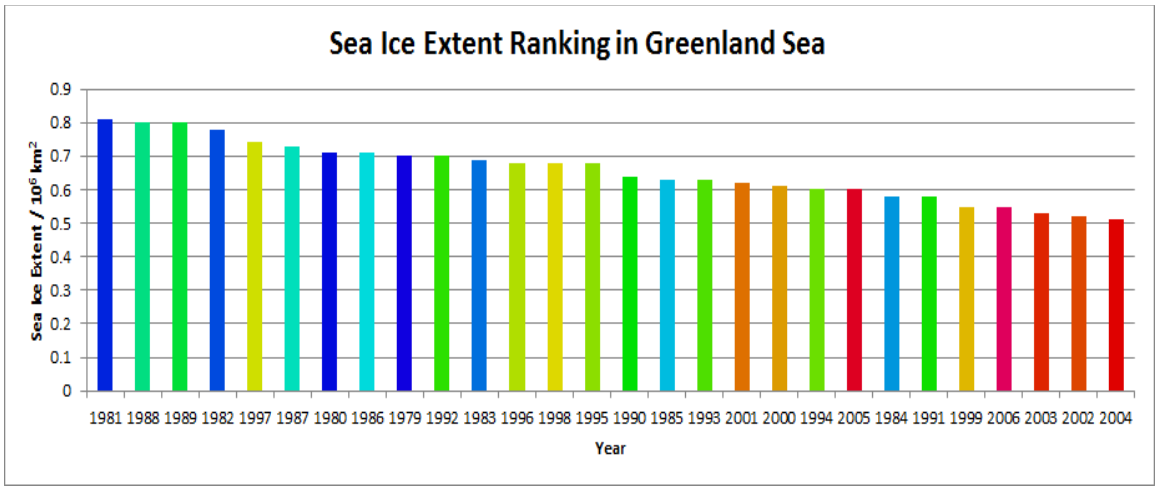

Figure 3.21 Sea Ice Extent Ranking Chart of the Greenland Sea

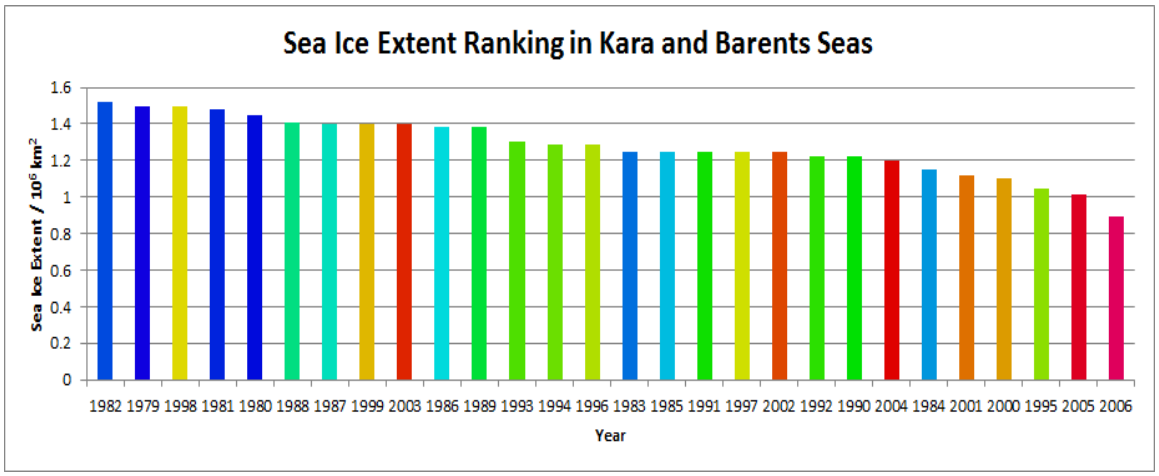

Figure 3.22 Sea Ice Extent Ranking Chart of the Kara and Barents Seas

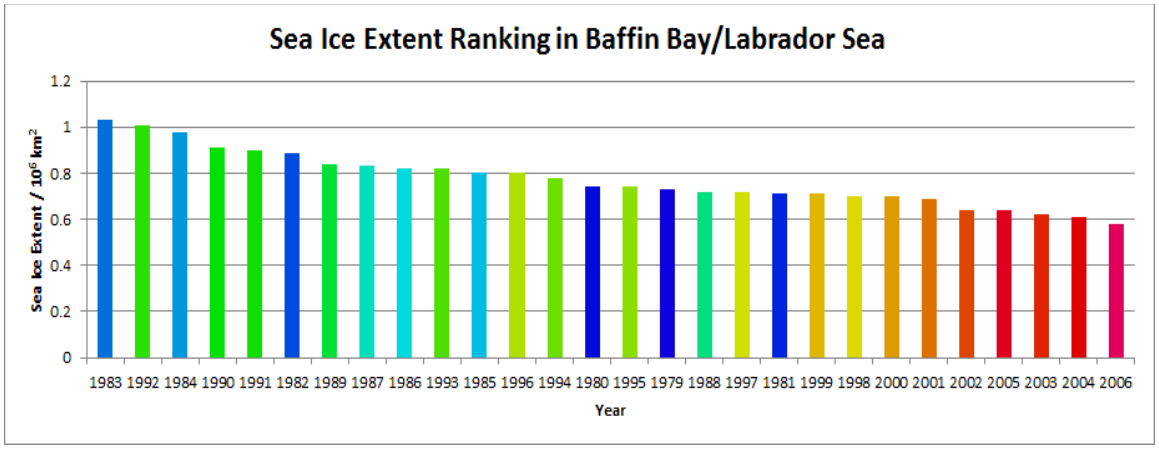

Figure 3.23 Sea Ice Extent Ranking Chart of the Baffin Bay

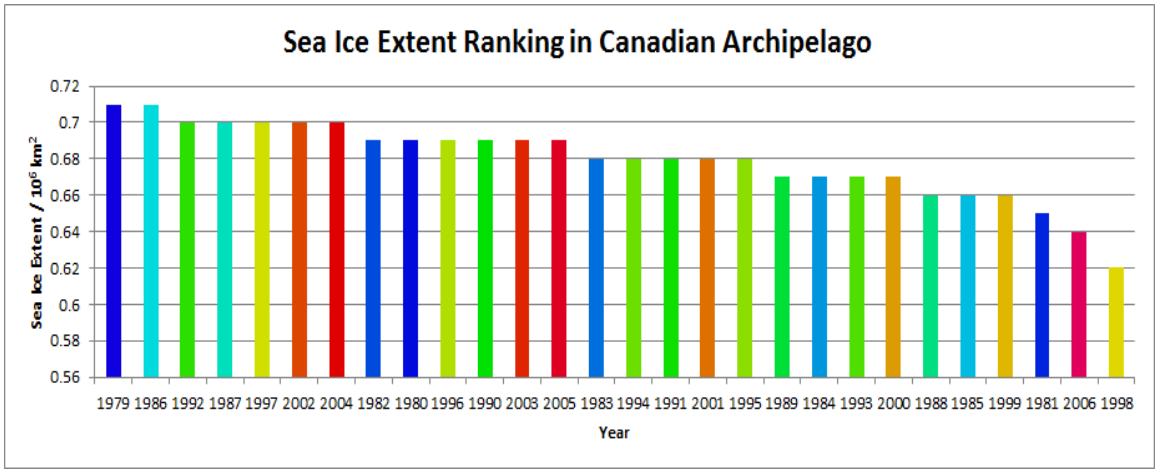

Figure 3.24 Sea Ice Extent Ranking Chart of the Canadian Archipelago

In section 3.1, analyzing the general trend of the Arctic sea ice extent variability, it can be concluded that in majority of the Arctic sub-regions, sea ice extent is decreasing in the long term. From the sea ice extent ranking chart of the whole Arctic region, it reaches the similar conclusion with the Arctic sea ice extent variability and trend estimation. There is a downward trend in the sea ice extent variability. However, the sea ice extent ranking chart provides more and detailed information of the sea ice extent variability than the general trend. The sequential color scheme of the ranking chart provides the most intuitive method for analyzers to identify the clustering of years with similar colors and sea ice extents. Also, the anomalies can be easily identified as a different color bar among a cluster of bars with similar color.

According to the sea ice extent ranking chart of the whole Arctic region, in the late 1970s and early 1980s, sea ice extent is high, while after 1998, sea ice extent starts to decrease dramatically, especially the last five years, from 2002 to 2006. From this chart, sea ice anomalies can be easily found. For example, 1992 and 1995 are two significant anomalies which 1992 ranked fourth in sea ice extent in this nearly 30 year sequence,

while 1995 is ranked between 2000 and 2002 as the last but five sea ice extent ranking. These anomalies, which do not fall within their adjacent years, can be utilized to study the Arctic variability and trends. According to this chart, it can be generally concluded that over the past 30 years, Arctic sea ice extent is decreasing.

Similar sea ice extent ranking charts are created for all the sub-regions. The anomalies and sea ice variability trends can be identified through these charts. For example, in the chart for the Seas of Okhotsk and Japan, 2001 ranked second largest sea ice extent which indicates an incredibly cold year, while 1989 is the least sea ice extent year indicating a warm year in this region. In addition, the clustering of years indicates these years share very similar sea ice variability. For example, sea ice extent in the Baffin Bay and Labrador Sea has an obvious clustering between 2002 and 2006 as the least sea ice extent.

Arctic region	Anomaly Years with large extent	Anomaly Years with small extent
Whole Arctic	1992	1995
Seas of Okhotsk and Japan	2001, 2000	1991, 1989, 1984, 1990
Bering Sea	1999, 2000, 2006	1996, 1989, 1979, 1982
Hudson Bay	1992, 1989	1998, 1995
Baffin Bay/Labrador Sea	1992, 1990, 1991	1981
Gulf of St. Lawrence	1994	1981, 1983
Greenland Sea	1988, 1989, 1997	1991, 1984
Kara and Barents Seas	1998, 1999, 2003	1995, 1984
Arctic Ocean	1996, 1994	1990, 1995, 1993
Canadian Archipelago	1992, 1997, 2002, 2004	1998, 1981, 1985, 1988

Figure 3.25 Anomaly years from the sea ice extent ranking charts

In Figure 3.25, years with unusual sea ice extents are selected based on visual color inspection. In addition, based on the sea ice variability and trend analysis, sea ice extent in the Arctic scale is decreasing over the last 30 years; therefore an assumption is

made that sea ice extent of years after 1995 is more likely to be smaller than that of years before 1990 in the Arctic sub-regions except the subpolar. And this assumption has got some evidences that sea ice extent is decreasing in majority of the Arctic sub-regions, and in the sea ice extent ranking chart, sea ice extent bars for years after 1995 are more likely to be in the lower rankings. Therefore, in the anomaly year selection process, years after 1998 with small sea ice extent will not be counted as anomalies. On the other hand, years before 1985 with large sea ice extent will also not be counted as anomalies.

The advantages of performing this sea ice extent ranking in the whole Arctic and its sub-regions are several. The most important advantage of doing this analysis is that it gives a straightforward visualization of sea ice extent anomalies and its overall variability through time. The gradual color scheme allows easy identification of years with unusual sea ice extent, i.e., very different from its adjacent years. Also, given the overall trend of sea ice extent variability from the previous trend estimation, the sea ice extent ranking should follow a similar downward trend. However, the ranking results of some sub-regions did not show a clear sign of a downward trend. In some sub-regions, for example, the sea ice extent ranking charts of the Canadian Archipelago, the Bering Sea, and the Seas of Okhotsk and Japan could not give its viewers a first impression that sea ice extent in these areas are under a downward trend. Therefore, the sea ice extent ranking chart of these sub-regions provides a different perspective than the trend estimation, which in the trend estimation, the monthly sea ice extent deviations, especially the extreme ones, are sometimes not visually identical to viewers.

The second advantage is that in the sea ice extent variability and slope estimation

analysis, through the outliers or anomalies can be detected using various kinds of statistical approaches, the small size of sample set in this research limited the performance and credibility of statistical analysis. But in the sea ice extent ranking analysis, any alien color bars that happened to be among a cluster of different color bars can be classified as anomalies. The easiness and effectiveness in anomaly analysis constitutes the second advantage.

The third advantage is that the sea ice extent ranking charts can be used for future research of studying the Arctic sea ice interaction with the North Atlantic Oscillation. Assuming Arctic sea ice extent variability is impacted by NAO, the growth and retreat of sea ice extent would sync with NAO. For example, the Bering Sea and Greenland Sea are in the opposite position of the Arctic region. In Bering Sea, year 1999 ranked first in sea ice extent and in Greenland Sea, year 1999 ranked last but five. In addition, year 1981 ranked first in sea ice extent in Greenland Sea while in the Bering Sea, year 1981 ranked in the middle. Same situation occurs in 1991, 1982, and 1979. In addition to the Bering Sea and Greenland Sea, sea ice extents in the Canadian Archipelago and the Kara and Barents Seas indicate the same sea ice oscillation pattern. These coincidences can be used as clues for further studies of the mechanism of NAO impact on Arctic sea ice.

3.3 Sea Ice Extent Ranking Anomalies with North Atlantic Oscillation

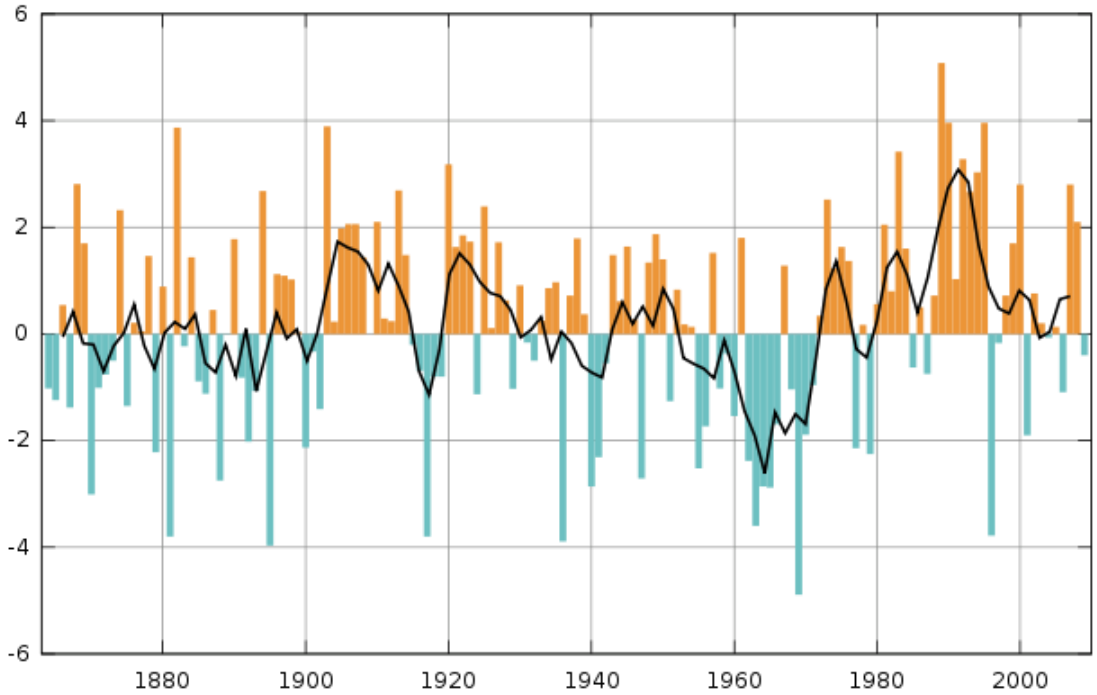

Figure 3.26 North Atlantic Oscillation Index Table (Marsupilami, 2010)

The North Atlantic Oscillation is a climatic phenomenon which refers to the fluctuations in the difference of atmospheric pressure at sea level between the Icelandic low and the Azores high, which is an east-west oscillation motions (R. Seager, Y. Kushnir, J. Nakamura, M. Ting, and N. Naik , 2010).

A high index year usually leads to increased westerlies, cool summers and mild wet winters in Central Europe and its Atlantic coast. On the other hand, if the index is low, westerlies are suppressed which leads to cold winters and the storms then track southerly toward the Mediterranean Sea (Hurrell et al., 2003). During the winter, when the index is high, the Icelandic low draws a stronger south-westerly circulation over the eastern half of the North American continent which prevents Arctic air from plunging

southward. In combination with the El Niño, this effect can produce significantly warmer winters over the northeastern United States and southeastern Canada (Hurrell et al., 2003). Conversely, when the NAO index is low, the eastern seaboard and southeastern United States can incur winter cold outbreaks (R. Seager et al., 2011).

The North Atlantic Oscillation Index from 1978 to 2006 (Figure 3.26) is above zero for the majority of years except 1979, 1985, 1987, 1996, 1997, 2001, 2004, 2006. In 1991 and 1992, the NAO indexes shares the same situations with the AO indexes, which are the top two highest indexes in a temporal span from 1860 to 2009.

Many of the very identical anomalies in the sea ice extent ranking charts can find their corresponding index peaks in the NAO index chart or the AO index chart. For example, sea ice extent of 1998 in the Kara and Barents Sea ranked 3rd largest from 1978 to 2006, surrounded by 1982, 1979, and 1981. And in the NAO index chart, there is a significant low index (lowest in the last 50 years) in the same period. In addition, sea ice extent of 1992 in the Hudson Bay ranked first followed by that of 1983 and 1986, while sea ice extent of 1993 and 1991 are in the middle ranking, which indicating that year 1992 in the Hudson Bay might be an unusual cold winter and/or cool summer. In the meantime, NAO index of 1992 is the highest in all the data available (from 1860 to 2009). Not only did these associations be found between sea ice extent anomalies and NAO indexes, but also with the AO indexes. The sea ice extent from 1989 to 1994 in the Gulf of St. Lawrence ranked in the first six places in the nearly 30 year sea ice extent ranking. While according to sea ice extent ranking in other sub-regions and the entire Arctic, it can be generally considered that in the early 1980s, sea ice extents kept a high level with a

considerable amount of high ranks. Since the Gulf of St. Lawrence and the Seas of Okhotsk and Japan are the most distant sub-regions away from the Arctic center, it can be implied that these sub-regions have a higher possibility of getting influenced by the Arctic Oscillation with increased amount of Arctic frigid air entering the middle latitude region. By the Arctic Oscillation Index chart, from 1989 to 1997 the indices formed a cluster of particular high peak over the past 100 years from 1900 to 2011.

3.4 TEMPORAL MIXTURE ANALYSIS

The Temporal Mixture Analysis developed by Piwowar and LeDrew, 1998 is utilized to create the fractional images to reveal the spatial distribution of temporal features of different sub-regions in this research.

3.4.1 Endmember selection and description of its seasonal variability

Endmembers are selected in each of the 9 sub-regions by finding the most "seasonal" pixel in the scatterplot approach by displaying sea ice concentration in March versus September.

The endmember selected from the Seas of Okhotsk and Japan behaves as a seasonal signal which has maximum sea ice coverage in late February and March to ice free in August. Any other months are in transition for freeze or melt. The maximum ice concentration in this region is about 80%.

The endmember selected from the Bering Sea is similar to the endmember of the Seas of Okhotsk and Japan but has a longer ice free period, and transition period.

The endmember selected from Hudson Bay represents a typical seasonal signal, where sea ice covers the entire region from December to May and almost melt up from July to early November.

The endmember selected from Baffin Bay and Labrador Sea behaves like endmember of Bering Sea with a much longer transition period. The maximum sea ice coverage usually happens in March with 50-60% concentration.

The endmember selected from the Gulf of St Lawrence shares the same

characteristics of that from Hudson Bay. Sea ice in the Gulf of St Lawrence usually reaches maximum concentration around 75% percent in February and March and completely melts up between May to December.

The endmember selected from the Greenland Sea is another typical seasonal pattern which reaches maximum sea ice extent in March with an ice concentration of 80% and starts to melt in April. In summer, sea ice concentration has a minimum to 10%. Usually in this region, sea ice extent kept varying every month with a long transition period.

The endmember selected from the Kara and Barents Seas is similar to the endmember of the Greenland Sea.

The endmember selected from the Arctic Ocean represents the non-seasonal pattern. Only late June to late October has little ice melt, and other months have 100% sea ice concentration. In summer, the minimum sea ice concentration is 70%.

The endmember selected from the Canadian Archipelago is very similar to the endmember of the Arctic Ocean. But this region has one more melt month and the minimum summer sea ice concentration is 50%.

3.4.2 Fractional images of the Temporal Mixture Analysis

After the 9 endmembers are selected from each region, the fractional image is created by unmixing each pixel. After the fractional images are created, the endmember fractions of each pixel can be used to see the spatial distribution of temporal features. Each endmember represents a certain temporal signature. In addition, because the

endmembers are selected in each subregion, pixels that are unmixed can be revealed to have temporal signatures similar to these of other sub-regions.

From the first image (Figure 3.27), it can be seen that this endmember selected in Hudson Bay represents a classic seasonal signal. This endmember describes a temporal characteristic of total ice cover from December to May and completely ice free from July to November. The majority of Hudson Bay is dominated sea ice that shares the temporal characteristics of this endmember. However, the northern part of Hudson Bay does notfit with this endmember very well with less than 30% segmentation. Not only does this endmember show positive observations in Hudson Bay, but also it can be found in the sea shore line along the Davis Strait and in the Chukchi Sea. This indicates some temporal similarity among these regions.

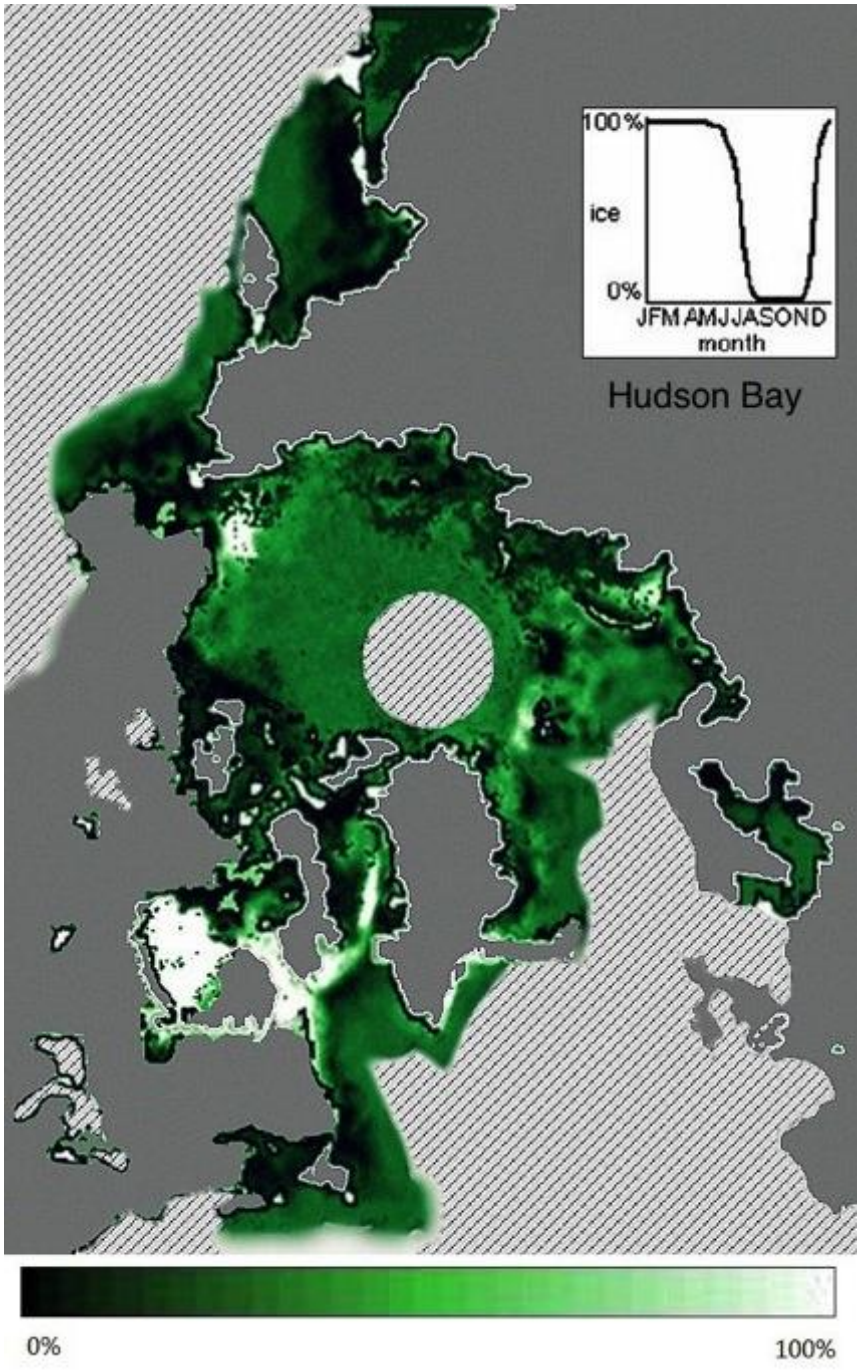

Figure 3.27 Fraction Image of Endmember 1

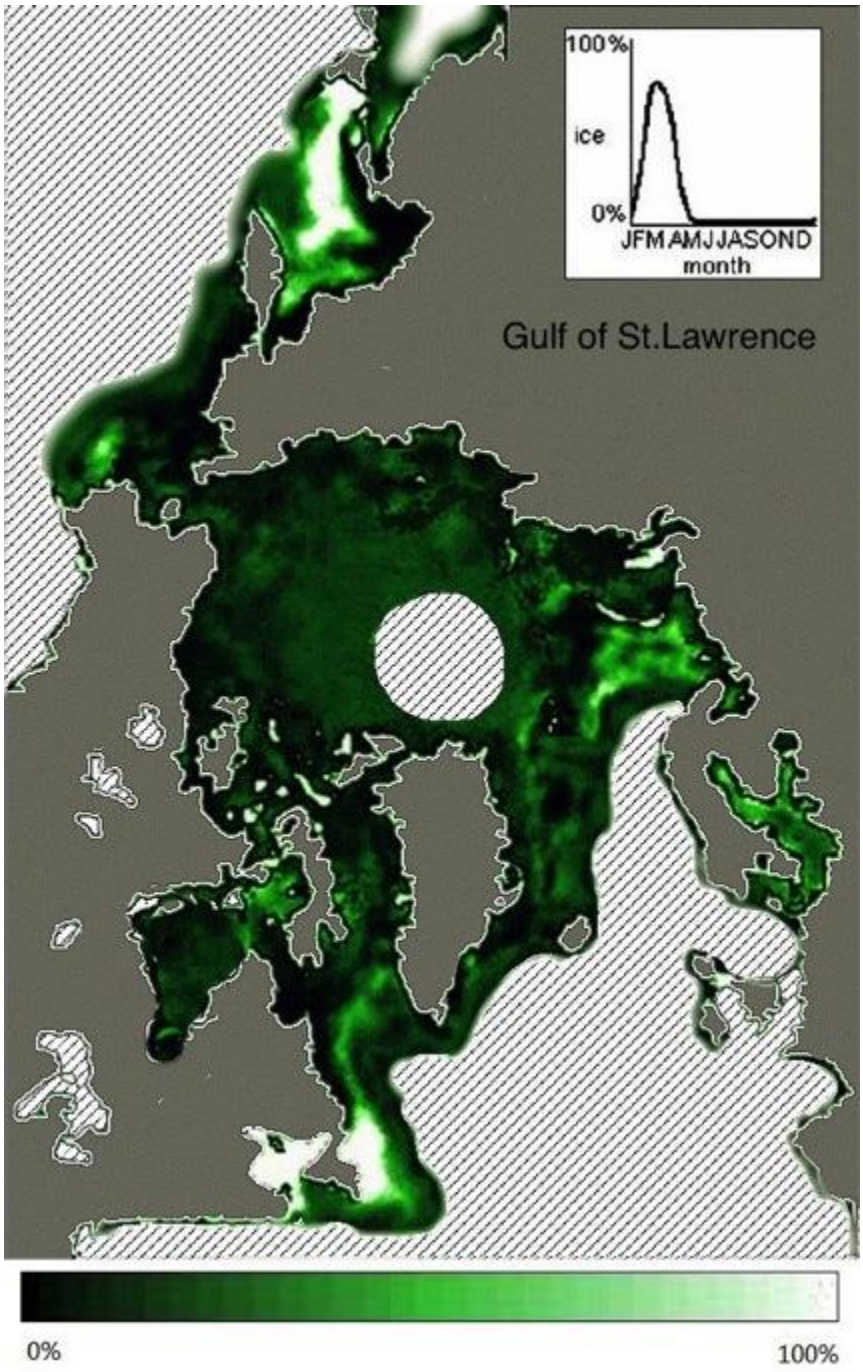

Figure 3.28 Fraction Image of Endmember 2

The second image (Figure 3.28) shows the endmember fraction selected in the Gulf of St. Lawrence. This endmember describes temporal characteristics of short ice cover duration and never make it to full ice cover in this region. Since the Gulf of St. Lawrence is not part of the Arctic region with lower latitude, the sea ice extent and concentration is much smaller compared to other regions. In this region, the maximum sea ice concentration is about 75% in February and March and become completely ice free from May to December. This temporal pattern describes the majority of area in the Gulf of St. Lawrence indicating high accuracy and less error in both raw data and endmember selection process. Interestingly, thousands of miles away in the opposite side of the Arctic region, the Seas of Okhotsk has a considerable amount of positive observations with approximately 70% of sea ice in that region. These positive observations in the Seas of Okhotsk formed a band started from the northeast then goes southwest until reaches the seashore. However, in the northwest corner of the Seas of Okhotsk, it's completely dark indicating no temporal fitting with this endmember at all.

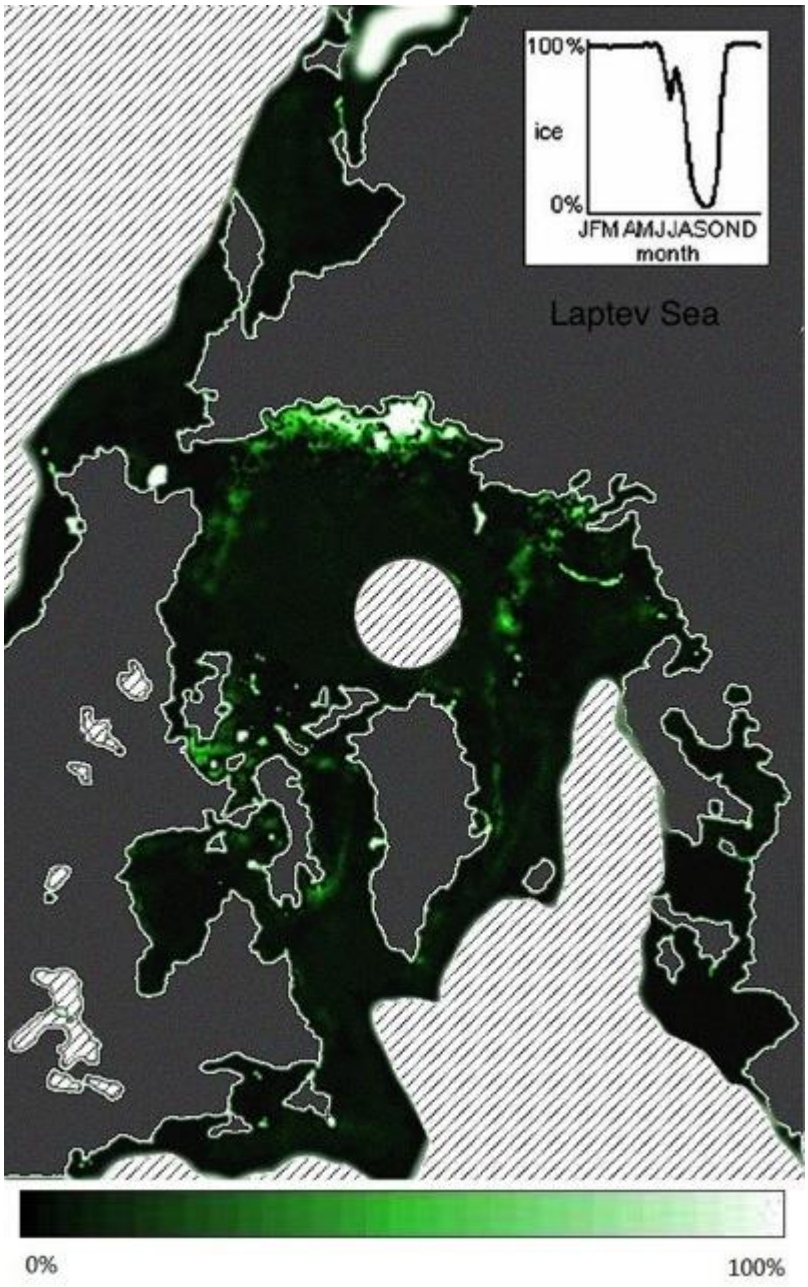

Figure 3.29 Fraction Image of Endmember 3

The third image (Figure 3.29) describes the fraction distribution in the Laptev Sea which is in the edge of the Arctic Basin with full sea ice coverage from October to May. In summer, sea ice concentration drops to almost zero in September. This endmember does not find any other positive observations outside of the Laptev Sea.

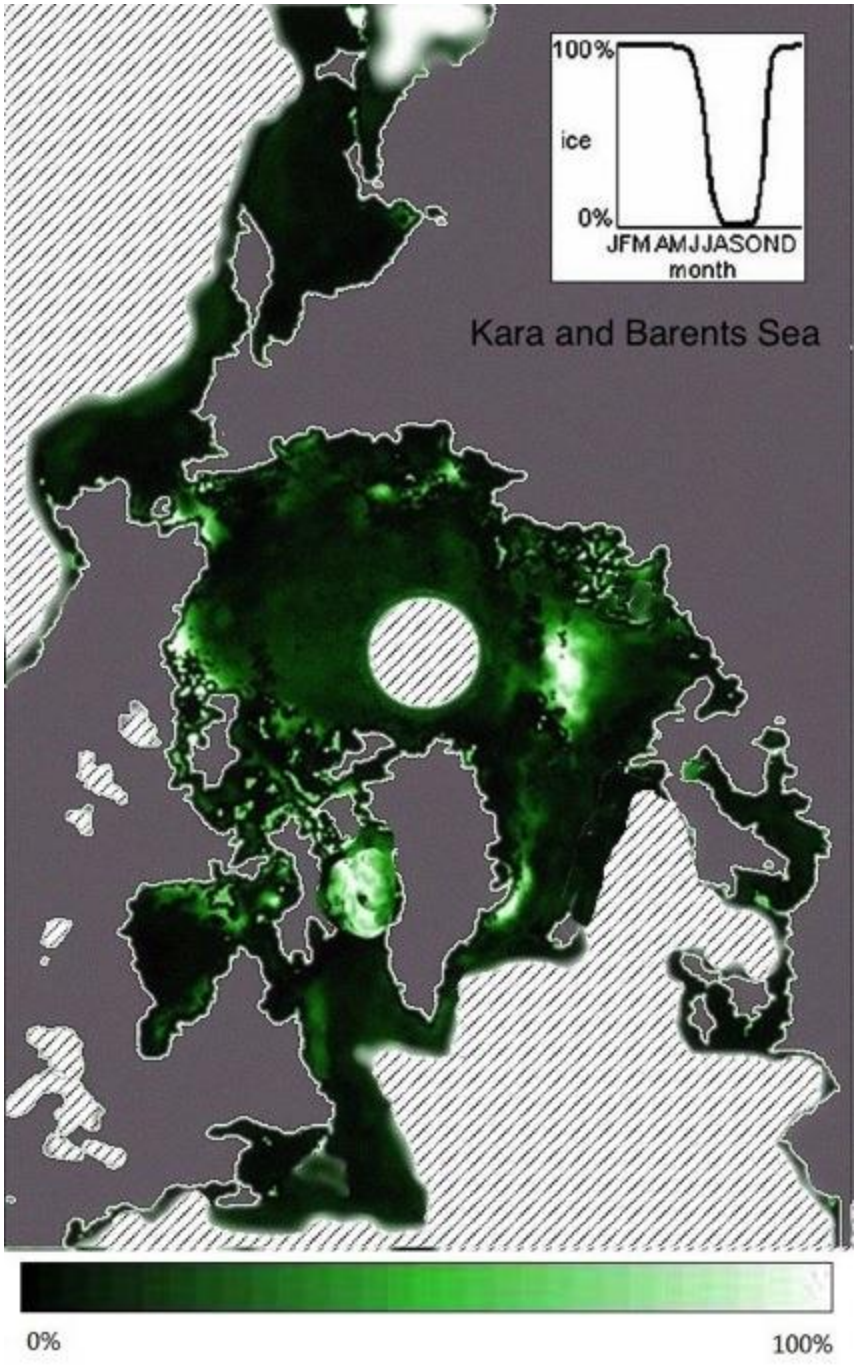

Figure 3.30 Fraction Image of Endmember 4

The fourth image (Figure 3.30) shows the endmember fraction selected in Kara and Barents Seas. This endmember shares similar temporal characteristics with the third endmember that is selected in the Laptev Sea. But this endmember has a one-month

shorter summer period. This endmember gives positive observations in the middle of Baffin Bay. In addition, it can also be found in the north part of the Kara and Barents Seas.

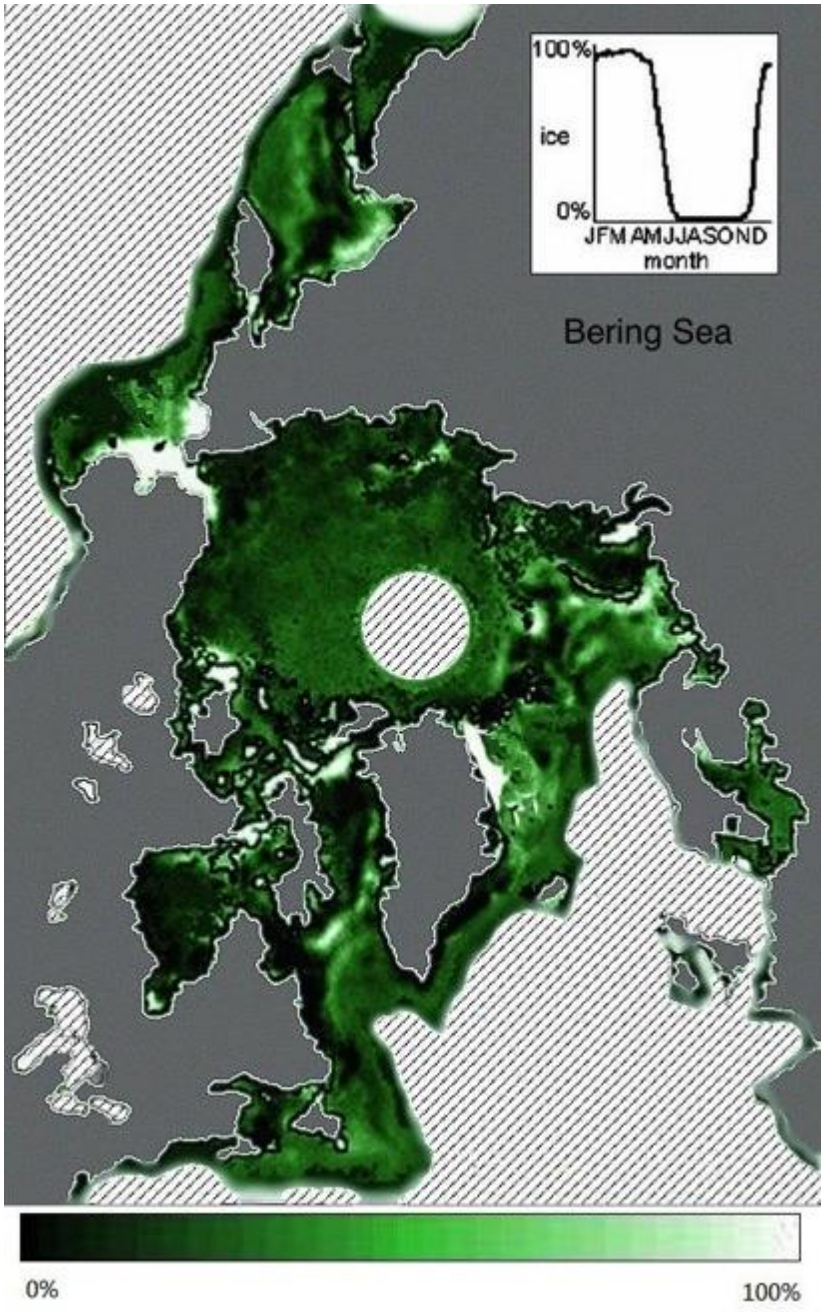

Figure 3.31 Fraction Image of Endmember 5

The fifth image (Figure 3.31) shows the endmember fraction selected in the Bering Sea. The temporal characteristics of this endmember are also a classic seasonal one. Sea ice coverage in this region is completely free from July to early November, than rapidly freeze to approximately 90% from late November to early December, then gradually freeze to full coverage until March, then slowly melt to 90% concentration from April to May, and rapidly melt to ice free in June. The majority of positive observations can be found in the northern part of Bering Sea. However, unlike other endmembers, this endmember has positive observations in many other regions with 70% to 90% confidence, such as the Kara and Barents Seas, Greenland Sea, Canadian Archipelago, and Baffin Bay. These positive observations are only found in smaller area or spots instead of a continuous large area.

The sixth image (Figure 3.32) shows the endmember fraction selected in the Greenland Sea. This endmember describes the temporal characteristics of a six months ice free duration followed by a two months winter. The maximum ice concentration reaches only 80% in March, then gradually melts to ice free until late May. This endmember only fits a small area in the Greenland Sea. Apart from the Greenland Sea, it also can be found in the Seas of Okhotsk, and the Bering Sea. Similar to the fifth endmember, this endmember also fits small areas. The second endmember fits the Seas of Okhotsk but completely not fit the northwest corner. The sixth endmember can fit that corner in the Seas of Okhotsk.

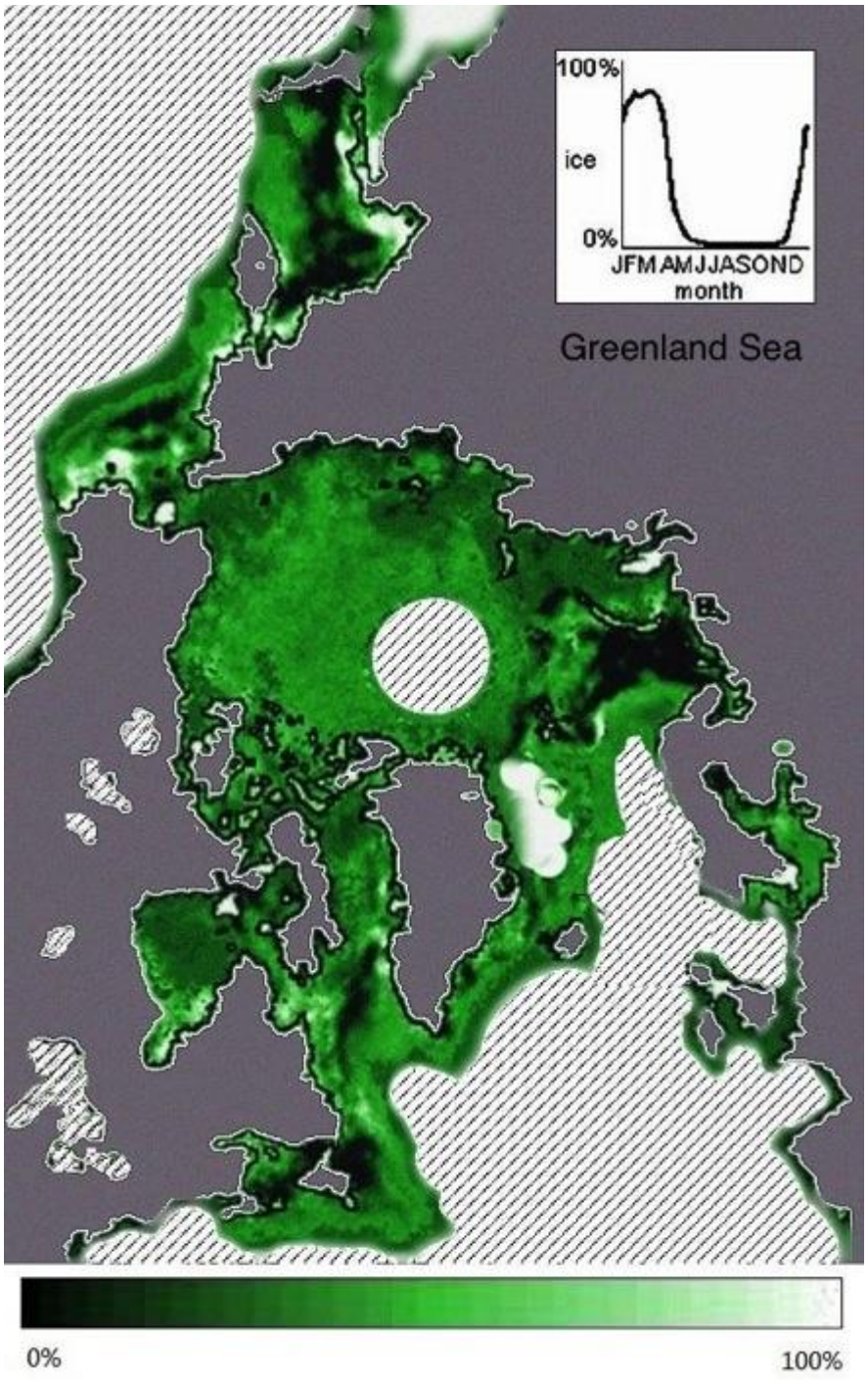

Figure 3.32 Fraction Image of Endmember 6

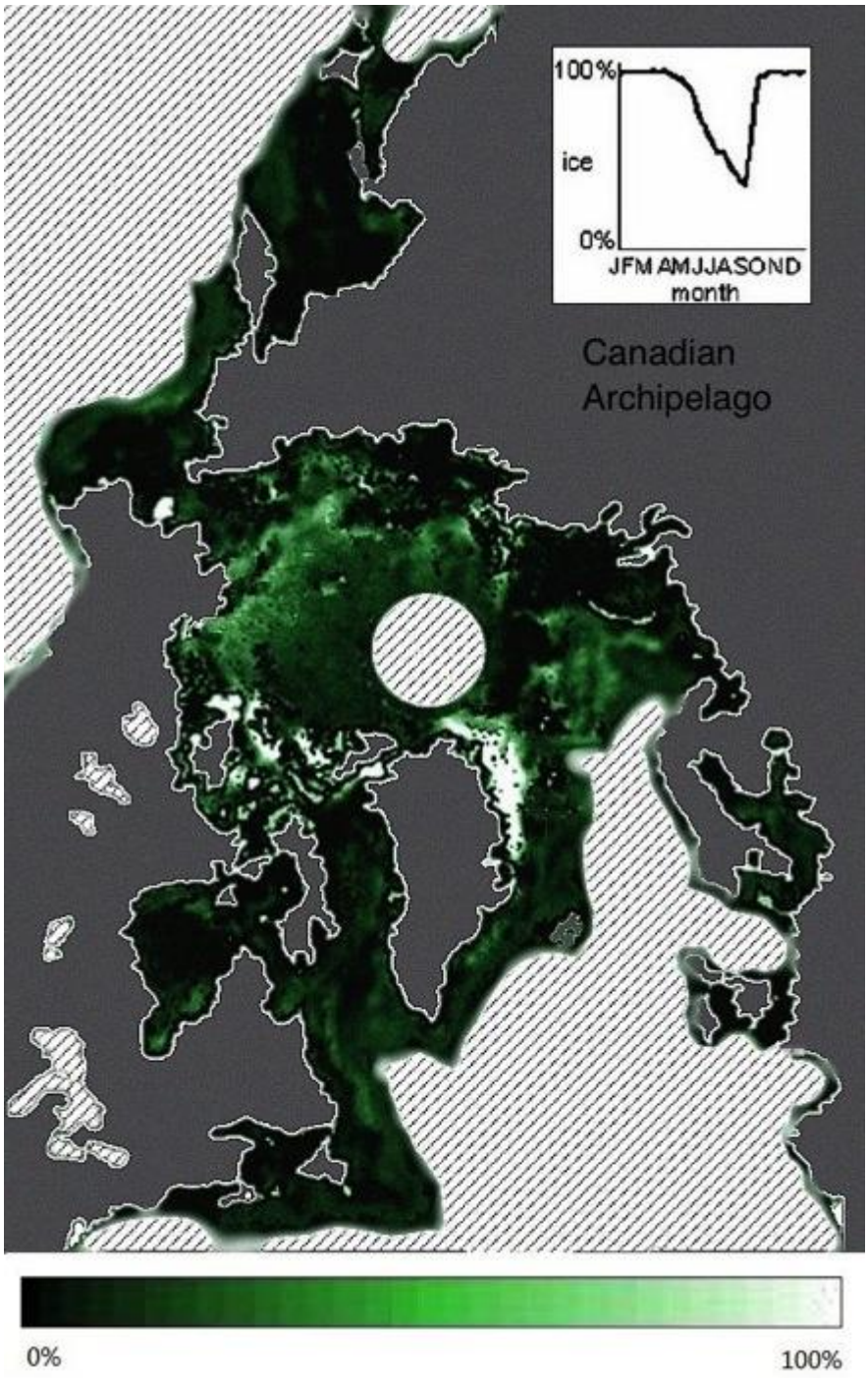

Figure 3.33 Fraction Image of Endmember 7

The seventh image (Figure 3.33) shows the endmember fraction selected in the Canadian Archipelago. This endmember describes a temporal characteristic of full ice

coverage from November to May, then starts to melt to a minimum of 40% ice concentration in late September then freezes again. This endmember fits part of the Canadian Archipelago, and interestingly it fits the west edge of the Greenland Sea.

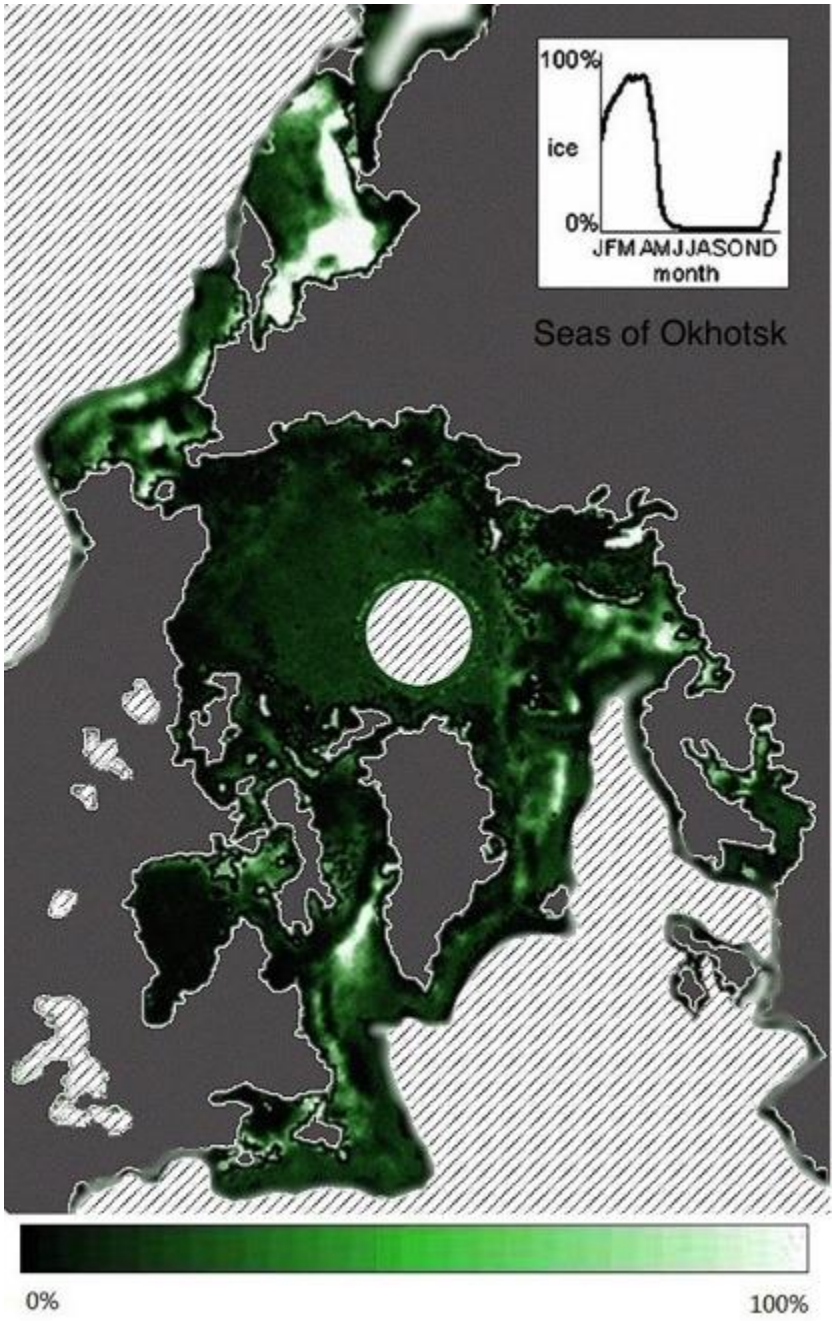

Figure 3.34 Fraction Image of Endmember 8

The eighth image (Figure 3.34) shows the endmember fraction selected in the Seas of Okhotsk. The temporal characteristics of this endmember are similar to endmember 6, but have longer summer duration for one month. This endmember fits the majority of area in the Seas of Okhotsk. Compared with endmember 2, endmember 8 has less positive observations in the Gulf of St. Lawrence. In addition, it has some minor fits in the Greenland Sea, Kara and Barents Seas, and the Bering Sea.

The ninth image (Figure 3.35) shows the endmember fraction selected in the Baffin Bay. The endmember selected in this region shares the same temporal characteristics with that selected in the Gulf of St. Lawrence, but with a month shorter summer duration. This endmember fits only the north part of the Baffin Bay, since Baffin Bay is a narrow long band, which makes it difficult to select an endmember that fits the entire region. Apart from the Baffin Bay, this endmember also fits the north part of the Bering Sea and the Seas of Okhotsk, but with less confidence.

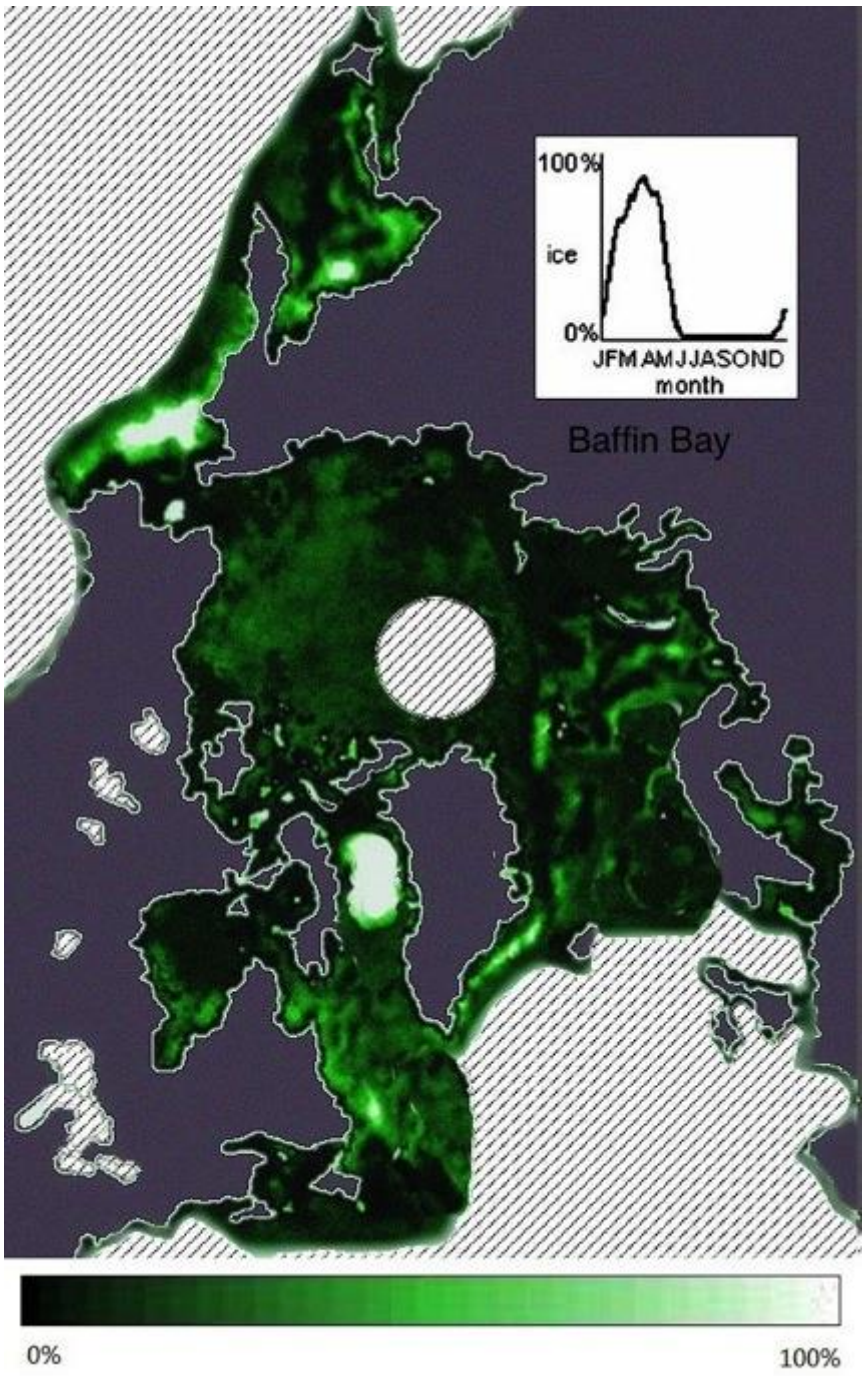

Figure 3.35 Fraction Image of Endmember 9

The RMS error image (Figure 3.36) is created in the process of temporal mixture analysis, which is a measure of the spectral residue that cannot be explained by the unmixing model. The amount of error is related to the performance of the model. If the error is large, it might indicate that the endmembers or unmixing rules are not selected or characterized correctly. In Figure 3.36, the RMS error statistics shows a mean error of 6% with a maximum error of 47%. From the RMS error image, it shows that in the central circle of the Arctic Ocean, because there is no data collected in that region, therefore, there is no error. Besides the central blank circle, level of RMS error remains low in the Arctic Basin, especially in high latitude. The boundaries between different sub-regions and sea shoreline are usually places with high RMS errors. In addition, the clustering of RMS errors can also be found in the eastern shoreline in the Baffin Bay and the Labrador Sea, north part of the Gulf of St. Lawrence, west part of the Greenland Sea, shoreline of the Kara and Barents Seas, and west part of the Seas of Okhotsk. The reason of why RMS errors would occur in these areas will be discussed in the discussion part.

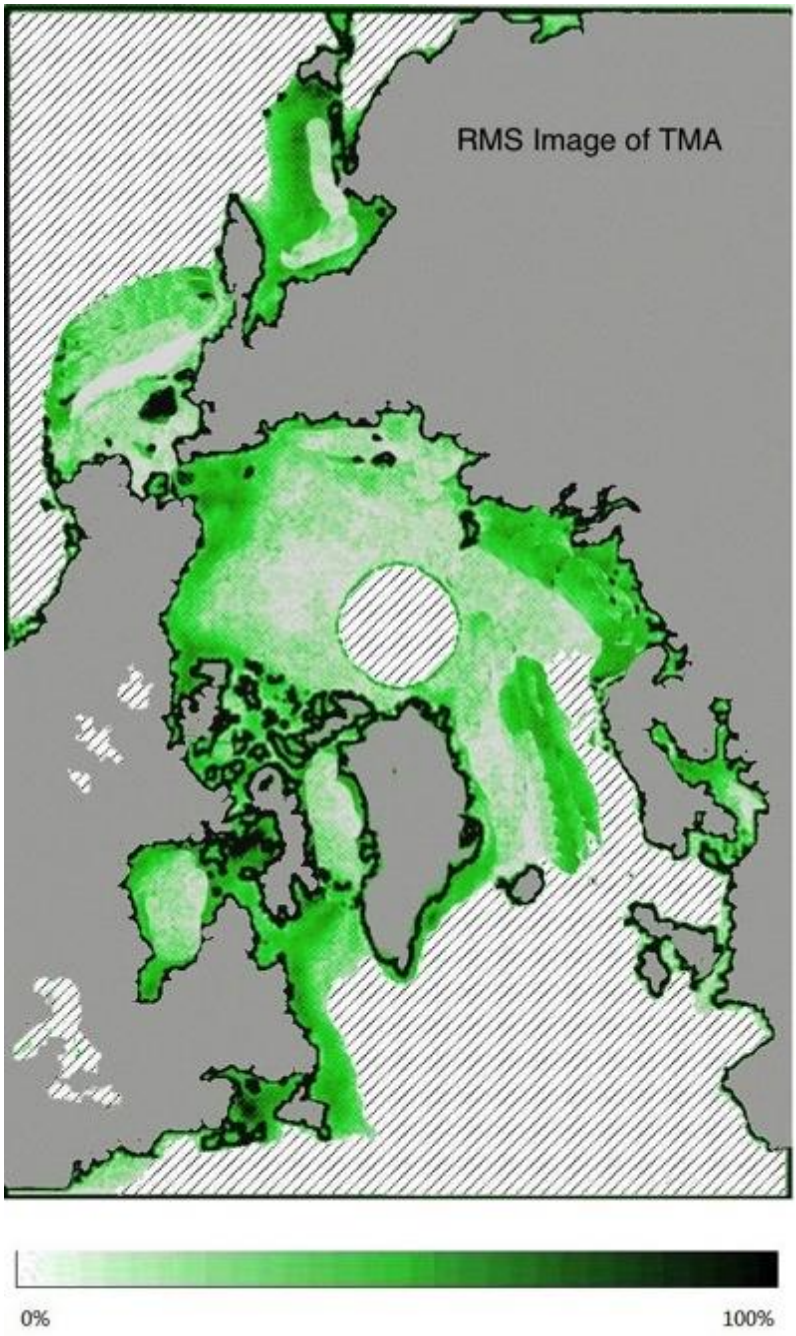

Figure 3.36 RMS Error Image of TMA

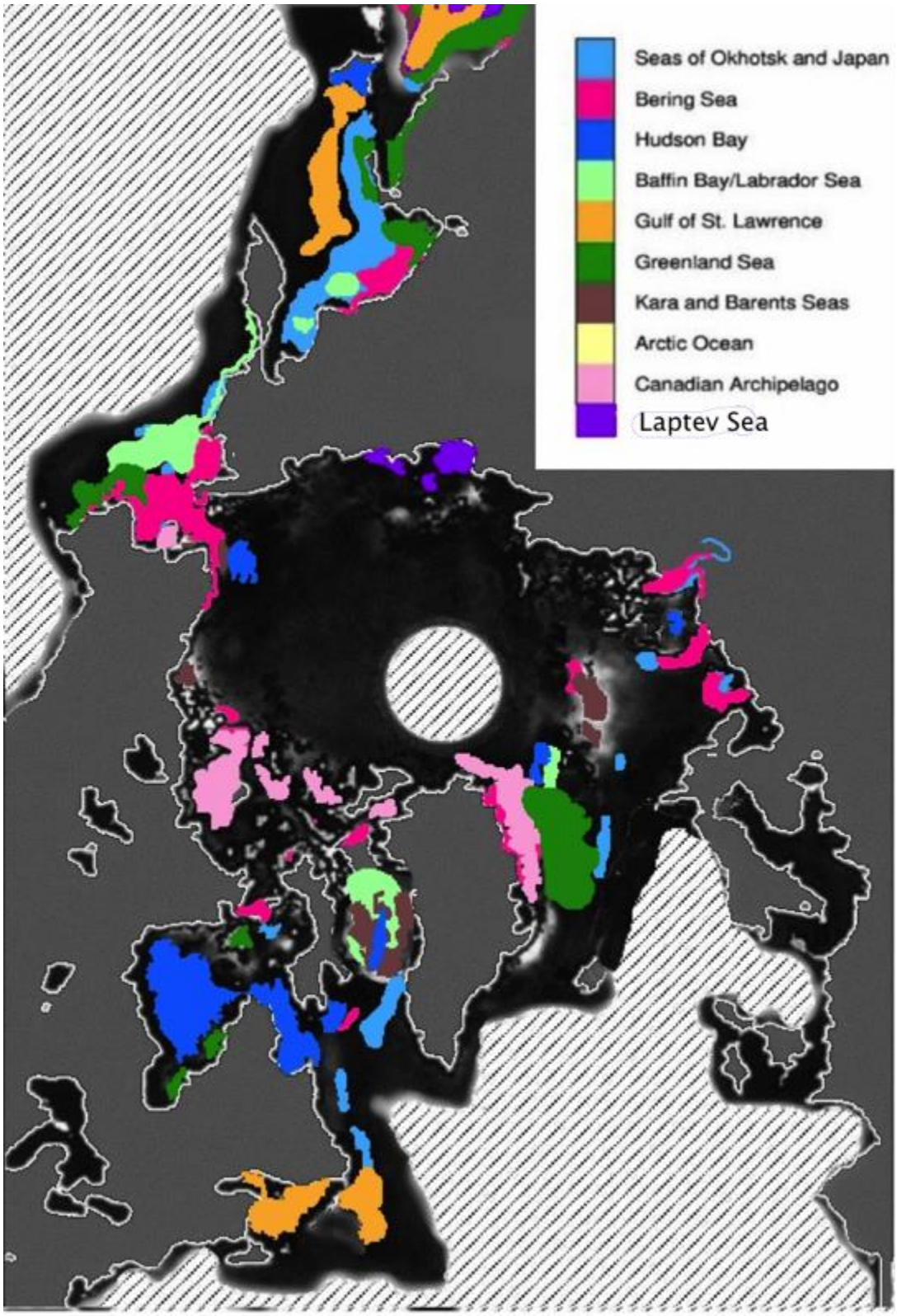

Figure 3.37 Color Mix of Endmembers

The endmember color mix image (Figure 3.37) is created to provide an overall view of the spatial distribution of temporal signatures derived from each subregion. This image is created by highlighting endmember fractions that are above 80% concentration with colors representing where they belong to. If a pixel does not have any endmember that has over 80% will be displayed as black. In addition, if a pixel has multiple endmember matchups, endmember with the highest concentration will be displayed above others. From Figure 3.37, it can be seen that the temporal characteristics of sea ice in the opposite side of the Arctic Basin are more likely to be similar with each other. In Hudson Bay and Gulf of St. Lawrence, their respective endmembers dominates these sub-regions with little fraction of other endmembers. However, most of other sub-regions contain multiple endmembers. The Seas of Okhotsk and Japan has a large amount of endmembers selected in other subregion. These endmembers are all seasonal endmember with different temporal characteristics, indicating sea ice in the Seas of Okhotsk and Japan is difficult to be described by using only one endmember, which can be proved in the RMS error analysis. If there is an overlay of colors, it might be two similar endmembers.

From Figure 3.37, the composition of endmembers can be analyzed in each sub-region. In the Seas of Okhotsk and Japan and the Greenland Sea, multiple endmembers can be found in this region with over 80% concentration. This indicates different temporal characteristics can be found in these regions that match a variety of different temporal signatures. However, different endmembers rather match different areas separately instead of overlaying each other indicating different temporal signatures

may exist within these subregions. Therefore further classification may be required in these two sub-regions for optimized endmember selection. In the Bering Sea and Baffin Bay, endmembers are more likely to overlap each other indicating complex and ambiguous temporal characteristics in these two regions. According to the sea ice variability and trend analysis, seasonal variations are higher in these two regions compared to others. This might explains the endmember lap that the temporal variability of sea ice in these regions may match one endmember in one period, and after a few years, it may match other endmembers. In the Hudson Bay, Canadian Archipelago, and the Gulf of St Lawrence, one endmember dominates the majority of the area. This indicates that endmembers selected in these regions match the majority of areas and high consistency in seasonal variation.

TMA describes the spatial distribution of different temporal signatures selected within these sub-regions; it also shows the spatial and temporal sea ice extent anomalies. In Figure 3.37, any other color appearance in a certain area is a signal of unconsidered temporal signature or inappropriate endmember selection. Also, in Figure 3.37, the large amount of black color implies none of the endmembers would match these areas with over 80% concentration. In addition, the black color in each subregion indicates a different temporal characteristic that has not been accounted for in the endmember selection process, because of the scale in the subregion classification. In the RMS error image, the clusters of errors can be considered as potential new endmembers following the same approach with Piwowar and LeDrew, 1997, which the four endmember modeling is a derivative from the two endmember modeling with two extra endmembers

selected from the error image. The TMA reveals sea ice temporal variability within each subregion and finds areas with different temporal characteristics.

3.5 Synthesis of Arctic Sea Ice Variability, Trend, and Anomaly Analysis

From the above Arctic sea ice variability and trend analysis, ranking analysis, and temporal mixture analysis, the general sea ice variability, trend, and anomalies are found.

The variability of the Arctic sea ice extent is spatially and temporally. And it forms a clustering nature to be similar with each other either spatially or temporally. Any phenomena that are different from the clustering nature can be classified as anomalies. Arctic sea ice extent varies from month to month, but forms a seasonal cycle that usually reaches its maximum extent at March and minimum at September mainly because of the latent heat. A variety of other environmental factors contribute greatly in sea ice variability such as the sea surface temperature, solar radiation, atmosphere, and ocean currents. Generally, sea ice covers larger area and lasts longer in the central Arctic compared with areas away, and sea ice variability varies accordingly. Apart from the seasonal variation, the yearly variation forms the long-term trend of Arctic sea ice extent. In addition, yearly averaged sea ice extents of years after 2000 are more likely to be smaller than those of years before 1985.

From the trend analysis using Sen's Slope Estimator and decadal averaged line (Figure 3.13), the overall trend of Arctic sea ice extent can be found. The sea ice extent is decreasing in the scale of the whole Arctic region and speed of decreasing grows from decade to decade. All subregions except the Bering Sea, Canadian Archipelago, and Gulf of St Lawrence show a clear decreasing trend according to the 95% confidence level Sen's Slope Estimator.

From the Arctic sea ice variability and trend analysis, the anomalies cannot be

easily statistically found. The sea ice extent ranking analysis and the temporal mixture analysis are used to analyze the anomalies both spatially and temporally. The sea ice extent ranking analysis gives years with abnormal high and low sea ice extent in Figure 3.25. And the temporal mixture analysis is used to find the spatial distribution of temporal anomalies within each sub-region. From the anomaly analysis, it shows years after 1995 are more likely to have abnormal low sea ice extents, and this phenomenon becomes very obvious after year 2000. This phenomenon coincides with the sea ice extent trend analysis that the Arctic sea ice extent is decreasing from 1979 to 2006 and the speed of decreasing increased from decade to decade.

The spatial distribution of temporal signatures shows different seasonal variation patterns across the Arctic region. Sub-regions that are close to the Arctic basin usually have their own and unique temporal signatures that do not occur in other sub-regions. This phenomenon might due to the high latitude cold environment while the lower latitude sub-regions do not have the same cold temperature to create similar multiyear ice dominated seasonal variation with the high latitude areas.

On the contrary, the lower latitude sub-regions such as the Bering Sea and Greenland Sea have more anomalies in the TMA analysis. The inconsistent seasonal variation and first-year ice dominated nature make sea ice extent in the lower latitude sub-regions easily affected by other environmental factors. Therefore, multiple temporal signatures can be found within one sub-region. In the Bering Sea and Hudson Bay, different endmembers overlay each other indicating different seasonal variations through the long-term time series. However, some other low latitude sub-regions such as the

Greenland Sea and the Seas of Okhotsk and Japan, have different endmembers matching different areas without overlaying each other. This phenomenon implies that these sub-regions have considerable amount of areas with different and similar to endmember from other sub-regions temporal characteristics.

Through the anomaly analysis, finding endmember clusters in other sub-regions across the Arctic basin can help support the oscillation pattern influence of the Arctic sea ice variability. Also, as the sea ice extent is decreasing, other temporal signatures would show up in several sub-regions as indicators of less winter maximum sea ice extent or delayed freeze time, which is similar to endmembers selected from lower latitude sub-regions. Therefore, the spatial location of anomalies implying the long-term decline trend can be revealed.

CHAPTER FOUR

DISCUSSION

Based on this research, there is a statistically significant trend that the Arctic sea ice extent is decreasing from 1979 to 2006. Analysis of arctic sea ice extents derived from satellite passive microwave data for the 28 years from 1979 to 2006 has found an overall downward trend of -45,100 ± 4,600 km^2 per year. Also, this downward trend has been found in all the sub-regions. The Arctic sea ice extent ranking analysis provides more information of the sea ice variability, trend, and of great use in anomaly detection of both the whole Arctic and its sub-regions. But in the ranking analysis, anomalies can only be found on the temporal resolution of year, and it cannot reveal anomalies within each subregion. Also, there is no effective assessment that could be applied to the ranking analysis to validate its credibility. Fortunately, the Temporal Mixture Analysis provides detailed analysis of the spatial distribution of temporal characteristics observed in the sub-regions. TMA cannot only provide the endmember distribution within its own subregion, but in other sub-regions as well.

4.1 RESULTS INTERPRETATION

From the Arctic sea ice variability and regression, ranking analysis, and Temporal Mixture Analysis, the general concept of Arctic sea ice temporal and spatial characteristics can be perceived. In the sea ice variability and trend estimation, the monthly sea ice extent data are presented in its temporal order with seasonal fluctuations. It is difficult to find the 28-year sea ice variability trend by visual inspection. With the aid of monthly deviation trend estimation, the regression line provides an answer that sea ice

extent is decreasing in the spatial scale of the whole Arctic. When it comes to different sub-regions, the trend estimation also gives the answer that sea ice extent is decreasing but with different confidence level. Regression analyses of the Bering Sea, Canadian Archipelago, Hudson Bay, and Gulf of St. Lawrence give very small ratios with 95% confidence level, which hold back the thoughts of making a conclusion that sea ice extents in these area are really decreasing.

The seasonal sea ice extent average line chart (Figure 3.13) pushed the trend estimation a step forward by revealing the fact that Arctic sea ice extent is decreasing not only in the 28-year time series analysis, but on a decadal basis. In Figure 3.13, sea ice extent of 1979-1990 average was larger than the 1979-2000 average, indicating sea ice decrease between 1990 and 2000. After 2000, the individual monthly sea ice extent data are far below the 1979-1990 average line and the 1979-2000 average line, indicating intensified sea ice decrease.

In the monthly deviation and trend estimation, the anomalies of monthly sea ice extent data can be identified by selecting the peaks and troughs. However, there is great uncertainty in whether a peak or trough is an anomaly or whether it's normal fluctuations. Therefore, except for a few extreme years, many peaks or troughs are left as uncertainties and cannot be classified as anomalies. The difference between an anomaly and normal fluctuations are determined by comparing the seasonal variation of sea ice extent of one year with its adjacent 2 years. If the seasonal difference is less than 10%, it will be counted as normal fluctuation; otherwise, it will be suspected as an anomaly, but not confirmed.

The sea ice extent ranking analysis can help solve the above problem in identifying anomalies. Instead of comparing each monthly sea ice extent data with the 28 year average, sea ice extents are ranked on a year basis from largest to smallest regardless of their temporal order. In these colored ranking charts, anomalies can be easily selected. This approach is effective in groupings that have clustering of bars with similar colors, allowing easy detection of a different color. But areas, for example, the Canadian Archipelago and the Gulf of St. Lawrence, that have small ratios in the trend estimation coincidentally have shuffle mixed color bars in the ranking analysis. In this case, anomalies cannot be easily detected, which make it a limitation for anomaly analysis.

The limitations of the ranking analysis can be summarized in three perspectives. Apart from the first one has been issued on the above paragraph, the second one is that it analyses data on a yearly basis, which fails to reveal the seasonal variations. The third one is that all the rankings treat its analyzed region as an integral unit, and fail to reveal the variations within its subregion.

In order to solve the limitations of the ranking analysis, the Temporal Mixture Analysis utilizes endmembers to best describe various seasonal variation signatures across the whole Arctic region, and then through the unmixing process to provide the fractional image of each endmember. The fractional images provide a visual impression of the spatial distribution of endmembers. The concentration of endmembers, i.e. temporal characteristics can be found not only in the subregion where the endmember is selected, but sometimes, other sub-regions also have high concentration of that particular endmember.

In the TMA analysis, the long-term variation of seasonal variations can be found in the Color Mix Figure of Endmembers (Figure 3.37). If a sub-region contains a number of and overlapping endmembers, the seasonal variation in this region is considered to have changed in the 30-year period. And this phenomenon is more likely to occur in areas far away from the central Arctic because these areas are dominated by first year ice. First year ice can be easily influenced by the changing atmospheric and temperature conditions that makes the seasonal variations different each year. While in the central Arctic, multiyear ice dominates the majority of areas, and multiyear ice is less sensitive to the changing atmosphere and temperature because of its large volume and latent heat from the ocean.

Apart from the seasonal variations, different temporal characteristics can also be found through TMA. In the Greenland Sea and Seas of Okhotsk and Japan, a number of endmembers can be found but covering different areas with little overlap. This indicates that part of this sub-region is temporally more similar to other sub-region than its own sub-region. Therefore, sub-regions like this should be further classified as two or more sub-regions instead of one in future researches.

In the sea ice extent ranking analysis, the oscillation pattern can be found by comparing the clustering of bars sharing similar colors. The TMA push it forward by displaying where exactly these areas are. If an endmember is found covering large areas in sub-regions that are in the opposite side of the Arctic basin, it can be considered that these sub-regions are likely to share similar temporal characteristics. With the help of the ranking charts, the time interval of the oscillation can be found. Piwowar, (2008),

published a paper analyzing the Arctic sea ice variability using TMA, and he used the Minimum Noise Fraction and Pixel Purity Index to help select the endmember while in this research, endmembers are selected based on known sea ice temporal/spatial variability in each sub-region. In the results analysis part, he used regional color mix of similar endmember to reveal the fraction of different endmembers. But in this research, the color mix image is improved to present the fraction distribution in the entire Arctic region. In addition, the detection of temporal signatures in other subregions, areas with different temporal characteristics within a subregion, and evolution of temporal characteristics through decades in certain areas can be identified in the color mix image, which improved from the regional color mix image that only gives fraction concentration without any interpretations.

4.2 The Error Analysis of Temporal Mixture Analysis and RMS Image

In spectral mixture analysis, there are a number of ways to evaluate the performance of the unmixing process. In this research, approaches utilized in SMA will be introduced for error evaluation for TMA through some minor adaptations.

4.2.1 RMS Error Analysis

A root mean square (RMS) is used to compare the model prediction results with the actual observations. In an unmixing process, a small RMS error of a pixel indicates the model suits this pixel well. If the error is large, it may indicate that it is an inappropriate model or endmember selection/categorization or unmixing rules, which requires changes in the modeling process.

From previous spectral mixture analysis studies, researchers usually make a RMS

error image of the unmixed study area. This method applied to temporal mixture analysis as well. When unmixing the Arctic sub-regions using the nine endmembers, a RMS error image is produced. In the RMS error image, it follows the same recognition pattern with the endmember fraction image, which areas with lighter color indicate a good condition of model fit. In the contrary, darker color areas indicate high errors.

From an overall view of the RMS error image derived from nine endmembers, it can be seen that the central Arctic basin has low errors for most of the endmembers because of the dominant non-seasonal sea ice all year round with little seasonal change throughout the year. In addition, sub-regions, which have large amounts of non-seasonal ice, also have less error than the seasonal sea ice areas. The reasons of why non-seasonal ice has less error than the seasonal ice can be from a number of perspectives.

First of all, temporal mixture analysis endmembers describe the seasonal sea ice variation within a year, i.e., the seasonal changes of sea ice. For all areas covered by non-seasonal sea ice, the non-seasonal sea ice endmember can fit them equally without any difference among different regions, which means that a single TMA endmember can easily describe all non-seasonal sea ice covered regions with low error. However, the seasonal sea ice has a wide range of temporal characteristics. For example, sea ice in the Hudson Bay covers the entire region from December to May and this area is completely ice free from July to November. The endmember of Hudson Bay describes when the sea water start to freeze and become sea ice, how fast is the freeze process, how much area is covered by sea ice, how long the frozen sea ice will last, when the sea ice will start to melt, and also in what speed, and how much ice will melt, and so on. Temporal

characteristics of sea ice in the Fram Strait, Greenland Sea, have unusual patterns in the melting process. Sea ice started to melt after March and slowly melt to approximately 50% around late July, then interestingly, it stopped melt and remain that sea ice coverage for almost a month until late August, then it resumed melting and reached the minimum sea ice coverage in September. The above-mentioned temporal characteristics of endmembers derived from two different regions differ a lot from each other, and so do the other seven endmembers. Hence, the seasonal sea ice requires multiple seasonal endmembers to describe the various kinds of temporal characteristics of sea ice in different regions. Therefore, the effectiveness of the nine endmembers to describe all the seasonal sea ice temporal characteristics is clearly not as good as the non-seasonal endmember, which is by default set to a condition that sea ice remains frozen all year round.

Second, in this research, a total of nine endmembers are selected from nine sub-regions. These nine sub-regions cover the entire Arctic region, but this fact does not imply that endmembers selected from these nine regions can well fit every pixel in the entire Arctic region. For example, the endmember selected in the Greenland Sea is located within the Fram Strait which is an important sea ice "tunnel" connecting the Arctic Ocean and the Atlantic Ocean. Therefore, the temporal characteristics in the Fram Strait are very different compared to other parts in the Greenland Sea. Hence, any endmember selected in the Greenland Sea would fail to describe the whole region. This issue will inevitably lead to errors in the unmixing process. The most feasible way to overcome this issue is add more endmembers which can better describe different

temporal characteristics. However, because of the limitless variation of climate conditions, such as ocean currents, atmospheric circulation, cyclones, solar radiation, etc., it is impossible to describe every temporal characteristics observed in the Arctic region. Therefore only the significant ones can be measured and analyzed.

Third, from the RMS error image, it can be seen that the boundaries between different sub-regions usually have a large amount of RMS errors compared to the central areas of a certain subregion, especially in boundaries between sub-regions which have very different temporal characteristics, or the edge effect. For example, the boundaries between Kara and Barents Seas and Greenland Sea, Baffin Bay and Hudson Bay, Gulf of St. Lawrence and Baffin bay. The more different the temporal characteristics are, the more error there might be in these boundaries. The most obvious reason is that the endmembers of each subregion is selected through the scatterplot of all the monthly sea ice averages, and it leads to a problem that the "purest" pixel representing temporal characteristics in this region usually happens to be within that area with a considerable distance away from the boundaries, while the temporal characteristics of sea ice vary a lot along the path connecting the "purest" pixel in one subregion and that in its adjacent subregion. In some situations, the changes of sea ice's temporal characteristics can be gradual and proportional to the distance between the two endmembers. For instance, the temporal signatures of sea ice in the Laptev Sea and the Kara and Barents Seas are very similar, therefore, the RMS error changes gradually along the path between two endmembers and there is no significant error clustering across the boundaries. On the other hand, the Hudson Bay and Baffin Bay are close-by sub-regions but their temporal

characteristics are dramatically different. Therefore, the edge effects of these two sub-regions are significant with RMS errors and errors in the Hudson Strait which indicates model unsuitability. The most obvious reason is that the climate systems of these two sub-regions are very different. The Hudson Bay is more like an inland lake surrounded by the North American continent and Baffin Island with small amount of water connected to the Baffin Bay and the Canadian Archipelago, while the Baffin Bay is directly connected to the Atlantic Ocean with large amount of open water. The difference between two climate systems in Hudson Bay and Baffin Bay causes the difference in their corresponding temporal characteristics.

4.2.2 Qualitative Evaluation

Qualitative evaluation can be made from the spatial patterns highlighted in each of the fractional images based on globally acknowledged characteristics of the analyzed zone. For example, any patterns that may not obvious belongs to this zone based on concomitant knowledge, however, actually appear in this zone. This occurrence may indicate possible incorrect construction of the model or some unaccounted features. Temporal mixture analysis is well acknowledged as efficient and effective for revealing hidden anomalies from other time series analysis.

In temporal mixture analysis, the qualitative evaluation process will be performed by comparing the distribution of endmember fractions with the actual sea ice variability trend in their corresponding area. In this analysis, since the endmembers are selected in each subregion, the sea ice variability of pixels in the lighter tones of the fraction images in each subregion undoubtedly matches the temporal characteristics of selected

endmembers. But other darker tones in these sub-regions do not seem to match the temporal characteristics of selected endmembers. However, the clustering of lighter tones of pixels of a certain endmember does not always fall within the endmember selection subregion. For instance, an endmember selected in the Gulf of St. Lawrence has a lot of lighter tones in the Gulf of St. Lawrence; however, far away from the gulf in the opposite side of the Arctic Ocean, there are another large area of clustering of lighter tones in the Seas of Okhotsk. In addition, similar situation can also be found in Greenland Sea and Bering Sea.

Through inspection of temporal sea ice variability in both the Gulf of St. Lawrence and the Sea of Okhotsk, the endmember clustering in these two regions does match the local sea ice seasonal variability. However, through the 28 year data of sea ice variability time series information, it can be seen that though the Gulf of St. Lawrence and Seas of Okhotsk shares a very similar temporal characteristics, their individual sea ice trend did not match with each other. By identifying the peaks of extraordinary high sea ice extent in both sub-regions, the similar conclusion can be made the sea ice trend and anomaly analysis that sea ice extent seasonal variability in Gulf of St. Lawrence and Seas of Okhotsk has a time shift for peak sea ice extents about 10 years, which implies Arctic oscillation which is also a decadal pattern. When looking into the seasonal sea ice extent of the two sub-regions, the decadal oscillation pattern is clearer especially in the winter sea ice extent averages. The Gulf of St. Lawrence and the Seas of Okhotsk are in the outer range of the Arctic region which indicates seasonal sea ice dominates these sub-regions. According to the sea ice extent seasonal averages, sea ice is completely melted

to sea water in summer time, and in spring and fall, sea ice extent remains at a low level, while in winter time, sea ice extent reaches to approximately three times of that in spring or fall. In the Seas of Okhotsk, sea ice extent in winter time is highest of 1.5 million km2 in 1979, then have three lows in 1984, 1991, and 1996, while in the Gulf of St. Lawrence, sea ice extent reaches three high peaks in 1985, 1989, and 1994. The sea ice extent peak area in the Seas of Okhotsk was observed in 1979, then in 1989, sea ice extent in the Gulf of St. Lawrence, reaches its peak area. Meanwhile, sea ice extent in the Gulf of St. Lawrence remains above the 28 year average between 1983 and 1997, but for the Seas of Okhotsk remains below the 28 year average for most of the years during that period.

Through the seasonal sea ice extent variability data, the qualitative evaluation validates the clustering of lighter tones in other sub-regions in the Gulf of St. Lawrence and Seas of Okhotsk situation. The reason may relate to climate perspectives such as similar latitude, ocean conditions, atmospheric circulation, etc., in these two sub-regions. And the time shift between peak sea ice extents may relate to the Arctic oscillation and the Atlantic oscillation.

However, not all the lighter tones indicating the endmember's temporal characteristics can successfully reveal the temporal characteristics of local pixels. For instance, the endmember fraction from Bering Sea which has a complete different temporal characteristics with the Greenland Sea, but there are a cluster of lighter tones along the Fram Strait. And as discussed before, the endmember selected from the Greenland Sea happens to be within the Fram Strait which has a very different climate system with other areas of the Greenland Sea. This issue shows the incapability of

describing the temporal patterns of pixels in the Greenland Sea. The reason of this issue is because of the very different types of temporal characteristics within one subregion, which a sub-regions is assumed to have a temporal characteristics that fits the majority of pixel in this area without too much variance.

4.3.3 Overflow Evaluation

In spectral mixture analysis, the sum of each endmember fraction must be 1.0 and each endmember fraction must be between 0 and 1. This rule should be effective in temporal mixture analysis as well. By examining the endmember fraction sum whether beyond the desired range 1.0, the TMA model can be evaluated for its effectiveness in describing each of the endmembers. In spectral mixture analysis, it is usually hard to find the purest spectral pixel of a certain land cover or band and use that pixel as an endmember. A fraction overflow generally shows up because pixels are more spectrally pure than the spectra defined by one or more of the endmember (Piwowar, 2008). Luckily, there is no large amount of overflow in this research. The only few are scattered in the central Arctic Ocean, and the subpolar region where there have most seasonal sea ice. The overflow in the Arctic Basin is probably because of the flooding of water over the multiyear ice. Although non-seasonal sea ice is found in the central Arctic Basin, it is not always identifiable in passive microwave imagery because summer melt water flooding the surface of the ice pack is frequently mistaken as ice with reduced concentration (Kwok, 2000; Meier, 2005). The overflow in the subpolar region is probably because of the limitation in the algorithm designed to estimate sea ice concentration data. According to the data documentation from NSIDC, this algorithm does not work well over open

ocean which instead predicting the expected zero value, it might predict sea ice concentration values as high as 35%, particularly in regions with excessive winds and stormy weather (Comiso, J. 1999).

In addition, in the endmember selection process of TMA, overflow can be detected from the scatter plot of sea ice extent in March versus September. If a pixel that happens to have higher sea ice concentration in September than in March, this pixel is an overflow which is due to land and atmospheric contamination of the SMMR signal of subpolar regions (Piwowar et al., 1997).

4.3 Advantages, Limitations, and Uncertainties of this research

In the sea ice extent calculation process, only sea ice concentration above 15% can be counted as sea ice extent. This process is used to avoid any interference of the atmosphere or random ice floes that might be accidentally counted as stable sea ice extent.

Also, as stated in the RMS error analysis, the manual classification of the Arctic sub-regions based on previous research gives a good understanding of the seasonal sea ice extent variability in these different areas. However, it would provide better consolidated and convincing results in all research to perform these classification analyses solely based on the data instead of arbitral segmentation. For example, to create possible processes that could find the boundaries between different temporal characteristics, and use these boundaries for subregion classification.

However, even if the subregion classification has been optimized, the boundaries would still be the region of high RMS errors. According to the Tobler's first law of geography (Tobler, 1970), things are more likely to share similar characteristics with

things that are close by than things are apart. Though the boundary area is divided by two sub-regions, its spatial and temporal characteristics still remain as an integral unit. Trying to analyzing the boundary region with two different endmembers would definitely cause error. The ideal situation is that the TMA would select endmember from every temporal signature to minimize the boundary effects.

Because of the complexity of sea ice variability, long term sea ice trend is usually hard to conclude its whether decrease or just normal fluctuation. In addition, any overfitting should be avoided in this sea ice extent trend trend estimation. Long term sea ice extent trend analysis incorporates strong seasonal effects that can greatly influence the trend estimation. Monthly sea ice extent regression can be influenced by the seasonal variation throughout the year, especially when the winter is particularly cold than usual year or an extremely hot summer. But a yearly average sea ice extent would be biased by arbitrarily averaging the 12 monthly data from January to December. In order to reveal the true long-term sea ice extent trend, seasonal adjustment would help greatly by alleviating the seasonal effects.

Another limitation of the TMA analysis is that it takes the 28 year sea ice extent data and tries to extract the temporal signatures in different regions. Though anomalies can be revealed, TMA does not consider the overall trend in sea ice extent variability. Seasonal sea ice variation in the 1980s might not be the same in years after 2000. Therefore, endmember selected in regions like that would not correctly describe the changes in seasonal sea ice variation.

Uncertainties, mostly recognized as “an information deficit”, cannot be avoided in

any modeling analysis. But it takes on an added dimension by utilizing scientific knowledge to support any modeling analysis by alleviating systematic error and bias (Brown, 2010). In Temporal Mixture Analysis, the spatial distributions of different temporal signatures are presented, which provides a new opportunity for analyzing past remote sensing record. But uncertainties also exist in TMA. For example, endmember selection, unmixing process, or error analysis could influence the model output. In addition, the remote sensing data capturing process is another source of uncertainty, such as atmospheric influence, sea water flood over ice, even the SMMR algorithms.

Algorithms designed to estimate sea ice concentration using passive microwave data frequently do not work well over Open Ocean (Comiso, J. 1999). When applied, instead of predicting the expected zero value, the algorithms predict sea ice concentration values as high as 35 percent, particularly in regions with excessive winds and stormy weather (Comiso, J. 1999). A climatological sea surface temperature mask was applied to remove pixels from regions where the ocean surface is above freezing. Also, land contamination (false ice along the coast due to pixels containing a mixture of land and ocean) were removed using a filter adapted from Cho et al. (1996). Even with these quality-control measures, some residual sea ice concentrations remain in the open ocean and along the coast.

4.4 Future Research Opportunities Following This Research

In future research of sea ice extent variability analysis, the most up-to-date sea ice extent data will be used. In this research, only monthly sea ice extent data is used for variability and trend analysis. But in future, by utilizing the daily sea ice extent data

would greatly improve the temporal resolution, and serves better in measuring the seasonal variability.

In temporal mixture analysis, endmembers will be selected in a different method. Through principle component analysis, minimum noise fraction, and pixel purity index, endmembers selected will better describe the temporal signatures across the study area instead of manual selection in each of the sub-regions. In addition, from the RMS error image, any clusters of error would also be potential endmembers. Incorporating new endmembers derived from the RMS error image could further improve the accuracy of TMA. As stated before, increased number of endmembers could subdivide the temporal signatures, which could better describe various kinds of temporal situation across the Arctic region.

Comparing the decadal oscillation pattern in sea ice variability trend and anomalies with the North Atlantic Oscillation index over the last few decades, there is a coincidence between them. Unfortunately, lack of reliable and continuous Arctic sea ice data, especially before the remote sensing era restricted systematic research of how North Atlantic Oscillation impact the Arctic sea ice, and whether NAO is the driving force in sea ice variability, motion, trend, etc.

The sea ice extent only is measured and analyzed in this research. The variability of sea ice thickness and volume is also very important in understanding the global climate. In particular, if Arctic sea ice volume decreases, it implies temperature rises and intensified sea ice melt. Therefore ice melts in glaciers, permafrost, ice sheet, etc., would also increase. If the temperature rises, it would imply global warming and intensified ice

melt in glaciers and ice sheet in the Antarctica. In future researches, by incorporating the sea ice thickness data, it would provide a more comprehensive understanding of Arctic sea ice.

CHAPTER FIVE

CONCLUSION

Most of the Arctic sea ice extent time series research focus on the identifying anomalies display the data in their temporal order, and try to identify the anomalies through various kinds of statistical methods. Two main questions were proposed in this research. The first one is to find the general trend in Arctic sea ice variability from 1979-2006 as well as different sub-regions. The second one is to find the spatial and temporal anomalies in sea ice extent variability across the Arctic region and different sub-regions. Traditional statistical methods would focus on the outliers in the time series, but fail to reveal the temporal characteristics or the inner relationship between clusters of anomalies in different regions.

In this research, the Arctic sea ice extent variation trend and anomalies from 1979 to 2006 are analyzed. In the sea ice anomaly analysis, the temporal anomalies of the whole Arctic region and the sub-regions are analyzed through the sea ice extent ranking. The sea ice extent ranking analysis provides a visual way to understand the anomalies in sea ice variation. The gradual color scheme adopted in the sea ice extent ranking is very useful for visual inspection of anomalies. Also, the comparison of sea ice extent ranking charts of some sub-regions reveals an oscillation pattern in sea ice growth/retreat in the east/west region of the Arctic Ocean. This pattern coincides with North Atlantic Oscillation to some extent, which provides a clue for future research to thorough investigates the sea ice feedback to North Atlantic Oscillation. The sea ice extent ranking analysis only treats the sub-regions as a whole unit, but in reality, there is sea ice

variation within each sub-region. And sometimes, sea ice variation within a sub-region could be more than that of different regions.

However, the spatial distribution of the temporal anomalies has not gained equal attention with the temporal anomalies in the long-term sea ice extent time series analysis. The Temporal Mixture Analysis, derived from spectral mixture analysis, is utilized to show the spatial distribution of temporal characteristics calculated in different sub-regions. TMA can reveal the spatial distribution of temporal characteristics, i.e. endmember, in other sub-regions. It can also reveal the concentration of that endmember in the subregion where it's selected, which is very useful for detection of any inappropriate subregion classification or endmember selection.

The TMA fraction images provide a straightforward method to understand the spatial distribution of temporal characteristics. Also, the inner variation of sea ice temporal characteristics can be revealed, which perfectly solved the limitation of sea ice extent ranking. In the sea ice extent general variability and trend analysis, the seasonal sea ice variation charts of different sub-regions indicates that some sub-regions share very similar temporal characteristics despite that they are far apart from each other.

The anomaly analysis in this research utilizes the sea ice extent ranking and temporal mixture analysis to reveal the spatial and temporal anomalies in the 1979 to 2006 period. The sea ice extent ranking analysis provides years with abnormal high or low sea ice extent in the Arctic region as well as different sub-regions. While the temporal mixture analysis provides an insight view of areas that anomalies would like to occur. Also, some sub-regions such as the Greenland Sea and Seas of Okhotsk and Japan

are revealed to have are multiple temporal characteristics in different parts of the sub-region.

This research provides a synthesized view of the spatial and temporal variability and anomalies of Arctic sea ice extent from 1979 to 2006. The sea ice ranking analysis provides a straightforward and non-statistical method of visualizing anomalies and see-saw oscillation pattern in the eastern and western area of the Arctic basin. And the TMA provides an unprecedented perspective of viewing the spatial and temporal variability at same time with scale insensitive entire Arctic analysis. The detection of temporal signatures in other subregions, areas with different temporal characteristics within a subregion, and evolution of temporal characteristics through decades in certain areas are the main improvements from previous researches.

In future research, the most up-to-date data can be used to analyze sea ice variability. Apart from using the monthly averaged sea ice concentration data, daily sea ice concentration data can be used for more detailed analysis. In the temporal mixture analysis, endmember selection process can be improved based on results of this research by utilizing more endmember in the Greenland Sea and Seas of Okhotsk. The sea ice dynamics could be explored to interpret the rapid sea ice cover decline in the recent decades. At last, not only the sea ice extent is of concern in understanding the Arctic climatology, but the sea ice thickness, volume, concentration, and motion. The analysis of variability in sea ice could help to build a comprehensive understanding of the Arctic environment and its interactions with the entire globe.

Ambaum, Maarten H. P., Brian J. Hoskins, David B. Stephenson, 2001: Arctic Oscillation or North Atlantic Oscillation?. J. Climate, 14, 3495–3507.

Anderson, M., J.L. Busse, and S. Drobot, 2012: A comparison between SSM/I passive microwave melt onset dates and satellite-derived albedo melt onset dates in the Arctic. International Journal of Remote Sensing, 33, 517-533, DOI: 10.1080/01431161.2010.542198.

Barry, R. G., M. C. Serreze, J. A. Maslanik, and R. H. Preller (1993), The Arctic sea ice-climate system: Observations and modeling, Rev. Geophys.,31(4), 397– 422, doi:10.1029/93RG01998.

Belchansky, G. I., D. C. Douglas, and N. G. Platonov (2004), Duration of the Arctic sea ice melt season: Regional and interannual variability,1979 – 2001, J. Clim., 17, 67–80, doi:10.1175/1520-0442(2004)017<0067:DOTASI>2.0.CO;2.

Bjørgo, E., O. M. Johannessen, and M. W. Miles (1997), Analysis of merged SMMR-SSMI time series of Arctic and Antarctic sea ice parameters 1978– 1995, Geophys. Res. Lett., 24(4), 413–416, doi:10.1029/96GL04021.

Burrus, C. S., Gopinath, R. A., and Guo, H. (1998). Introduction to wavelets and wavelet transforms. Prentice Hall.

Carsey, F. D. (1992). Microwave Remote Sensing of Sea Ice.

Cavalieri, D. J., C. L. Parkinson, P. Gloersen, J. C. Comiso, and H. J. Zwally (1999), Deriving Long-Term Time Series of Sea Ice Cover from Satellite Passive-Microwave Multisensor Data Sets, J. Geophys. Res., 104, 15,803-15,814.

Cavalieri, D.J. (2002), A link between Fram Strait sea ice export and atmospheric planetary wave phase. Geophysical Research Letters, 20(12):10.1029/2002GL014684.

Comiso, J. 1999, updated 2012. Bootstrap Sea Ice Concentrations from Nimbus-7 SMMR and DMSP SSM/I-SSMIS, [2012]. Boulder, Colorado USA: National Snow and Ice Data Center. Digital media.

Comiso, J.C., C.L. Parkinson, R. Gersten, and L. Stock (2008). Accelerated decline in the Arctic sea ice cover. Geophys. Res. Lett., 35(L01703), 6 pp 10.1029/2007GL031972

Corder, G.W. & Foreman, D.I. (2009) Nonparametric Statistics for Non-Statisticians: A Step-by-Step Approach, Wiley ISBN 978-0-470-45461-9

Davis, F. W., Ridd, M. K., Quattrochi, D. A., Lam, N. S., Walsh, S. J., Michaelsen, J. C., et al. (1991). Environmental analysis using integrated GIS and remotely sensed data: some research needs and priorities. Photogrammetric Engeneering and Remote Sensing , 689-97.

Decision 411, Duke University, 2005, www.duke.edu/~rnau/411diff.htm

Gershenfeld, N. (1999). The nature of mathematical modeling. p.205-08

Hipel, K. W., & McLeod, A. I. (1994). Time series modelling of water resources and environmental systems.

Holland, P. R. and R. Kwok (2012), Wind-driven trends in Antarctic sea ice drift, Nat Geosci., doi: 10.1038/NGEO1627.

Howell, S.E.L., C.R. Duguay, and T. Markus 2009. Sea ice conditions and melt season duration variability in the Canadian Arctic Archipelago: 1979-2008, Geophysical Research Letters. 36, L10502, doi:10.1029/2009GL037681

Hurrell, J. W., Kushnir, Y., Ottersen, G., and Visbeck, M. (2003). The North Atlantic Oscillation - Climatic Significance and Environmental Impact.

Kwok, R. (2000), Recent changes in Arctic Ocean sea ice motion associated with the North Atlantic Oscillation, Geophys. Res. Lett., 27(6), 775–778, doi:10.1029/1999GL002382.

Kwok, R. (2011), Satellite remote sensing of sea ice thickness and kinematics: A review, J. Glacio., 56, 200.

Kwok, R. and G. F. Cunningham (2012), Deformation of the Arctic Ocean ice cover after the 2007 record minimum in summer ice extent, CRST, 76-77, doi: 10.1016/j.coldregions.2011.04.003.

Laxon S. W. , K. A. Giles , A. L. Ridout , D. J. Wingham , R. Willatt , R. Cullen , R. Kwok , A. Schweiger , J. Zhang , C. Haas , S. Hendricks , R. Krishfield , N. Kurtz , S. Farrell, and M. Davidson. 2013. CryoSat-2 estimates of Arctic sea ice thickness and volume , Geophysical Research Letters , 40, doi: 10.1002/grl.50193 .

LeDrew, E.F. (1987), Developmental Processes for Five Depression Systems Within the Polar Basin. Journal of Climatology, 8, 125-153.

Liu, J., J. A. Curry, and Y. Hu (2004), Recent Arctic sea ice variability: Connections to the Arctic Oscillation and the ENSO, Geophys. Res. Lett.,31, L09211, doi:10.1029/2004GL019858.

Lorenz, Edward N. (1951). "SEASONAL AND IRREGULAR VARIATIONS OF THE NORTHERN HEMISPHERE SEA-LEVEL PRESSURE PROFILE". Journal of Meteorology 8 (1): 52–59. Bibcode 1951JAtS....8...52L. DOI:10.1175/1520-0469(1951)008<0052:SAIVOT>2.0.CO;2. ISSN 1520-0469. Retrieved 2010-08-28.

Maslanik, J. A., M. C. Serreze, and R. G. Barry (1996), Recent decreases in Arctic summer ice cover and linkages to atmospheric circulation anomalies, Geophys. Res. Lett., 23(13), 1677–1680, doi:10.1029/96GL01426

Michael Pidwirny (2006). "Introduction to the Oceans". www.physicalgeography.net. Retrieved 2006-12-07.

Mysak, L. A., R. G. Ingram, J. Wang, and A. van der Baaren (1996), The anomalous sea-ice extent in Hudson Bay, Baffin Bay and the Labrador Sea during three simultaneous NAO and ENSO episodes, Atmos. Ocean, 34(2), 313– 343.

Overland, J. E., M. Wang, and S. Salo (2008), The recent Arctic warm period, Tellus, Ser. A, 60, 589– 597.

Parkinson, C. L. (2000), Recent trend reversals in Arctic sea ice extents: Possible connections to the North Atlantic Oscillation, Polar Geogr., 24(1), 1 – 12.

Parkinson, C. L., and D. J. Cavalieri (1989), Arctic sea ice 1973–1987: Seasonal, regional, and interannual variability, J. Geophys. Res., 94(C10), 14,499–14,523, doi:10.1029/JC094iC10p14499.

Parkinson, C. L., and D. J. Cavalieri (2008), Arctic sea ice variability and trends, 1979–2006, J. Geophys. Res., 113, C07003, doi:10.1029/2007JC004558.

Parkinson, C. L., D. J. Cavalieri, P. Gloersen, H. J. Zwally, and J. C. Comiso (1999), Arctic sea ice extents, areas, and trends, 1978– 1996, J. Geophys. Res., 104(C9), 20,837– 20,856, doi:10.1029/1999JC900082Overland, J. E., M. Wang, and S. Salo (2008), The recent Arctic warm period, Tellus, Ser. A, 60, 589– 597.

Piwowar, J. M., & LeDrew, E. F. (2001). On the Autoregressive nature of Arctic sea ice concentrations.

Piwowar, J. M., Peddle, D. R., & LeDrew, E. F. (1998). Temporal mixture analysis of Arctic sea ice imagery: a new approach for monitoring environmental change.

Piwowar, J., & LeDrew, E. F. (1995). HyperTemporal Analysis of remotely sensed sea ice data for climate change studies. Progress in physical geography , 216-242.

Polyakov, I. V., J. Walsh, R. Kwok (2012), Recent changes of arctic multiyear sea-ice coverage and the likely causes, BAMS, doi: 10.1175/BAMS-D-11-00070.1.

Priestley, M.B. (1988) Non-linear and Non-stationary Time Series Analysis, Academic Press.

R. Seager, Y. Kushnir, J. Nakamura, M. Ting, and N. Naik (July 2010). "Northern hemisphere winter snow anomalies: ENSO, NAO and the winter of 2009/10". Lamont-Doherty Earth Observatory, Columbia University.

Reddy, M. P. (2001). Descriptive Physical Oceanography.

Serreze, M. C., J. E. Walsh, F. S. Chapin III, T. Osterkamp, M. Dyurgerov, V. Romanovsky, W. C. Oechel, J. Morison, T. Zhang, and R. G. Barry (2000), Observational evidence of recent change in the northern high latitude environment, Climate. Change, 46, 159–207, doi:10.1023/ A:1005504031923.

Stroeve, J. C., M. C. Serreze, M. M. Holland, J. E. Kay, J. Maslanik, and A. P. Barrett. 2012. The Arctic's rapidly shrinking sea ice cover: a research synthesis. Climatic Change 110(3-4): 1,005-1,027, doi:10.1007/s10584-011-0101-1.

Stroeve, J. C., V. Kattsov, A. Barrett, M. Serreze, T. Pavlova, M. Holland, and W. N. Meier. 2012. Trends in Arctic sea ice extent from CMIP5, CMIP3 and observations. Geophysical Research Letters 39, L16502, doi:10.1029/2012GL052676.

Stroeve, J., Holland, M. M., Meier, W., Scambos, T., & Serreze, M. (2007). Arctic sea ice decline: Faster than forecast. Geophysical Research Letters, 34(9), L09501. doi:10.1029/2007GL029703

Tang, C. C., Ross, C. K., Yao, T., Petrie, B., DeTracey, B. M., & Dunlap, E. (2004). The circulation, water masses and sea ice of Baffin Bay.

Theil, H. (1950), "A rank-invariant method of linear and polynomial regression analysis. I, II, III", Nederl. Akad. Wetensch., Proc. 53: 386–392, 521–525, 1397–1412, MR 0036489.

Torrence, C., & Compo, G. P. (1998). A practical guide to wavelet analysis.

Wilcox, Rand R. (2001), "Theil–Sen estimator", Fundamentals of Modern Statistical Methods: Substantially Improving Power and Accuracy, Springer-Verlag, pp. 207–210, ISBN 978-0-387-95157-7.